NASA TECHNICAL MEMORANDUM

NASA TM X-2779

THROAT-BYPASS BLEED SYSTEMS FOR INCREASING THE STABLE AIRFLOW RANGE OF A MACH 2.50 AXISYMMETRIC INLET WITH 40-PERCENT INTERNAL CONTRACTION

by Bobby W. Sanders and Glenn A. Mitchell

Lewis Research Center
Cleveland, Ohio 44135

NATIONAL AERONAUTICS AND SPACE ADMINISTRATION • WASHINGTON, D. C. • MAY 1973

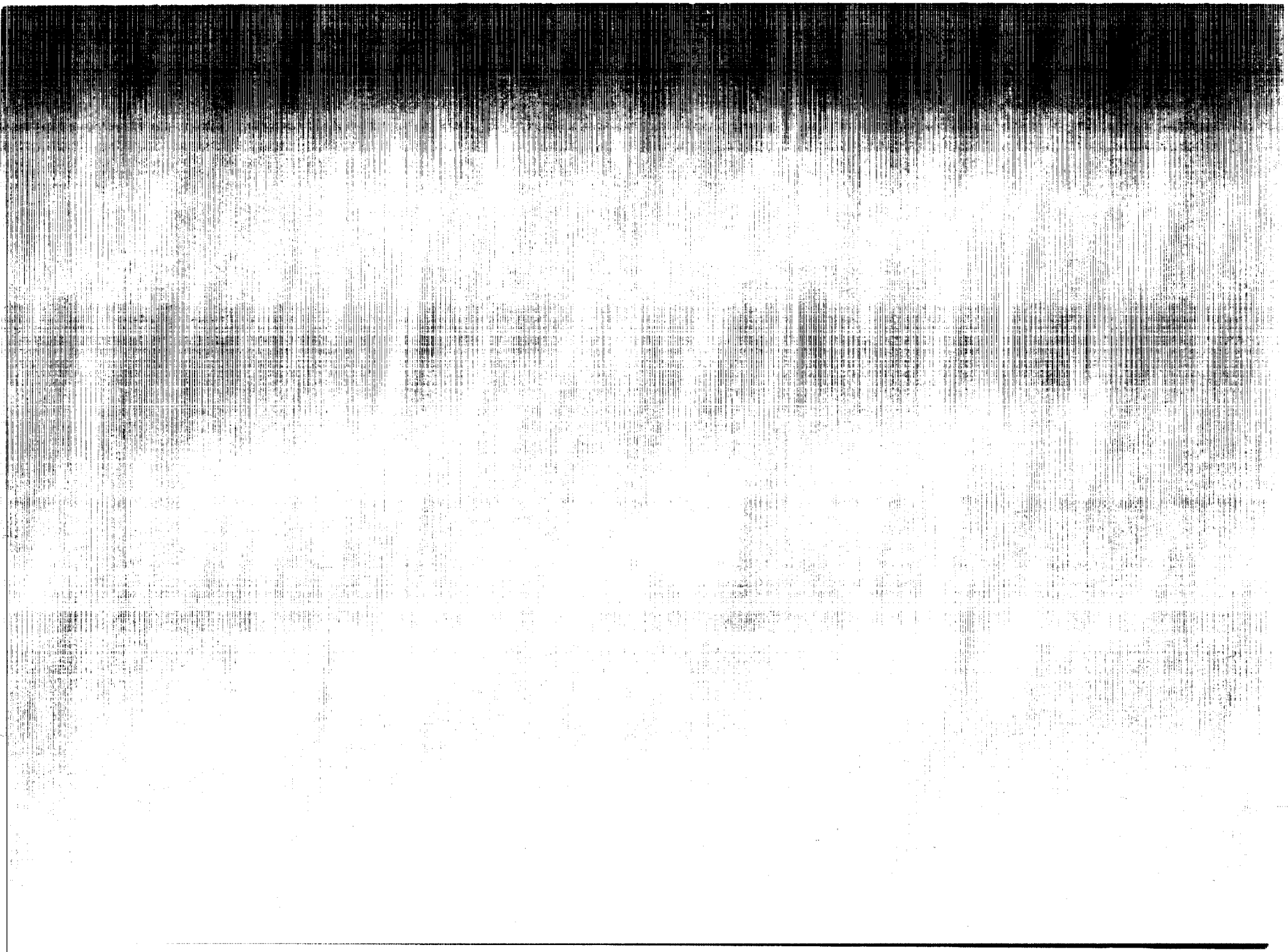

1. Report No.	2. Government Accession No.	3. Recipient's Catalog No.
NASA TM X-2779		

4. Title and Subtitle	5. Report Date
THROAT-BYPASS BLEED SYSTEMS FOR INCREASING THE STABLE AIRFLOW RANGE OF A MACH 2.50 AXISYMMETRIC INLET WITH 40-PERCENT INTERNAL CONTRACTION	May 1973
	6. Performing Organization Code
7. Author(s)	8. Performing Organization Report No.
Bobby W. Sanders and Glenn A. Mitchell	E-7240
	10. Work Unit No.
9. Performing Organization Name and Address	501-24
Lewis Research Center National Aeronautics and Space Administration Cleveland, Ohio 44135	11. Contract or Grant No.
	13. Type of Report and Period Covered
12. Sponsoring Agency Name and Address	Technical Memorandum
National Aeronautics and Space Administration Washington, D.C. 20546	14. Sponsoring Agency Code

15. Supplementary Notes

16. Abstract

The results of an experimental investigation to increase the stable airflow range of a supersonic mixed-compression inlet are presented. Various throat-bypass bleeds were located on the inlet cowl. The bleed types were distributed porous normal holes, a forward-slanted slot, or distributed educated slots. Large inlet stability margins were obtained with the inlet throat bleed systems if a constant pressure was maintained in the throat-bypass bleed plenum. Stability limits were determined for steady-state and limited transient internal airflow changes. Limited unstart angle-of-attack data are presented.

17. Key Words (Suggested by Author(s))	18. Distribution Statement
Air intakes; Supersonic-cruise inlets; Shock stability; Inlet bleed; Throat-bypass bleed	Unclassified - unlimited

19. Security Classif. (of this report)	20. Security Classif. (of this page)	21. No. of Pages	22. Price*
Unclassified	Unclassified	87	$3.00

* For sale by the National Technical Information Service, Springfield, Virginia 22151

THROAT-BYPASS BLEED SYSTEMS FOR INCREASING THE STABLE AIRFLOW RANGE OF A MACH 2.50 AXISYMMETRIC INLET WITH 40-PERCENT INTERNAL CONTRACTION

by Bobby W. Sanders and Glenn A. Mitchell

Lewis Research Center

SUMMARY

An experimental investigation was conducted to evaluate the effectiveness of various types of inlet throat-bypass bleed in providing an increased inlet stable airflow range. The inlet used in the investigation was an axisymmetric, bicone, mixed-compression type with 40 percent of the supersonic area contraction occurring internally at the design Mach number of 2.50. Data were obtained at this design Mach number for distributed porous, forward-slanted-slot, and distributed educated-slot bleed types. A porous boundary-layer bleed arrangement was located on the centerbody in order to achieve high performance during normal operation.

With the inlet operating at a high-performance condition, each of the throat-bypass bleed types provided a large stability range prior to inlet unstart. In terms of inlet diffuser-exit-corrected airflow, each of the bleed types provided a reduction in corrected airflow prior to unstart (stability range) of 20 percent or greater if a constant pressure was maintained in the stability bleed plenum from the initial condition to inlet unstart. Unstart angle-of-attack tolerance for most of the bleed configurations tested was equal to or greater than 4.5°. The maximum unstart angle-of-attack obtained was 7.6°. Data show that the angle-of-attack tolerance of the inlet was increased by locating all centerbody bleed upstream of the throat and distributing the cowl bleed over a large axial length in the inlet throat region.

INTRODUCTION

The function of a supersonic inlet is to supply the airflow required by an engine at the highest possible pressure level while maintaining minimum drag. To minimize inlet cowl drag for sustained flight at speeds above Mach 2.0, it becomes essential that some

portion of the supersonic area contraction be accomplished internally. An inlet of this type is commonly referred to as a mixed-compression inlet. For mixed-compression inlets, optimum internal performance is provided by maintaining the terminal shock at the inlet throat. This operation provides high pressure recovery and minimizes distortion at the engine face. These inlets, however, have a discontinuous airflow characteristic known as unstart. If an airflow transient causes the terminal shock to move upstream of the throat, the shock is unstable and is abruptly expelled ahead of the cowling. This shock expulsion or unstart causes a sharp reduction in mass flow and pressure recovery and a large drag increase. Inlet buzz, compressor stall, and/or combustor blowout may also occur. Obviously, an inlet unstart is extremely undesirable because of the adverse effects not only on the propulsion system itself, but also on the aerodynamic qualities of the aircraft. If inlet unstart does occur, complex mechanical variations to alter the inlet geometry are required to re-establish initial design operating conditions.

Both external airflow transients such as atmospheric turbulence and internal airflow changes such as a reduction in engine airflow demand can cause the inlet to unstart. For an internal airflow change, the inlet should provide a margin in corrected airflow below the value for optimum performance without incurring unstart. This margin is defined as the stable airflow range. Conventional mixed-compression inlets may be designed to have a limited stable range that is provided by the capacity of the performance bleed system to spill increased airflow as the terminal shock moves upstream in the throat region. With performance bleed exit areas that are fixed, this stable range may not be adequate to absorb many of the airflow transients that are encountered by a supersonic propulsion system. An increased stable airflow range is currently provided for these inlets by operating them supercritically with a resultant loss in performance. Since any loss in inlet efficiency is reflected directly as a loss in thrust of the propulsion system, supercritical operation is undesirable.

To provide the necessary inlet stability without compromising steady-state performance, the inlet can be designed to allow the throat bleed to function as a throat bypass. This system prevents unstart by allowing the throat bleed to compensate naturally for changes in diffuser exit airflow demand. References 1 and 2 have shown that large increases in bleed may be provided as the inlet operation proceeds from supercritical to minimum stable conditions, without prohibitive amounts of bleed during normal operation, if the bleed exit area can be controlled to maintain a near-constant pressure in the throat-bypass bleed plenum. This exit-area variation might be provided either by an active control that senses shock position and regulates the bleed exit area or by high-speed valves that react to bleed plenum pressure changes that occur when the terminal shock changes position. Experimental results that are presented in references 2 and 3 show that high-speed valves can operate automatically to provide large stable margins.

An inlet test program was undertaken in the Lewis 10- by 10-Foot Supersonic Wind Tunnel to evaluate the effectiveness of several different types of such stability bleed

systems. This investigation was conducted with a Mach 2.5 mixed-compression inlet having 40 percent of the design supersonic area contraction occurring internally. Throat-bypass bleed airflow was removed through either distributed porous holes, distributed educated slots, or a forward-slanted slot. The open cowl bleed areas were designed to remove approximately 20 percent of the inlet capture airflow during minimum stable operation if a near-constant bleed plenum pressure was maintained.

Some selected results of this test program are reported in reference 2. Steady-state and transient inlet stability limits for several different types of throat-bypass-bleed and bleed-exit-area controls were included. The data presented herein are for variable-choked-exit bleed plugs that were manually positioned. These plugs were utilized to backpressure the various types of stability bleed systems and to determine the requirements of possible self-acting or automatic valve bleed-exit controls. Inlet stability limits were determined for steady-state and limited internal airflow transients. Limited unstart angle-of-attack data are also presented. These data were obtained at a free-stream Mach number of 2.50 and a Reynolds number, based on the cowl-lip diameter, of 3.88×10^6.

U. S. customary units were used in the design of the test model and for recording and computing of the experimental data. These units were converted to the International System of units (SI) for presentation in this report.

APPARATUS AND PROCEDURE

Inlet Model

The inlet used in this investigation was a Mach 2.50 axisymmetric, mixed-compression type with 40 percent of the design supersonic area contraction occurring internally. Figure 1 shows the test model installed in the wind tunnel test section. The inlet was attached to a cylindrical nacelle 0.635 meter in diameter in which a J85-GE-13 engine or a cold pipe, choked-exit plug assembly could be installed. At the design Mach number, sizing of the inlet to match the airflow requirements of the J85-GE-13 resulted in an inlet capture diameter of 47.32 centimeter. For this study, only the coldpipe was used. The model incorporated a translating centerbody to effect inlet start. A flight version of this inlet with 40-percent internal contraction would require a collapsing centerbody for starting and off-design operation (ref. 3).

Some of the basic inlet design details are presented in figure 2. Local theoretical airflow conditions on the cowl and centerbody, inlet contours, and diffuser area variation are shown for the inlet design Mach number and spike position. Initial supersonic compression was accomplished by a two-cone surface, 10° and 18.5°. The internal oblique

shock from the cowl lip was canceled at its impingement point on the centerbody by a turn in the centerbody surface. The remaining supersonic compression was accomplished isentropically to obtain an average theoretical supersonic throat Mach number of 1.30 with an average recovery of 0.9855. At design centerbody position, the geometric throat was located at $x/R_c = 3.26$. A computer program which incorporated the method of characteristics was used to design the supersonic portion of the inlet diffuser (ref. 4). Downstream of the geometric throat, the inlet included a 1^o equivalent conical expansion throat region and a main subsonic diffuser which included an overboard bypass system. A more complete discussion of the inlet design characteristics is presented in reference 5. Internal surface coordinates of the inlet in terms of the cowl-lip radius are presented in table I.

Inlet details are shown in figure 3. Bleed was located in the throat region on the cowl and centerbody surfaces. Throat-bypass bleed was removed through the cowl surface only. An isometric sketch that shows the ducting of cowl bleeds is presented in figure 4. Throat-bypass bleed was ducted through the cowling to two coldpipes with choked plugs, one on either side of the nacelle. Centerbody bleed was ducted through hollow support struts to exit plugs. Remotely actuated plugs that were used to vary the main duct and bleed airflows are shown in figure 1(b).

The subsonic portion of the inlet diffuser incorporated two remotely controlled bypass systems: a high-response sliding-louver overboard system, and a low-speed ejector bypass for engine and nozzle cooling airflow. For steady-state data, the bypasses were closed. However, there was a small amount of leakage airflow through these systems. Cascades were installed in the entrance to the bypass cavity during a previous test program to eliminate a resonant condition. A discussion of this resonance that resulted from the open cavity is presented in reference 6. Vortex generators were installed on the centerbody at inlet station 3 (fig. 3). Details of the vortex generator design are shown in figure 5. These vortex generators were one-half of a NACA-0012 airfoil with the mean camber line of the airfoil as the parting line. The leading edge was rounded.

Photographs and sketches of the test model that have been presented thus far have shown a rather bulky external profile. Since major variations were made in the cowl bleed and bleed ducting during the investigation, a bulky cowl was used to accommodate model changes and hence was not representative of flight-type hardware. Low external cowl drag is essential for a supersonic inlet; therefore, a sketch that shows a possible arrangement of a stability bleed system in an inlet for flight is presented in figure 6.

Inlet Bleed

The various bleed configurations that were investigated are shown in figures 7 to 9: distributed porous holes (fig. 7), a forward-slanted slot (fig. 8), and distributed educated slots (fig. 9). The design of these bleeds was for the most part based on bleed characteristic information contained in references 7 to 9. These bleed characteristics and the test data that are reported in references 1 and 5 were used to determine the location and amount of open bleed area for each of the different bleed types that would provide the desired amount of throat-bypass airflow. Each of the types of throat-bypass bleed was designed to provide a bleed mass-flow ratio of about 0.20 at the inlet minimum stable condition. Open bleed for the distributed porous throat bypass was increased to extend over the same axial cowl region as the educated stability bleed. This open bleed area gave the distributed porous bleed a capacity for a bleed mass-flow ratio of about 0.30.

Centerbody performance bleed variations are presented with the porous throat-bypass configurations in figure 7. Centerbody bleed pattern C was used for most of the porous cowl bleed configurations and for all forward-slanted slot and educated bleed configurations. All the porous bleed regions in figure 7, cowl and centerbody, were composed of circumferential rows of holes. Holes in adjacent rows were staggered for a more uniform open-area distribution. These holes were 0.3175 centimeter (0.125 in.) in diameter and were drilled normal to the local inlet surface. They were located on 0.4763-centimeter (0.1875-in.) centers to obtain a nominal porosity of 40 percent. Nominal thickness of the metal in the bleed regions was equal to the bleed hole diameter.

As shown in figure 7, the porous pattern and amount of open bleed were varied by filling selected holes. A pictorial representation of the forward-cowl bleed region with part of the holes filled is shown. As indicated for the distributed porous configurations, several bleed patterns for each of the bleed regions were studied. The first configurations (NA, NB, and NC) were tested to obtain a centerbody bleed geometry that was consistent with an acceptable on-design inlet performance and compatible with throat-bypass bleed systems for inlet shock stability. The intent was not to optimize the centerbody bleed for performance, but only to obtain a configuration that provided terminal shock stability ahead of the throat. The remainder of the porous configurations were tested so that the amount and extent of throat-bypass bleed, as well as variations of forward- and aft-cowl bleed, could be studied. As indicated, porous throat-bypass bleed was located upstream (15 bleed rows) and downstream (8 bleed rows) of the geometric throat. Bleed variations were as follows: all bleed open, upstream bleed open, and equal amounts of open bleed upstream and downstream of the geometric throat. All configurations in figure 7 had only porous bleed except configuration NG, which included a small slot for the aft-cowl bleed. Throat-bypass and aft-cowl bleed exhausted into a common plenum; therefore, the airflow from these two regions is presented in the data as throat-bypass bleed.

Forward-slanted-slot configurations are presented in figure 8. Two slot sizes are shown. These slots were flush with the local inlet surface and were slanted upstream with a 20° angle. The upstream corner was sharp and the downstream lip was nominally located at the geometric throat. Four lip shapes were investigated with the large slot: the basic sharp lip, a rounded lip, a lip relieved to obtain a 10° ramp angle with the local surface with a sharp leading edge, and a 10° relieved lip with a rounded leading edge. These large slots had a height of 1.363 centimeters. An insert was installed on the upstream surface of slot SA to obtain the small slot SS. Slot height of this small slot was 0.650 centimeter. Porous forward-cowl bleed was the same for all slot configurations. Alternate holes in three bleed rows were open. Aft-cowl bleed was sealed; therefore, it is not shown in figure 8. Centerbody configuration C (fig. 7) was used with all forward-slanted-slot configurations.

Educated throat-bypass bleed, figure 9, was an approximation of the ideal rearward-slanted-hole concept. Educated bleeds are designed to limit the amount of bleed through the perforations when the flow approaching the perforation is supersonic and to permit a large amount of bleed when the flow approaching the perforations is subsonic. Because of the difficulty of drilling slanted holes in the cowl surface, circumferential slots rather than holes were used. In order to educate these slots, the downstream edge was relieved to obtain a 10° angle with the local surface. Slot width was 0.318 centimeter with 1.27 centimeters between slots. This provides an equivalent local porosity of 25 percent. These slots covered the same local area of the cowl as the porous configurations of figure 7. Forward-cowl bleed that was also educated was ducted into the throat-bypass bleed plenum instead of overboard. Aft-cowl bleed was sealed. Centerbody configuration C (fig. 7) was used with all educated-bleed configurations.

Instrumentation

Static-pressure distributions along the top centerline of the cowl and centerbody were measured. Axial locations of the static-pressure instrumentation are presented in tables II and III. Bleed and subsonic diffuser total-pressure instrumentation are presented in figure 10. Forward-cowl bleed flow rate was determined from a measured total and static pressure (fig. 10(a)) and the measured exit area. Airflow from the cowl throat-bypass and centerbody bleeds was determined by coldpipe, choked-exit plug assemblies. Throat-bypass bleed total pressure was obtained from two total-pressure rakes that were located just downstream of the open bleed at $x/R_c = 4.051$. Pressures from these rakes were averaged to determine the throat-bypass bleed recovery. Centerbody and overboard bypass total pressures were measured by single tubes, as indicated in figure 10(a).

Total-pressure rakes that are shown in figure 10(b) were used to determine the local flow profiles in the subsonic diffuser. These rakes are also shown in figure 3. Overall inlet total-pressure recovery and distortion were determined from six, 10-tube, total-pressure rakes that were located at the diffuser exit, inlet station 5. Each rake consisted of six equal-area-weighted tubes with additional tubes added at each side of the extreme equal-area-weighted tubes in positions corresponding to an 18-tube area-weighted rake.

Forward-slanted slot pressure instrumentation is presented in figure 11. Slot rakes were circumferentially indexed to avoid interference effects. These rakes were located just upstream and downstream of the upstream shoulder of the slot, and in the slot passage. Static-pressure tubes on the upstream slot surface are also shown.

RESULTS AND DISCUSSION

This part of the report is presented in five sections. The first section is a discussion of the type of data plots that are used to present inlet stability data. The second, third, and fourth sections are a presentation of data that were obtained for the distributed porous, forward-slanted slot, and distributed educated-slot throat bypasses, respectively. The ability of the inlet to absorb transient internal airflow disturbances is presented in the fifth section.

Inlet Stability Data

The basic types of plots that are used in this report to present inlet shock stability data are illustrated in figure 12. Several performance conditions have been labeled for ease of data correlation.

Throat-bypass bleed characteristics are illustrated in figure 12(a). A series of straight lines (AB, CD, etc.) represent the bleed performance obtained for several, different, fixed, bleed-exit areas. Inlet performance is presented in figure 12(b) by a standard pressure-recovery - mass-flow plot. Note that each pressure-recovery - mass-flow curve is for a fixed bleed-exit area which corresponds to the straight lines (AB, CD, etc.) for figure 12(a). Each of these curves is generated by reducing the inlet diffuser-exit airflow from a supercritical value and causing the terminal shock to move upstream until unstart occurs. By utilizing this mode of operation, locii (dashed curves) of supercritical bleed airflows (ACEG) and minimum stable bleed airflows (BDFH) are obtained. The minimum airflows correspond to supercritical operation, and maximum airflows are obtained at minimum stable conditions. The supercritical and minimum stable airflow curves in figure 12(a) are similar to bleed characteristic data that are reported in

references 7 to 9. In these references the performance of different types of bleed is presented in the form of a flow coefficient as a function of bleed local recovery.

Airflow index (AI) for these inlet conditions is shown in figure 12(c). Values of airflow index represent the percentage change in corrected airflow between any inlet operating condition and the minimum recorded corrected airflow, point H. Figure 12(c) illustrates the amount of stable margin available if the bleed-exit area can be controlled from any inlet operating condition to unstart at point H. As indicated in figure 12(a), the maximum throat-bypass airflow is for point H. However, the fixed exit area that is required to obtain this maximum bleed rate also provides prohibitive amounts of supercritical bleed, point G. If the fixed bleed-exit area is reduced to obtain an acceptable supercritical bleed level (point C), the amount of bleed and consequently the stable margin at the minimum stable condition (point D) is also reduced. Similar results were reported in references 1 and 2. From an acceptable inlet operating condition at point C (i.e., acceptable high-recovery level and small amount of bleed), figure 12(c) shows that a relatively large airflow index can be obtained if the bleed-exit area can be varied to obtain inlet unstart at condition H. An exit-area control of this type is likely to be difficult to provide, since point H corresponds to a lower bleed plenum total pressure and since a negative pressure gradient on the bleed plenum is required with increasing exit area.

A more realistic exit-area control would be one that could perhaps provide a near-constant pressure in the throat-bypass bleed plenum from supercritical to minimum stable inlet conditions. An inlet stability index map such as illustrated in figure 12(d) can be generated based on a constant-pressure control. This constant-pressure stability index is a parameter that is similar to airflow index. The difference between the two indices is that, whenever a bleed exit control is specified (constant pressure in this case), the percentage change in corrected airflow will be defined as stability index. Each point in figure 12(d) represents the stability index available at that condition if it is assumed that the minimum stable condition is reached by the inlet along a line of constant bleed pressure (typical constant-pressure control in fig. 12(c)). The values of constant-pressure stability index are determined from figure 12(c) by using the equation:

$$SI_{cp} = 100\left(1 - \frac{100 - AI_{op}}{100 - AI_{min\ s,cp}}\right)$$

where AI_{op} is the airflow index at any inlet operating condition and $AI_{min\ s,cp}$ is the airflow index in figure 12(c) where a constant bleed pressure line from the operating point intersects the minimum stable curve BDFH. The stability index is not a simple difference of airflow indices. For airflow index AI, the operating point is referenced to the minimum corrected airflow (point H) to obtain the percentage change in corrected airflow. Stability index SI is the ratio of the difference in corrected airflow between the

operating point and the constant-pressure minimum stable point expressed as a percentage of the operating-point corrected airflow. The preceding equation accounts for the difference in reference (minimum stable) airflows between the stability and airflow indices. Inlet bleed conditions with bleed recoveries lower than the maximum bleed condition (point H) are referenced to this condition to determine the stability index. Therefore, the constant-pressure stability index for the lower bleed recovery conditions in figure 12(d) are the same as airflow index in figure 12(c).

To obtain a typical inlet performance plot and to allow comparison of different inlet configurations, figures 12(e) to (g) are shown. The constant-pressure stability index computed for each inlet operating condition is presented as a function of inlet total-pressure recovery in figure 12(e). A constant-pressure-stability-index curve (IJKL) as shown in figure 12(f) is obtained from figure 12(e) by selecting an inlet match total-pressure recovery as indicated by the dashed line. Figure 12(f) shows the amount of stability margin that is available when the inlet is operated at the selected match total-pressure recovery for various amounts of initial cowl bleed airflow. A typical inlet performance plot for point J from figure 12(f) is shown in figure 12(g). The supercritical inlet performance curve is determined up to the selected inlet recovery by the initial bleed airflow (point J) and the selected match inlet recovery. The constant-pressure stability index at point J represents the difference between two corrected airflow lines, one through the selected match condition $\left[(W\sqrt{\theta}/\delta)_{op}\right]$ and the other $\left[(W\sqrt{\theta}/\delta)_{min\ s}\right]$ intersecting the locus of minimum stable conditions on the inlet performance map (fig. 12(b)) at the corresponding minimum stable point. Inlet performance between the match condition and minimum stable operation is represented by a straight line since the true fairing is unknown.

Distributed Porous Throat Bypass

A comparison of the inlet performance for the distributed porous throat-bypass configurations is presented in figure 13. Data from which these curves were obtained are presented in figures 14 to 26. From these data a performance curve like the curve presented in figure 12(f) was obtained. These curves (fig. 13) were generated by selecting initial inlet-engine match conditions of 89-percent inlet total-pressure recovery and 2- to 3-percent inlet capture airflow for the total cowl bleed. Mass-flow ratio for the supercritical portion of the inlet performance curve up to the 89-percent recovery match condition is determined by the initial selected conditions. With these conditions, a constant-pressure stability index was obtained from plots like figure 12(e). This constant-pressure stability index represents two corrected airflow curves, one through the selected match condition and the other intersecting the locus of minimum stable conditions on the inlet performance map. This intersection point is represented in figure 13

by the left-most extent of the performance curve. A straight line was faired from the match condition, 89-percent recovery, to the minimum stable condition that was determined from the constant-pressure stability index.

No comparison curves for configurations NA and NB are shown in figure 13. Neither of these configurations provide an inlet recovery of 89 percent at the selected cowl bleed amount. The value of 89-percent recovery was selected for comparison purposes only, since most of the test configurations provided at least this performance level. Figure 13 shows that the largest values of stability index were provided by configurations NF, NG, and NH.

Test data for distributed porous configurations NA to NH are presented in figures 14 to 26. Figures 14 to 19, 21, and 23 present the basic data plots illustrated in figure 12 for each of the porous configurations. These figures also contain, in addition to the basic plots, the variation of inlet recovery with throat-bypass bleed, centerbody and forward-cowl bleed performance, and compressor face distortion. Figure 20 presents pressure distributions through the inlet and total pressures at the throat-exit, mid-diffuser, and diffuser-exit stations for various selected inlet conditions. Figures 24 to 26 show inlet static-pressure distributions for configurations ND, NE, and NF at initial conditions and at unstart angles of attack. The porous configurations are presented in the order in which they were tested for convenience of indicating the desirable and undesirable performance characteristics.

Performance for configuration NA is presented in figure 14. Figure 14(a) shows that large amounts of airflow can be removed through the throat-bypass stability bleed system at inlet minimum stable conditions for large bleed-exit areas. Mass-flow ratios greater than 0.20 were obtained. Of course, as previously indicated, a fixed exit that would allow these large airflows also provides a prohibitively large supercritical bleed mass-flow ratio of about 0.14. At constant bleed pressure, configuration NA provided a large increase in bleed mass-flow ratio from supercritical to minimum stable conditions (0.02 to 0.17 for a constant throat-bypass bleed recovery of 0.36). Although this stability mass-flow ratio increase of 0.15 was a rather large change in airflow, these large flow rates were obtained with a considerable loss in inlet total-pressure recovery at the minimum stable conditions (fig. 14(b)). Since stability index is a percentage change in corrected airflows which accounts for changes in inlet recovery as well as in mass flow, the drop in inlet total-pressure recovery at the minimum stable condition tends to reduce the apparent improvement in stability (fig. 14(c)). A more desirable configuration would provide higher inlet recovery levels at the maximum bleed, minimum stable conditions and, therefore, more inlet stability.

Maximum recovery for this configuration was slightly less than 0.89. At this inlet recovery the constant-pressure stability index was zero (minimum stable condition for zero throat-bypass bleed), as shown in figure 14(d). For configuration NA the initial inlet-engine match recovery must be reduced to a lower level before a sizable

constant-pressure stability index can be obtained (fig. 14(e)). For example, a reasonable level of constant-pressure stability index was obtained if the inlet recovery was reduced to obtain an initial total-pressure recovery of 0.855 at the no-stability bleed condition. At this condition the throat-bypass recovery was 0.39. If this bleed recovery level was held constant, an increase in bleed mass-flow ratio of about 0.10 from initial conditions to the unstart limit was obtained (fig. 14(a)). This provides a constant-pressure stability index of about 13.7 percent (figs. 14(d) and (e)). Throat-bypass mass-flow ratio as a function of inlet recovery is presented in figure 14(f). Centerbody and forward-cowl bleed performance are presented in figure 14(g). The curves in this figure indicate that both forward-cowl and centerbody bleed mass flows increased as the terminal shock was moved from supercritical (minimum bleed) to minimum stable (maximum bleed) conditions. The maximum values of bleed indicated by these data were not obtained for all minimum stable points. Inlet distortion for configuration NA is presented in figure 14(h). The centerbody bleed pattern used in this configuration was the same as the optimum centerbody bleed presented in reference 5.

Changing the centerbody bleed pattern of configuration NA to obtain configuration NB (fig. 7) improved inlet total-pressure recovery at the larger bleed minimum stable conditions, as shown in figure 15(b) by the open symbols. This increase in mimimum stable inlet recovery was primarily the result of opening the mid-centerbody bleed region. Evidently, bleed in this region was more compatible with the throat-bypass bleed location on the cowl. Figure 15(a) shows a throat-bypass mass-flow ratio increase of about 0.15 from an initial mass-flow ratio of 0.027 if the bleed recovery was maintained at a constant level of 0.30. Therefore, this configuration, like configuration NA, could provide a reasonable increase in mass flow to the unstart limit if a constant plenum pressure was maintained. Even though configuration NB provided higher inlet recoveries than configuration NA, it did not provide the performance levels that were selected for comparison of configurations. The amount of bleed airflow required to provide 89-percent inlet recovery was larger than the selected level of 2- to 3-percent total cowl bleed for comparison. At an inlet recovery of 89 percent, the total-cowl-bleed mass-flow ratio for configuration NB was 0.046 (0.027 throat-bypass bleed and 0.019 forward-cowl bleed). At this inlet operating condition, the constant-pressure stability index was 12.5 percent (fig. 15(f)).

The performance that was obtained for increased centerbody bleed is presented by the solid symbols in figure 15(b). For supercritical conditions, the centerbody-bleed mass-flow ratio was increased from 0.023 to 0.031. Although a mass-flow ratio of 0.031 was slightly larger than the desired level of about 0.025 (ref. 5), data show a significant improvement in maximum bleed airflow and inlet recovery at minimum stable conditions (fig. 15(b)). The results of a basic performance study on this inlet are presented in reference 5. The increased centerbody bleed was provided by increasing the choked-exit area of the control plugs, which effectively reduced the bleed plenum

pressure. Analysis of the centerbody surface pressure at the forward bleed region and just inside the bleed plenum for the minimum stable conditions indicates possible bleed recirculation (ratio of centerbody surface to bleed plenum pressure less than 1.0) for the small-centerbody-bleed mass-flow ratio of 0.023 and no recirculation for the increased bleed. Centerbody bleed regions were not compartmented; therefore, bleed recirculation from the high-pressure (downstream) region to the lower pressure (upstream) region may have limited the most forward movement of the terminal shock for the smaller centerbody bleed amount by causing the inlet to unstart prematurely. Thus, the maximum capabilities of the throat-bypass system were not obtained.

Bleed recirculation resulted from a higher plenum pressure than the local surface pressure. Since this configuration (NB) had a large open unchoked bleed area on the centerbody, a high plenum pressure was necessary to maintain a nominal level of bleed airflow ($m_{cb}/m_0 = 0.025$) for supercritical operation. The data for configuration NB indicate that the desired level of centerbody bleed should be obtained at plenum pressures that do not cause recirculation. A desired level of bleed could be provided at a reduced plenum pressure if the amount of open bleed were reduced (unchoked bleed only). This was accomplished by sealing part of the mid-centerbody bleed of configuration NB to obtain configuration NC, as shown in figure 7.

Data for configuration NC are presented in figure 16. Both forward-cowl and throat-bypass bleeds, in addition to the centerbody bleed, were changed to obtain this configuration (fig. 7). Performance for configuration NC was similar to configuration NB. Both of these configurations provided higher inlet total-pressure recoveries at minimum bleed conditions than did configuration NA. Figure 16(b) shows an inlet total-pressure recovery larger than 0.89 at minimum bleed conditions. Figure 16(a) shows an increase of throat-bypass mass-flow ratio from supercritical to minimum stable conditions of only about 0.10 for constant bleed recovery. However, this configuration did provide a fair amount of stability at minimum bleed flow, as shown in figure 16(f). This figure shows a constant-pressure stability index of 8.1 and 9.3 percent for total-cowl-bleed mass-flow ratios of 0.02 and 0.03, respectively. The stability index of 9.3 percent was chosen for the inlet performance comparison that is presented in figure 13. For the supercritical condition, the centerbody-bleed mass-flow ratio was 0.026 (fig. 16(h)). This value was about equal to the nominal desired level of 0.025. Configuration NC had an acceptable centerbody bleed for the inlet stabilization study. This inlet configuration provided acceptable inlet performance at minimum bleed conditions and provided a reasonable stable range. The centerbody bleed pattern of configuration NC, with one minor exception for configuration NH, was used with all the remaining stability bleed systems.

Figure 17 presents the performance of configuration ND. This configuration had the same amount of open throat-bypass bleed as configuration NC. However, the open porous region was shifted downstream, as shown in figure 7. A more downstream position for the stability bleed resulted in large improvements in inlet performance. The

increased performance is evident from a comparison of figures 16(b) and 17(b). Configuration ND provided inlet performance equal to or greater than the initial design values of 20-percent throat-bypass mass flow at constant bleed recovery from supercritical to minimum stable conditions (fig. 17(a)). Configuration ND also provided a constant-pressure stability index of 20 percent for a high-inlet-recovery, low-bleed initial condition (fig. 17(f)). As shown in figure 17(f) a constant-pressure stability index of 22.6 percent was obtained from initial conditions of 89-percent inlet total-pressure recovery and a total-cowl-bleed mass-flow ratio of 0.02. These values were selected for the comparison of configurations in figure 13. For this condition the throat-bypass bleed recovery was 0.35. Diffuser-exit distortion was 12 percent (fig. 17(i)). Figure 17(e) shows that this configuration can provide a constant-pressure stability index greater than 10 percent at an initial inlet recovery of 91 percent. This high recovery, however, does require a larger amount of bleed airflow.

Unstart angles of attack of 4.96° and 7.6° were obtained from initial inlet conditions indicated in figure 17(b). The unstart angles of attack were obtained from the initial inlet conditions (fig. 17(b)) by increasing the model angle of attack until the angle just prior to inlet unstart was determined. For the 4.96° angle-of-attack tolerance, the stability bleed plugs were closed (sealed). Since the stability airflow was equal to zero for this condition (forward-cowl bleed only), the data should be similar to that obtained for the basic inlet model in reference 5. The basic inlet had only performance bleed on the cowl surface. However, this unstart angle of attack of 4.96° was larger than the maximum value of 3.9° that was presented in reference 5. The basic inlet that is presented in this reference only provided variations in forward- and aft-centerbody bleed. Mid-centerbody bleed as shown in figure 7 was not available in reference 5 but was incorporated in the design of the inlet stability systems. Therefore, the 1.06° increase in angle-of-attack tolerance was probably obtained by a change in centerbody bleed location. At the initial conditions for the unstart angle of attack of 7.6°, the throat-bypass performance was about 30-percent recovery at 0.025 bleed mass-flow ratio (fig. 17(a)). This bleed recovery of 0.30 was maintained at a constant level by varying the throat-bypass exit plugs as the model angle of attack was increased to inlet unstart. These data indicate that some amount of bleed airflow through the throat bypass can also provide a sizable improvement in angle-of-attack tolerance.

Sealing the aft-cowl bleed region of configuration ND to obtain configuration NE (fig. 7) only slightly changed the inlet performance. The performance of configuration NE is presented in figure 18. The slight change in performance is reflected in the comparison of these configurations in figure 13. As indicated in this figure for the same initial condition, configuration ND provided a constant-pressure stability index of 22.6 percent compared to 22 percent for configuration NE. Unstart angles of attack that were obtained for configuration NE are indicated at the initial conditions in figure 18(b). Unstart angles of attack that were obtained for zero throat-bypass airflow and constant

throat-bypass recovery, as indicated in figure 18(b), are the same as for configuration ND. Maintaining a fixed throat-bypass exit area to inlet unstart from the same initial conditions as used for the constant throat-bypass recovery unstart angle provided approximately the same unstart angle as the value obtained for the constant bleed recovery.

Configuration NF utilized the same throat-bypass bleed as configurations ND and NE. Forward- and aft-cowl bleed regions were sealed. This configuration (fig. 19) did provide an increased stability margin over configurations ND and NE when compared at an initial recovery of 0.89 and a total-cowl-bleed mass-flow ratio of 0.02. This comparison (fig. 13) shows that configuration NF provides a constant-pressure stability index of 28.4 percent, while the other two configurations (ND and NE) have about 22 percent. A comparison of figures 17(b), 18(b), and 19(b) indicates that the increased stable margin for configuration NF resulted primarily from increased inlet recovery at the maximum-bleed, minimum stable conditions. An initial inlet-engine match condition with the inlet total-pressure recovery of 0.89 was chosen for a comparison of stability range since most of the configurations provide this level of performance. However, configuration NF can provide a much higher performance level. This configuration at the cost of an additional supercritical-bleed mass-flow ratio of 0.007 can provide a constant-pressure stability index greater than 20 percent at an initial inlet recovery of more than 92 percent (fig. 19(e)).

An unstart angle of attack of 4.46° was obtained for configuration NF for both fixed-exit and constant-bleed recovery controls. Initial inlet conditions ($\alpha = 0^{\circ}$) are shown in figure 19(b). This unstart angle of 4.46° was about the same as the angle-of-attack tolerance of 4.96° that was obtained for configurations ND and NE at zero throat-bypass airflow conditions. For these unstart angles, ND and NE had a sealed throat-bypass bleed (plugs closed) and about 1.5-percent bleed through the forward cowl for boundary-layer removal (figs. 17(h) and 18(h)). Cowl boundary-layer control for configuration NF was provided by removing a small amount of bleed (about 2.5 percent) through the throat-bypass bleed region. Therefore, positioning the performance bleed upstream provided an improvement in angle of attack from 4.46° to 4.96°. Similar results were reported in references 3 and 10. In figures 17(b) and 18(b), it can be seen that 4.96° angle of attack was obtained with only forward-cowl bleed and no throat-bypass bleed (for right-most curve with throat-bypass bleed plugs closed). If the throat-bypass plugs were opened to allow about 0.02 supercritical mass-flow ratio, the maximum unstart angle of attack increased to 7.4°. This improvement, when compared to the 4.96° that was obtained with only forward-cowl bleed, was a function of removing airflow from a larger axial region on the cowl, as well as a function of additional bleed mass-flow ratio of 0.02 (0.015 to 0.035).

Figure 20 shows pressure distributions through the inlet and diffuser total-pressure profiles for configuration NF. One supercritical (86-percent inlet recovery) and several

minimum stable conditions are presented. These plots are typical of those that are obtained for the porous configurations.

Maximum throat-bypass airflow of all the configurations tested was provided by configuration NG (fig. 21(a)). A mass-flow ratio of 0.295 was obtained at a bleed recovery of 0.324. For this configuration, all the available stability bleed was open, and a small forward-slanted slot was installed at the aft-cowl bleed location. Figure 21(b) shows that high inlet recoveries were obtained for low-bleed conditions and for the minimum stable conditions. These high inlet recoveries help to provide large values of stability index. The dip in the unstart limit curve of figure 21(a) at about 0.03 bleed mass-flow ratio may be the result of cowl bleed recirculation which caused the inlet to unstart prematurely. Possible recirculation of the bleed airflow exists on the cowl when the open bleed is distributed over a rather large axial length. High local pressures that are obtained at the downstream part of the bleed when the terminal shock moves upstream (minimum stable conditions) can cause bleed to recirculate through the low-pressure, or upstream, part of the bleed region. Bleed recirculation pressure ratios for the distributed porous configurations are presented in figure 22. For this plot, the local cowl static pressure at the upstream edge of the open bleed was ratioed to the bleed plenum pressure (sketch) for each of the data points of the unstart limit curve. These pressure ratios are presented as a function of the minimum-stable-bleed mass flow. A pressure ratio less than 1.0 indicates the possibility of bleed recirculation. Figure 22 shows possible bleed recirculation for all the porous configurations except configuration NB at the lower throat-bypass mass-flow ratios. Therefore, the dip in the unstart limit curve of figure 21(a) for configuration NG may have been the result of bleed recirculation. These data only suggest this possibility and are not conclusive proof. For the large bleed mass flows, figure 22 shows that the possibility of bleed recirculation is reduced for configurations which had forward-cowl bleed - configurations NA to NE.

Configuration NG at the inlet performance comparison condition had a constant-pressure stability index of 30.4 percent with a total cowl bleed mass-flow ratio of 0.03 (fig. 21(f)). To obtain this stability index a constant throat-bypass recovery of 0.34 was required. Unstart angles of attack that are presented in figure 21(b) are much smaller than those for previous configurations. The initial inlet recovery for the unstart angle-of-attack data was about 3 percent larger than for previous unstart data. Therefore, a comparison of data cannot be made.

Configuration NH provided the largest constant-pressure stability index of the porous configurations. Data for this configuration are presented in figure 23. The limits of the throat-bypass bleed were not obtained because of a restriction in the bleed ducting for this configuration. This is evident in figure 23(a) because of the flat characteristic of the unstart limit curve. This curve does not include a drop in recovery for the largest mass-flow ratios that were obtained for previous configurations. If larger bleed ducting areas were available, this configuration would certainly have provided larger amounts of

throat-bypass airflow prior to inlet unstart. For example, if a constant throat-bypass recovery of 0.35 were maintained from supercritical to minimum stable conditions, an extension of the minimum stable curve in figure 23(a) indicates that mass-flow ratios larger than 0.30 may have been obtained if large exits were available. At the inlet comparison condition, figure 23(f) shows that configuration NH provided a constant-pressure stability index of 32 percent at 2-percent total-cowl-bleed mass flow.

Figure 23(b) shows that the unstart angles of attack for this configuration were 3.13° and 3.44°. A direct comparison of the unstart data with other porous configurations cannot be made because both cowl and centerbody bleed regions were varied, as shown in figure 7. However, based on the analysis of the effect of centerbody bleed location on unstart angle in the discussion of figure 17, it is suspected that the low unstart angles for configuration NH resulted from the sealed forward-centerbody bleed.

Pressure distributions on the leeward side of the cowl and centerbody for configurations ND, NE, and NF at unstart angles of attack are presented in figures 24, 25, and 26, respectively. For reference, pressures for the initial condition at 0° angle of attack are also presented in the figures. Unstart data for two initial values of throat-bypass bleed are shown in figure 24. As shown in figures 24(a) and (c) for configuration ND, the pressure distributions at angle of attack indicate that the airflow was compressed to pressures higher than sonic values on the cowl at an x/R_c of 3.0. Reference 10 indicates that this additional compression of the internal supersonic airflow on the leeward side of the inlet as a result of an angle-of-attack increase was the critical region where local choking caused the inlet to unstart. As the inlet angle of attack increases, the cowl-lip oblique shock angle increases as a result of the increased local surface angle relative to the local airflow. The result was an upstream movement of the shock impingement location on the centerbody surface. This shift of shock impingement location is evident in figure 24(b). At 0° angle of attack the shock impingement was at an x/R_c of 2.75, while at the unstart angle-of-attack condition an upstream position of $x/R_c = 2.6$ was obtained. On design, this cowl shock was canceled at its impingement point; however, at an angle-of-attack condition it would reflect back to the cowl surface. The additional compression results in regions where the pressures are higher than sonic values on the cowl surface. Further increases in angle of attack would unstart the inlet. Similar results are reported in references 3 and 10.

Unstart angle-of-attack pressure distributions for configuration NE are shown in figure 25. Data for a fixed-throat bypass bleed exit and a variable exit to maintain a near-constant bleed recovery are presented. These results are similar to those for configuration ND (fig. 24).

Pressure distributions in figure 26(a) for configuration NF at angle of attack do not show the local choking region on the cowl. A pressure rise is indicated at an x/R_c of about 3.0. However, a choking value that may result in an inlet unstart is not indicated. A shift in oblique-shock impingement point on the centerbody is indicated in figure 26(b).

The impingement point moved from an x/R_c of 2.75 to an x/R_c of 2.67. This upstream movement of the shock impingement on the centerbody was similar to the results that were obtained for configurations ND and NE, but a choking pressure did not occur on the cowl.

Inlet unstart can also result from an upstream movement of the terminal shock ahead of the inlet throat to a position in the supersonic diffuser where it is unstable as the angle of attack is increased. Normally, the terminal shock is farther upstream on the windward side of the inlet than on the leeward side at angle of attack (ref. 10). Figure 26 indicates that the terminal shock on the leeward side moved upstream of the initial $\alpha = 0^{\circ}$ condition when the inlet was moved to 4.46°. The terminal shock moved from an x/R_c of about 3.6 to 3.3, but the shock was still downstream of the geometric throat ($x/R_c = 3.26$). The terminal shock position on the windward side was unknown since pressure instrumentation was not installed on this side of the inlet. Although the probable cause of unstart at angle of attack for configuration NF was an upstream movement of the terminal shock on the windward side of the inlet, the cause of unstart cannot be verified from the available data. An extension of the unstart angle-of-attack data that are presented herein for configurations NE and NF is presented in reference 10.

Since the choice of an inlet configuration ultimately depends on its mission, a best configuration of those that have been presented cannot be selected. These configurations do, however, provide desirable characteristics that are required for a mixed-compression inlet. Configuration NE provided high inlet performance for match conditions while providing a large stable range and angle-of-attack tolerance. This configuration provided high throat-bypass bleed recovery levels at minimum stable conditions for the smaller fixed bleed exits. Higher bleed recoveries result in larger bleed airflows at the minimum stable condition for a given fixed exit. These high bleed recoveries can offer an increased inlet stable range if variable bleed exits such as vortex valves are used. Vortex valves have a relatively steep bleed-recovery - mass-flow characteristic; therefore, the vortex valve is able to exhaust more airflow at the higher bleed recoveries before inlet unstart. Bleed airflow characteristics of vortex valves are presented in references 2 and 11.

Configuration NF when compared to configuration NE had a smaller angle-of-attack tolerance but provided a larger stable range. Configuration NH provided the maximum stability margin but had a rather limited angle-of-attack tolerance when compared to configurations NE and NF. Of these three configurations, NF was chosen as the porous configuration for presentation in reference 2. These configurations (NF and NH) have the advantage of all the cowl bleed exhausting through the throat-bypass bleed region. Therefore, valves or the secondary airflow pumping of the exhaust nozzle may be used to control boundary-layer bleed removal as well as the stability airflow. Matching of inlet bleed to nozzle secondary airflow requirements is presented in reference 12.

Forward-Slanted Slot Throat Bypass

Data for the forward-slanted slot configurations are presented in figures 27 to 34. A comparison of the slot configurations for the same initial inlet engine match condition as was used for the comparison of the porous configurations is presented in figure 27. Figure 27 shows that each of the large-slot throat-bypass bleeds provided about the same constant-pressure stability index of 20 percent. For this comparison, the sharp-lipped configuration SA and rounded-lip configuration SB provided a slightly larger bleed mass flow at the minimum stable condition than configurations SC and SD. Configurations SC and SD obtained about the same stable range by providing a slightly higher inlet recovery at the minimum stable condition.

Figure 28 shows the performance that was obtained for configuration SA. This slot had a sharp lip which was flush with the cowl surface (fig. 8). The bleed characteristics that are presented in figure 28(a) are typical of those that were obtained for the slot configurations. These data indicate that significantly higher bleed recoveries for supercritical conditions can be achieved with the slot configuration than were obtained with a typical porous configuration (fig. 19(a)). High bleed recoveries are desirable because of the payload penalties that are associated with the overboard exhaust of low-energy airflows (ref. 13). Maximum throat-bypass mass-flow ratio was 0.19. By referring to figure 28(a), it is obvious that the slot configuration as for the porous configurations, when used with a constant throat-bypass pressure control, can provide a large increase in stability mass-flow range. The large gap in throat-bypass mass-flow ratios between about 0.05 and 0.15 was the result of selecting fixed-exit areas to define the throat-bypass and inlet performance and was not a result of inconsistent inlet performance.

Inlet performance for slot SA (fig. 28(b)) indicates that the increase in inlet recovery from an initial condition (match comparison condition) to inlet unstart was smaller than obtained with a porous throat bypass like configuration NF (fig. 19(b)). As indicated in the comparison of the slot configurations, all configurations provided a constant-pressure stability index of about 20 percent from the initial inlet condition. Figure 28(f) shows that configuration SA had a stability index of 19.6 percent at a total-cowl-bleed mass-flow ratio of 0.02. This mass-flow ratio includes a supercritical forward-cowl mass-flow ratio of 0.011 (fig. 28(h)) and a mass-flow ratio of 0.009 through the throat-bypass slot. Even though configuration SA had one-half the amount of open forward-cowl bleed of configuration ND, as shown in figure 7, the bleed mass-flow ratio was not reduced by one-half. Comparison of the minimum forward-cowl bleed in figures 28(h) and 17(h) shows that the reduction in open bleed area only reduced the bleed mass-flow ratio from 0.016 to 0.011. This indicates unchoked bleed holes since choked bleed does provide a linear function of bleed amount with open bleed area.

Unstart angles of attack are indicated at the initial inlet performance condition in figure 28(b). From this initial inlet performance, fixed-bleed exits provided an unstart

angle-of-attack tolerance of 4.77°. If a near-constant pressure was maintained in the throat-bypass bleed plenum from this same initial condition, the unstart angle increased to 6.6°. To provide a constant plenum pressure, the throat-bypass bleed plugs had to be opened as the inlet angle of attack was increased. Therefore, the increase in unstart angle from 4.77° to 6.6° was provided by an increase in the amount of throat-bypass bleed airflow as the inlet moved to the unstart angle.

Performance of configuration SB is presented in figure 29. This forward-slanted slot configuration included a rounded downstream lip, as shown in figure 8. The throat-bypass performance, inlet performance, stability index, and unstart angle of attack were approximately equal to those that were obtained for configuration SA.

Pressure distributions that were recorded for configuration SB at selected inlet conditions are presented in figures 30 and 31. These pressure distributions are typical for the forward-slanted slot configurations. Inlet surface static pressures, diffuser total-pressure profiles, slot rake total-pressure profiles, and slot surface static pressures are shown.

Pressure distributions for supercritical inlet conditions are presented in figure 30. Diffuser static-pressure distributions (figs. 30(a) and (b)) indicate that the terminal shock was downstream of the slot ($x/R_c = 3.26$) at an x/R_c of about 3.6 for the larger diffuser-exit mass flows (low throat-bypass airflow). For these conditions the gradual pressure rise indicates a shock train. However, the terminal shock was at the slot location for the smaller diffuser-exit mass flows. Even though the terminal shock was upstream for these conditions, the inlet recovery, as indicated in figures 30(a) and (b), was about the same.

Slot total-pressure distributions for the supercritical conditions are presented in figures 30(f) to (h). Figure 30(f) shows that the total-pressure profile for slot rake A did not vary for the different amounts of throat-bypass bleed for supercritical inlet operation. Total-pressure profiles for slot rake B in figure 30(g) indicate a separation region near the upstream slot surface. The depth of this separation at the rake station was about equal to the slot height at low throat-bypass mass flows but was equal to about 0.4 of the slot height at maximum throat-bypass mass flows. Reattachment of the airflow occurs upstream of slot rake C because the pressure profiles that are shown in figure 30(h) for this slot rake do not indicate separated airflow.

Slot static-pressure distributions in figure 30(i) indicate an expansion at the slot shoulder ($L/R_c = 0$). The largest pressure reduction occurs for the larger throat-bypass airflows (small diffuser-exit mass flows). From this initial expansion, the airflow compresses to a location just downstream of the slot lip station ($L/R_c = 0.169$). Downstream of this compression the pressure distributions are typical of those that are obtained by varying the backpressure on a diffuser or diverging nozzle. An increase in bleed-exit area which decreases the backpressure and allows larger throat-bypass mass flows

results in an increased expansion of the airflow to higher Mach numbers prior to the slot terminal-shock recompression.

Pressure distributions for configuration SB at minimum stable conditions are shown in figure 31. For comparison, a supercritical condition is also presented. Figure 31(a) indicates a pressure level above the supercritical values on the cowl surface at an x/R_c of 2.86, which was upstream of the geometric throat station of $x/R_c = 3.26$. An increase in surface pressure upstream of the throat was also obtained on the centerbody (fig. 31(b)). This indicates that the terminal shock moved upstream of the geometric throat for the minimum stable conditions. This higher local pressure in the region of the forward-cowl bleed results in a more effective bleed system. As a result of an increase in forward-cowl bleed mass flow from supercritical to minimum stable conditions, the boundary-layer height at rake A was reduced, as shown in figure 31(f). Figure 31(g) shows that the separation region at slot rake B was, also, present for the minimum stable conditions. No separation was evident for rake C (fig. 31(h)). Downstream of the slot upstream shoulder ($L/R_c = 0$), the pressure distributions in figure 31(i) for minimum stable conditions are similar to those that were obtained for the supercritical conditions. However, expansion around the shoulder was not as large. This figure also shows the increase in surface pressure upstream of the shoulder for the minimum stable conditions.

The performance of configuration SC is presented in figure 32. These data are similar to the data that were obtained for configurations SA and SB. The effect of relieving the downstream lip of a forward-slanted slot can be seen by comparing figures 28(a) and 32(a). Configuration SC (fig. 32(a)) with the downstream lip relieved as shown in figure 8 provided lower bleed recoveries for supercritical conditions than those that were obtained for configuration SA (fig. 28(a)).

The general trend of an inlet stability bleed system for a given exit area is that minimum bleed airflows are obtained for supercritical conditions and the bleed mass flow increases as the terminal shock is moved upstream to inlet unstart. Unlike this general trend, the larger exit areas for configuration SC (fig. 32(a)) provide a reduction and then an increase in throat-bypass mass flow as the terminal shock was moved from supercritical to minimum stable conditions. For example, figure 32(a) shows that the supercritical values of 0.12 mass-flow ratio at 0.36 bleed recovery reduces to 0.105 mass-flow ratio at 0.32 bleed recovery prior to increasing to 0.16 mass-flow ratio at 0.50 bleed recovery for the minimum stable condition. The effect of this decrease in throat-bypass mass flow can easily be seen in figure 32(b) as an increase in diffuser-exit mass flow when the inlet recovery was increased from about 0.85 to about 0.90.

Performance of configuration SD was similar to the other large-slot bleeds. Figure 33 shows the performance that was obtained for this configuration. Additional unstart angle-of-attack data were recorded for this configuration, as indicated in figure 33(b). Unstart angles were recorded for supercritical, critical, and minimum stable conditions. At the supercritical condition of about 86-percent inlet recovery, a fixed

exit area and constant recovery for the throat-bypass bleed provided about the same unstart angle of 6.7°. A constant throat-bypass recovery at initial inlet conditions of about 90-percent recovery also provided this same angle, while an angle of 5.47° was obtained for a fixed, throat-bypass, bleed exit area. An unstart angle of 1.44° was recorded for both types of bleed-exit control at the minimum stable condition. The small variation in unstart angles for the initial condition of about 90-percent inlet recovery with a fixed bleed-exit area for the slot configurations was the result of a slight change in inlet recovery. A comparison of the initial condition for unstart angle-of-attack data in figures 28(b), 29(b), 32(b), and 33(b) shows that, as the inlet recovery for the initial conditions was reduced, the unstart angle changes from 4.59° to 5.63°.

Pressure distributions on the leeward side of the cowl and centerbody for configuration SB at unstart angle of attack are presented in figure 34, along with data for slot rake A. This configuration was selected as being typical of the large-slot configurations. For reference, pressures for the initial 0° condition are also presented. These pressure distributions are similar to those that were presented for the porous bleeds in figures 24 to 26. Local sonic pressures occur on the cowl at an x/R_c of about 3.0 for the unstart angles. Data for slot rake A (fig. 34(c)) indicate an improved boundary layer on the top, or leeward side, of the inlet for the unstart angle-of-attack conditions. This improved boundary layer indicates that the forward-cowl bleed was more effective in the region of higher (sonic) pressures on the cowl. More effective bleed would tend to relieve the local choking for angle-of-attack operation; therefore, without forward-cowl bleed the inlet would be expected to unstart at a lower angle of attack. These expectations were substantiated by the previously presented angle-of-attack results of configurations ND, NE, and NF.

Performance for the small-slot configuration SS is presented in figure 35. Slot height for this configuration was about one-half the height of the large-slot configurations. The largest minimum stable bleed recovery of all configurations tested was obtained with this configuration. Figure 35(a) shows that a throat-bypass recovery of 0.64 was obtained at minimum stable conditions. The lowest supercritical throat-bypass recovery of all the forward-slanted slot configurations was obtained for the configuration at the small bleed-exit areas. A configuration like SS, which has low bleed recovery at supercritical conditions and high bleed recovery at minimum stable conditions, is desirable if vortex valves are to be used as the bleed-exit control. Except for slot size, this configuration was identical to configuration SA. A comparison of figures 35 and 28 shows the result of decreasing the slot size. Configuration SS as shown in figure 35(b) provided high inlet recovery for low-bleed conditions. At an inlet recovery of 0.89 a constant-pressure stability index of 13.8 percent was obtained. Total-supercritical-cowl-bleed mass-flow ratio for this condition was 0.011.

Distributed Educated-Slot Throat Bypass

Comparison of educated bleed configurations in figure 36 shows that both configurations EA (no forward stability bleed) and EB (with forward stability bleed) provided a large stability range. Of the two configurations, EA provided the larger constant-pressure stability index of 20 percent.

Performance data for the educated throat-bypass bleed systems are presented in figures 37 to 40. Typical inlet pressure distributions are shown in figure 38 and pressure distributions for angle-of-attack conditions are presented in figure 40.

These configurations, like the porous and large-slot bleeds, provided a large stability index if a constant bleed plenum pressure was maintained from supercritical to minimum stable conditions. When educating bleed, the desire is to reduce the flow coefficient relative to that of normal bleed geometries for supersonic local conditions without reducing the flow coefficient with local subsonic airflow. A comparison of the flow characteristics of the educated-slot (fig. 37(a)) and porous (fig. 19(a)) bleeds at supercritical conditions is valid since the open bleed areas for both configurations were approximately equal and the Mach number over the bleed region was about constant. Except near zero throat-bypass bleed, the educated bleed (fig. 37(a)) produced lower bleed plenum pressures than the porous normal hole bleed (fig. 19(a)), thus indicating a lower flow coefficient for the educated bleed. Since the extents of the open bleeds are different (figs. 7 and 9), comparison of bleed types at subsonic local conditions (minimum stable) cannot be made. Several factors invalidate this comparison. For example, premature inlet unstart may occur as a result of bleed recirculation because the open bleed was extended over too large a region on the cowl.

Figure 37(b) shows that the minimum stable inlet pressure recovery rise was similar to that of the better porous bleed configurations. Configuration EA provided a slightly higher unstart angle of attack than a similar porous configuration (NF) - 4.96° and 5.53° compared to 4.46°. Neither configuration had forward-cowl bleed. However, the throat-bypass bleed of configuration EA extended farther upstream than for configuration NF. This upstream bleed, as previously indicated, may have allowed the increased angle tolerance. Inlet pressure distributions for configuration EA are presented in figure 38.

Figure 39 shows the performance of configuration EB. This configuration yielded lower bleed recoveries at the smaller throat-bypass bleeds for minimum stable conditions (fig. 39(a)) than did configuration EA (fig. 37(a)). The unstart limit curve shown in figure 39(a) is similar to the results of configuration NG that are presented in figure 21(a). Upstream movement of the terminal shock over the bleed region may have resulted in bleed recirculation since the bleed region had been extended over a large axial distance on the cowl. Unstart angle-of-attack data were not obtained for this configuration.

Pressure distributions for unstart angles of attack that were recorded for configuration EA are shown in figure 40. This configuration did not have a region of local choking pressures on the forward cowl. As shown in figure 40(a), the pressure rise at an x/R_c of about 3.0 was similar to the results of configuration NF that are presented in figure 26(a). Configuration EA, like configuration NF, did not have forward-cowl bleed. Therefore, the cause of inlet unstart was probably the same for both configurations. Since a local choking pressure was not obtained on the leeward side of the cowl, unstart probably resulted because of too large an upstream movement of the terminal shock on the windward side of the inlet into an unstable region.

Transient Stability Index

The ability of the inlet utilizing throat-bypass stability bleed systems to absorb internal airflow transients was investigated. Unstart limits for inlet configuration NF when subjected to internal airflow transients are presented in figure 41. Data presented in this figure are for a small fixed exit area on the throat-bypass bleed. This exit was downstream of a small and large bleed plenum, as indicated in the figure. The small plenum included the bleed plenum from the open bleed to a station just downstream of the throat-bypass total-pressure instrumentation (fig. 10(a)). A small exit area was installed at this station for the small plenum data. The large bleed plenum included all the throat-bypass bleed ducting to the choked-exit plugs which were used as the exit area. Internal airflow disturbances were obtained with initial inlet conditions of 0.90 total-pressure recovery with about 0.02-mass-flow-ratio fixed bleed through the throat-bypass bleed system. These internal airflow disturbances were created by moving the overboard bypass doors toward a closed position. The single sine wave pulse used to reduce the overboard bypass airflow is shown in figure 41. Bypass door airflow was calibrated at steady-state conditions in terms of corrected airflow. At each frequency (fig. 41), the maximum door amplitude that the inlet would tolerate without unstarting was determined and converted by means of the calibration to a change in corrected airflow. This value was referenced to the total diffuser-exit airflow at the initial conditions to obtain the transient stability index that is presented in figure 41.

As shown in this figure, the smallest transient stability index values were obtained for a small bleed plenum volume. Basically, these data represent the capacity of a conventional inlet and coldpipe to absorb an internal airflow transient. For these data, the inlet was attached to a coldpipe-plug system which added 2.59 cubic meters to the 1.39 cubic meters of the inlet·subsonic diffuser and overboard-bypass system. Conventional inlets would normally have a small bleed plenum between the open boundary-layer bleed and the overboard exit. The change in transient stability index between small- and large-plenum data indicates the improved capability that can be provided by using a stability

bleed system connected to a fixed exit by means of a large plenum. Actually, if only a system that can absorb the higher frequency transients is required, a system such as the large plenum and the throat-bypass bleed can provide the capability of absorbing very large transients, above 50 percent of the engine corrected airflow for a transient with a frequency of 27 hertz (fig. 41). The capability of this system at low frequencies was rather limited; therefore, other systems in addition to the throat-bypass bleed and large plenum are required to provide a large tolerance to internal airflow disturbances for the entire frequency range. For example, the addition of an overboard bypass such as presented in reference 14 with only a moderate bypass frequency response to improve the lower frequency capability would allow a large capability at all frequencies. Another system is presented in reference 2. Data that are presented in this reference show that a throat-bypass bleed combined with self-acting pressure relief valves to regulate the bleed can also provide large values of transient stability index for all airflow transient frequencies. A stability airflow system which utilizes the exhaust nozzle pumping characteristics may also provide the capacity of absorbing large internal airflow changes, both steady state and transient. The secondary airflow pumping of an exhaust nozzle has a characteristic similar to the pressure relief valves of reference 2; therefore, the nozzle would provide a large steady-state and low-frequency transient stability index. Large values of transient stability index at high frequencies would be provided by the large bleed plenum between the inlet throat-bypass bleed and the exhaust nozzle.

CONCLUDING REMARKS

An experimental program was conducted to evaluate the effectiveness of various types of inlet throat bleed (or bypass) in providing an increased inlet stable airflow range. The inlet used in this investigation was an axisymmetric, bicone, mixed-compression type with 40 percent of the supersonic area contraction occurring internally at the design Mach number of 2.5. Data were obtained at the inlet design Mach number for distributed porous, forward-slanted-slot, and distributed educated-slot throat-bypass systems. The following results were obtained:

1. With an inlet operating at a high-performance condition, a large stable airflow range can be provided by maintaining a near-constant plenum pressure on an inlet throat-bypass bleed system.

2. Each of the types of bleed (distributed porous, forward-slanted slot, and distributed educated slot) provided a large inlet stability range.

3. Centerbody-bleed location is an important factor in the development of an inlet configuration that provides a large stable airflow range.

4. The largest stable airflow ranges were obtained for the distributed porous bleed configurations.

5. From an initial inlet operating condition of 89-percent recovery and a total-cowl-bleed mass-flow ratio of about 0.02 (total-inlet-bleed mass-flow ratio of about 0.046), each of the throat-bypass bleed types tested provided a bleed configuration with a constant-pressure stability index greater than 20 percent.

6. The angle-of-attack tolerance of this inlet can be increased by adding centerbody performance bleed at a position just upstream of the throat station.

7. Locating bleed forward on the cowl surface in the supersonic diffuser can provide an increase in angle-of-attack tolerance. Distributing the performance bleed over a large axial region on the cowl surface, with additional bleed airflow, can also provide a sizable increase in unstart angle-of-attack tolerance.

8. Most of the inlet configurations tested provided unstart angles of attack of about 4.5° or larger.

9. Maximum unstart angle-of-attack tolerance obtained was 7.6° with selected distributed porous bleed configurations.

10. The small-forward-slanted-slot configuration provided the lowest and highest bleed recovery at supercritical and minimum stable conditions, respectively.

11. The ability of an inlet to absorb internal airflow transients is significantly increased by incorporating a large bleed plenum between the open stability bleed and the bleed plenum exit.

Lewis Research Center,
National Aeronautics and Space Administration,
Cleveland, Ohio, January 17, 1973,
501-24.

APPENDIX - SYMBOLS

A	flow area, m^2
A_c	cowl-lip capture area, 0.1757 m^2
AI	airflow index, $AI = 100\left\{1 - \left[(W\sqrt{\theta}/\delta)_{min\ s}/(W\sqrt{\theta}/\delta)_{op}\right]_5\right\}$
D_5	inlet distortion, $D_5 = \left[(P_{max} - P_{min})/P_{av}\right]_5$
f	frequency
H	annulus or rake height at local diffuser station, cm
h	distance from inlet surface, cm
L	axial distance from upstream shoulder of slot throat-bypass bleeds, cm
M	Mach number
m/m_0	mass-flow ratio
P	total pressure, N/m^2
p	static pressure, N/m^2
R_c	inlet cowl-lip radius, 23.66 cm
r	radius, cm
SI_{cp}	constant-pressure stability index, $SI_{cp} = 100\left\{1 - \left[(W\sqrt{\theta}/\delta)_{cp,\,min\ s}/(W\sqrt{\theta}/\delta)_{op}\right]_5\right\}$
SI_t	transient stability index, $SI_t = 100\left\{1 - \left[(W\sqrt{\theta}/\delta)_{t,\,min\ s}/(W\sqrt{\theta}/\delta)_{op}\right]_5\right\}$
STA	station, cm
T	total temperature, K
W	weight flow rate, kg/sec
$W\sqrt{\theta}/\delta$	corrected airflow, kg/sec
x	axial location, cm
x/R_c	axial distance ratio, inlet radii
α	angle of attack, deg
δ	$P/(10.13\times10^4\ N/m^2)$
θ	T/288.2 K
θ_l	cowl-lip position parameter, $\tan^{-1}[1/(x/R_c)]$
φ	circumferential position, deg

Subscripts:

av	average
b	bleed
bp	bleed plenum
by	overboard bypass
cp	constant bleed pressure
ct	cowl total
gt	geometric throat
l	local
max	maximum
min	minimum
min s	minimum stable inlet operating point
op	inlet operating point
t	transient
tb	throat bypass
uns	unstart
0	free stream
5	diffuser-exit station

REFERENCES

1. Sanders, Bobby W.; and Cubbison, Robert W.: Effect of Bleed-System Back Pressure and Porous Area on the Performance of an Axisymmetric Mixed-Compression Inlet at Mach 2.50. NASA TM X-1710, 1968.

2. Sanders, Bobby W.; and Mitchell, Glenn A.: Increasing the Stable Operating Range of a Mach 2.5 Inlet. Paper 70-686, AIAA, June 1970.

3. Bowditch, David N.; Coltrin, Robert E.; Sanders, Bobby W.; Sorensen, Norman E.; and Wasserbauer, Joseph F.: Supersonic Cruise Inlets. Aircraft Propulsion. NASA SP-259, 1971, pp. 283-312.

4. Anderson, Bernhard H.: Design of Supersonic Inlets by a Computer Program Incorporating the Method of Characteristics. NASA TN D-4960, 1969.

5. Wasserbauer, Joseph F.; and Choby, David A.: Performance of a Bicone Inlet Designed for Mach 2.5 with Internal Distributed Compression and 40-Percent Internal Contraction. NASA TM X-2416, 1972.

6. Coltrin, Robert E.; and Calogeras, James E.: Supersonic Wind Tunnel Investigation of Inlet-Engine Compatibility. Paper 69-487, AIAA, June 1969.

7. McLafferty, George: A Stepwise Method for Designing Perforated Supersonic Diffusers. Rep. R-12133-5, United Aircraft Corp., Nov. 17, 1949.

8. McLafferty, George H.; and Ranard, E.: Pressure Losses and Flow Coefficients of Slanted Perforations Discharging from Within a Simulated Supersonic Inlet. Rep. R-0920-1, United Aircraft Corp., 1958.

9. McLafferty, George: A Study of Perforation Configurations for Supersonic Diffusers. Rep. R-53372-7, United Aircraft Corp., Dec. 1950.

10. Choby, David A.: Tolerance of Mach 2.50 Axisymmetric Mixed-Compression Inlets to Upstream Flow Variations. NASA TM X-2433, 1972.

11. Gebben, Vernon D.: High-Capacity Compact Vortex Valve for Increasing Stability of Supersonic Mixed-Compression Inlets. NASA TN D-6662, 1972.

12. Talbot, J. E.; and Furness, B.: A Fully Integrated Propulsion System for a Supersonic Transport Aircraft. Aerodynamics of Power Plant Installation, Part 2. AGARDograph 103, pt. 2, 1965, pp. 513-538.

13. Koenig, Robert W.: Inlet Sensitivity Study for a Supersonic Transport. NASA TN D-3881, 1967.

14. Crosby, Michael J.; Neiner, George H.; and Cole, Gary L.: Restart and High Response Terminal Shock Control for an Axisymmetric Mixed-Compression Inlet with 60-Percent Internal Contraction. NASA TM X-1792, 1969.

TABLE I. - INLET COORDINATES

(a) Centerbody

Axial distance from cone tip, x/R_c	Inlet cowl-lip radius ratio, r/R_c
0	0
10^o Conical section	
1.0323	.1820
18.5^o Conical section	
2.7620	.7608
2.800	.7696
2.850	.7794
2.900	.7874
2.950	.7937
3.000	.7986
3.050	.8025
3.100	.8045
3.150	.8043
3.200	.8030
3.250	.8015
3.300	.8000
3.350	.7982
3.400	.7964
3.450	.7944
3.500	.7925
3.550	.7906
3.600	.7886
3.650	.7862
3.700	.7834
3.750	.7798
3.800	.7757
3.850	.7711
3.900	.7655
3.950	.7590
4.000	.7513
4.050	.7426
4.100	.7330
4.150	.7230
4.200	.7133
4.250	.7036
4.300	.6924
4.350	.6810
4.400	.6692
4.450	.6577
4.500	.6455
4.550	.6330
4.600	.6205
4.650	.6085
4.700	.5960
4.750	.5825
4.800	.5700
4.850	.5573
4.900	0.5448
4.950	.5320
5.000	.5195
5.050	.5075
5.100	.4983
5.150	.4895
5.200	.4805
5.250	.4715
5.300	.4622
5.350	.4534
5.400	.4444
5.450	.4352
5.500	.4264
5.550	.4175
5.600	.4085
5.650	.3995
5.700	.3900
5.750	.3815
5.800	.3732
5.850	.3650
5.900	.3566
5.950	.3488
6.000	.3412
6.050	.3339
6.100	.3266
6.150	.3196
6.200	.3130
6.250	.3068
6.300	.2985
6.350	.2910
6.400	.2845
6.450	.2780
6.500	.2716
6.550	.2655
6.600	.2597
6.650	.2545
6.700	.2501
6.750	.2464
6.800	.2430
6.850	.2410
6.900	.2400
6.950	.2396
7.000	.2394
Cylinder	
7.8858	.2394

(b) Cowl

Axial distance from cone tip, x/R_c	Inlet cowl-lip radius ratio, r/R_c
2.1167	1.0000
2.150	1.0028
2.200	1.0070
2.250	1.0111
2.300	1.0154
2.350	1.0193
2.400	1.0228
2.450	1.0261
2.500	1.0290
2.550	1.0317
2.600	1.0340
2.650	1.0360
2.700	1.0373
2.750	1.0382
2.800	1.0386
2.850	1.0386
2.900	1.0381
2.950	1.0370
3.000	1.0356
3.050	1.0337
3.100	1.0320
3.150	1.0304
3.200	1.0290
3.250	1.0275
3.300	1.0262
3.350	1.0251
3.400	1.0239
3.450	1.0227
3.500	1.0215
3.550	1.0204
3.600	1.0192
3.650	1.0176
3.700	1.0160
3.750	1.0144
3.800	1.0124
3.850	1.0100
3.900	1.0071
3.950	1.0037
4.000	1.0000
4.050	.9955
4.100	.9908
4.150	.9858
4.200	.9808
4.250	.9756
4.300	.9702
4.350	.9659
4.400	.9595
4.450	0.9538
4.500	.9481
4.550	.9426
4.600	.9374
4.650	.9324
4.700	.9276
4.750	.9232
4.800	.9191
4.850	.9153
4.900	.9120
4.950	.9087
5.000	.9050
5.050	.9044
5.100	.9049
5.150	.9058
5.200	.9071
5.250	.9086
5.300	.9102
5.350	.9118
5.400	.9132
5.450	.9145
5.500	.9157
5.550	.9166
5.600	.9173
5.650	.9177
5.700	.9179
Cylinder	
6.1747	.9179
Bypass gap	
6.7847	.8868
6.800	.8865
6.850	.8855
6.900	.8846
6.950	.8837
7.000	.8823
7.050	.8805
7.100	.8785
7.150	.8760
7.200	.8734
7.250	.8707
7.300	.8677
7.350	.8654
7.400	.8639
7.450	.8631
7.500	.8627
7.550	.8623
7.600	.8621
Cylinder	
7.8858	.8621

TABLE II. COWL STATIC-PRESSURE TAP LOCATIONS

[Top centerline.]

(a) Distributed porous configuration	(b) Forward-slanted slot configuration	(c) Educated configuration
Axial distance from cone tip, x/R_c	Axial distance from cone tip, x/R_c	Axial distance from cone tip, x/R_c
2.684	2.684	2.684
2.807	2.807	2.807
2.859	2.859	2.838
2.894	2.894	2.892
2.930	2.930	2.945
2.964	2.964	2.999
2.999	2.999	3.053
3.038	3.038	3.106
3.066	3.069	3.160
3.101	3.311	3.213
3.136	3.343	3.267
3.170	3.390	3.321
3.205	3.434	3.375
3.240	3.489	3.434
3.275	3.639	3.489
3.310	3.677	3.639
3.345	3.779	3.677
3.380	3.950	3.779
3.434	4.192	3.950
3.489	4.519	4.192
3.639	4.847	4.519
3.677	5.202	4.847
3.779	5.529	5.202
3.950	6.119	5.529
4.192	6.742	6.119
4.519	7.311	6.742
4.847		7.311
5.202		
5.529		
6.119		
6.742		
7.311		

TABLE III. - CENTERBODY STATIC-

PRESSURE TAP LOCATIONS

[Top centerline.]

Axial distance from cone tip, x/R_c	Axial distance from cone tip, x/R_c
2.308	3.317
2.603	3.353
2.670	3.389
2.716	3.441
2.751	3.489
2.775	3.543
2.802	3.586
2.834	3.629
2.858	3.671
2.893	3.714
2.963	3.795
3.030	3.875
3.102	3.951
3.140	4.192
3.173	4.519
3.210	4.847
3.247	5.202
3.285	7.311

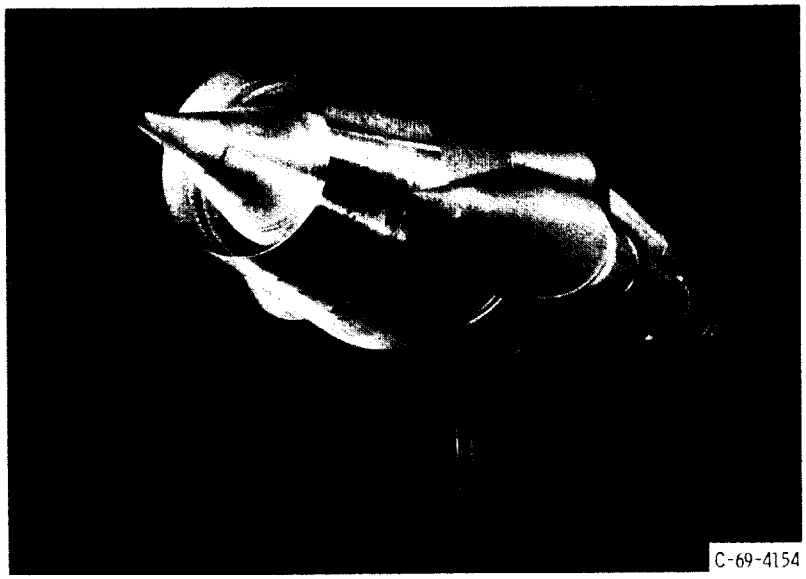

(a) Front view.

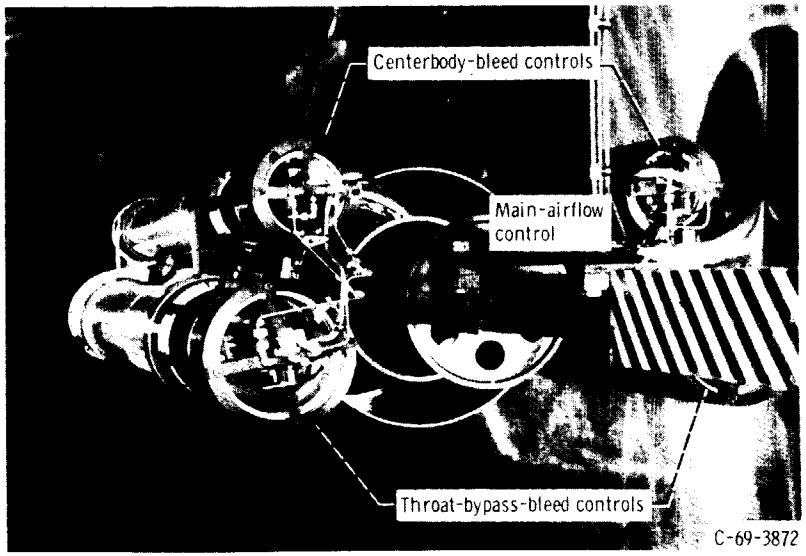

(b) Model installation showing choked-exit mass-flow throttling controls.

Figure 1. - Model installed in 10- by 10-Foot Supersonic Wind Tunnel.

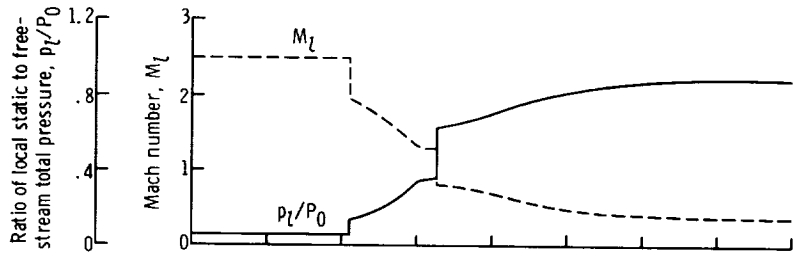

(a1) Cowl surface conditions.

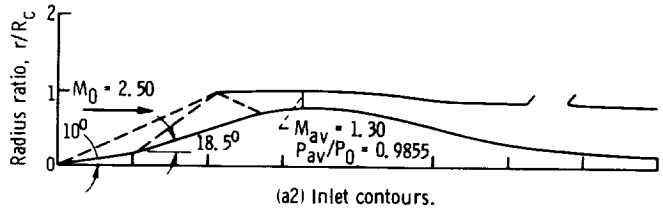

(a2) Inlet contours.

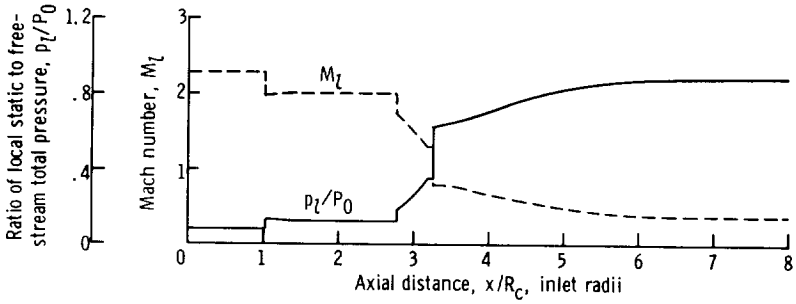

(a3) Centerbody surface conditions.

(a) Inlet dimensions and airflow conditions. Free-stream Mach number, $M_0 = 2.50$.

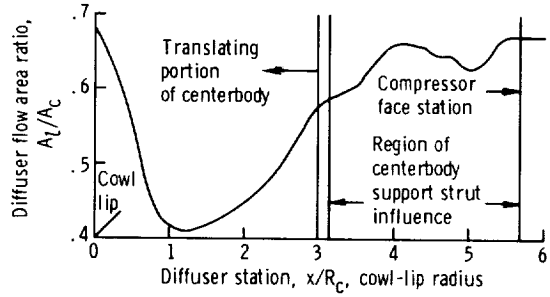

(b) Diffuser area variation.

Figure 2. - Aerodynamic details. Cowl-lip position parameter, $\theta_l = 25.27^0$.

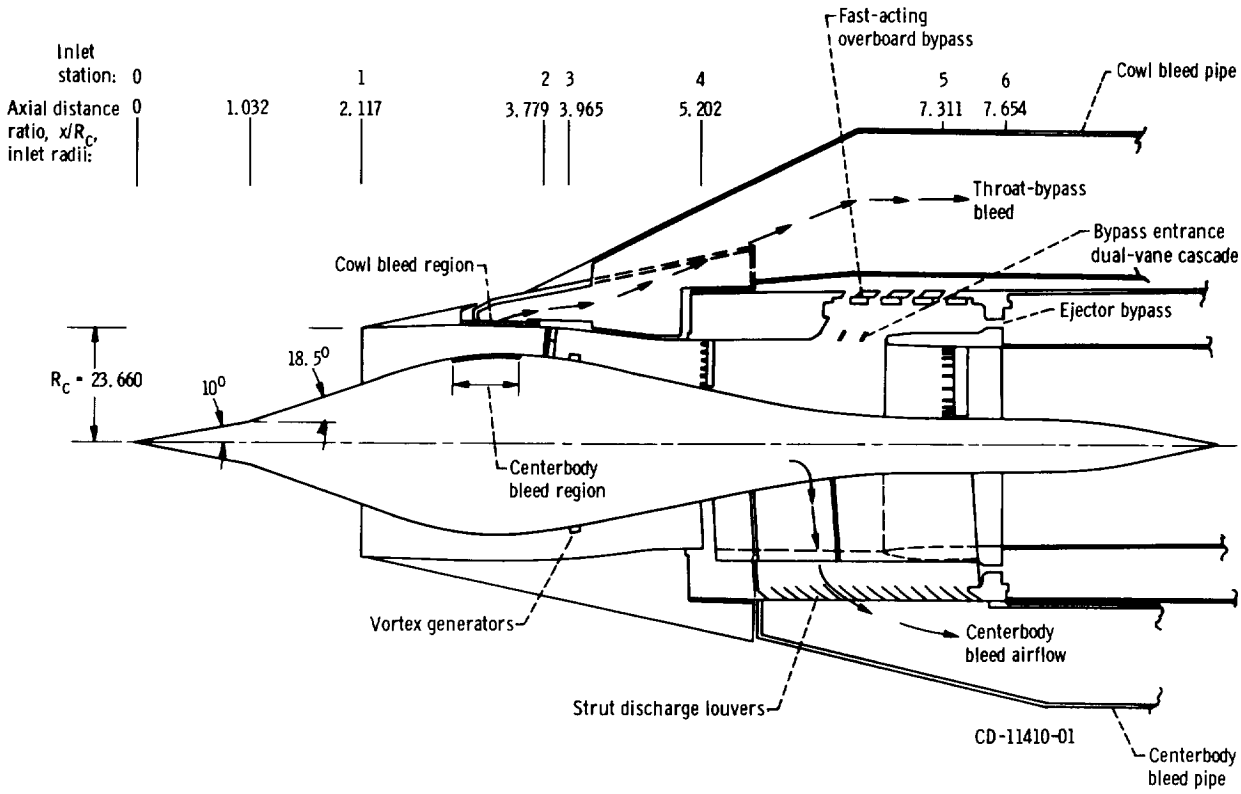

Figure 3. - Inlet details. Dimensions are in centimeters.

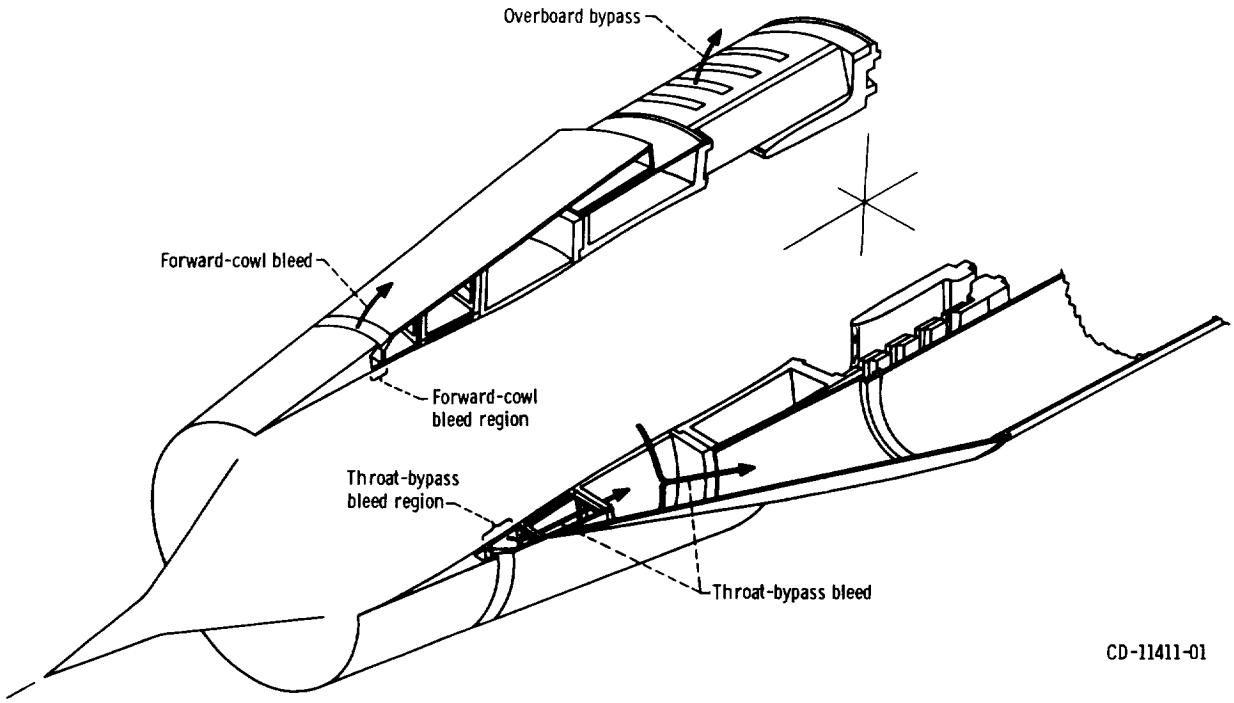

Figure 4. - Sketch of inlet cowl which shows bleed ducting.

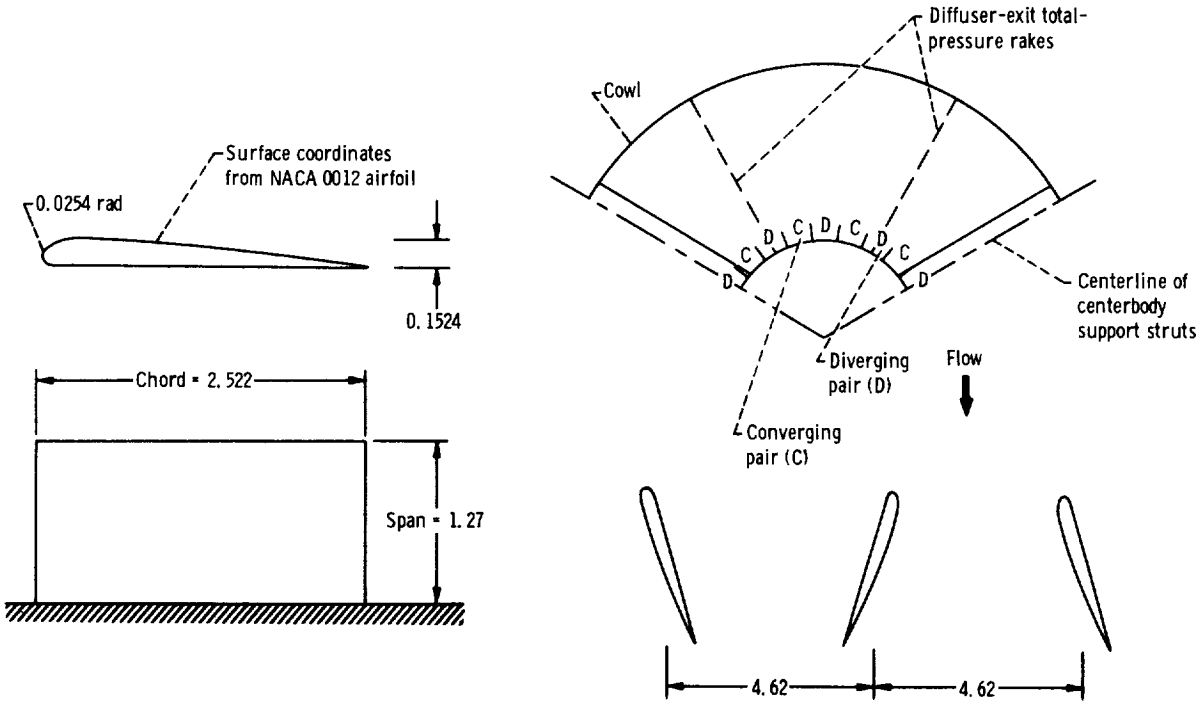

Figure 5. - Vortex generator design. Dimensions are in centimeters.

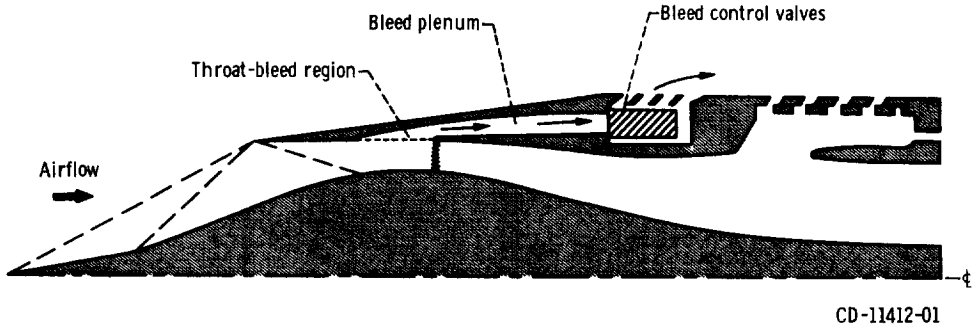

Figure 6. - Possible arrangement of a stability bleed system for a flight inlet.

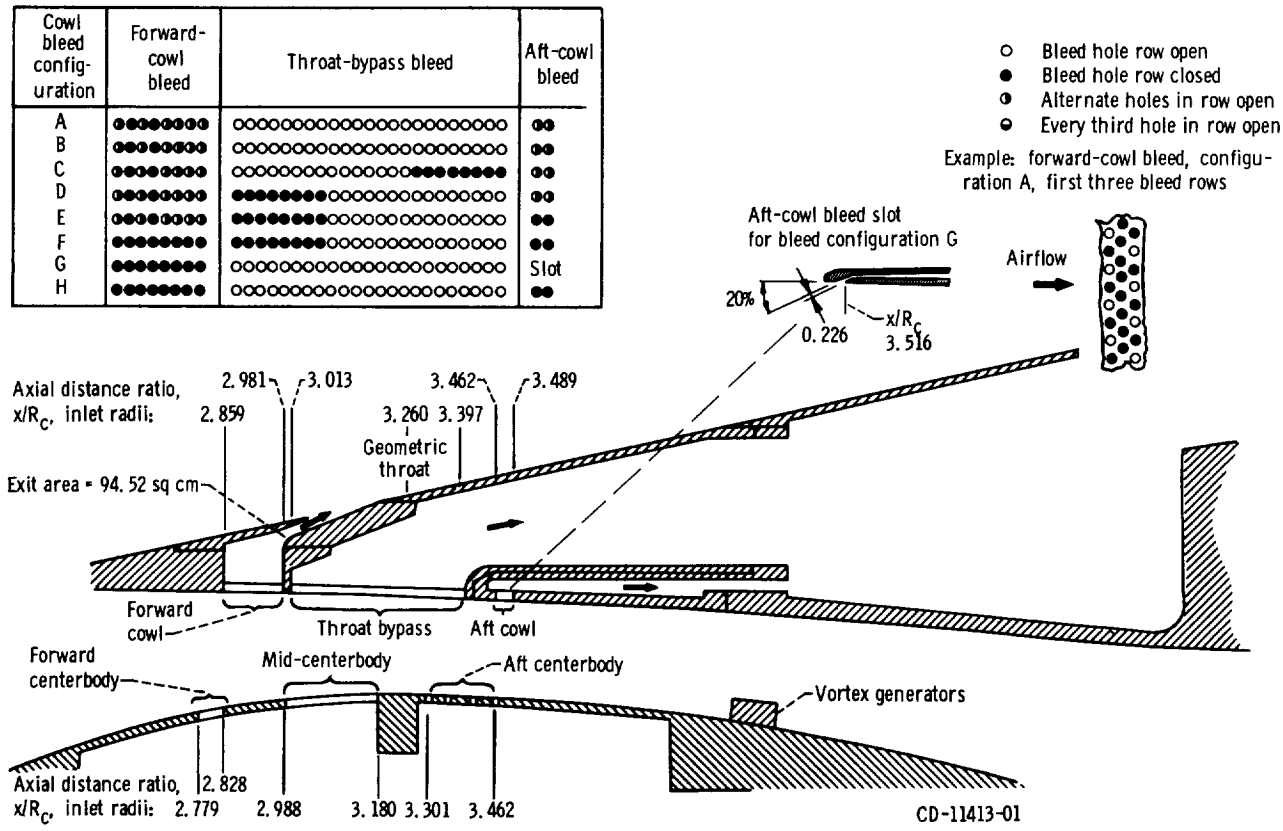

Centerbody-bleed configuration	Forward bleed	Midbody bleed	Aft bleed
A	●●●●	●●●●●●●●●●●●	●●●●
B	●●●●	○○○○○○○○○○○○	●●●●
C	●●●●	●●●●●●●●●●●●	●●●●
D	●●●●	●●●●●●●●●●●●	●●●●

Bleed configuration	Cowl-bleed configuration	Centerbody-bleed configuration
NA	A	A
NB	B	B
NC	C	C
ND	D	C
NE	E	C
NF	F	C
NG	G	C
NH	H	D

Figure 7. - Sketch of model which includes cowl distributed porous throat-bypass bleed system and centerbody performance bleed system. Dimensions are in centimeters.

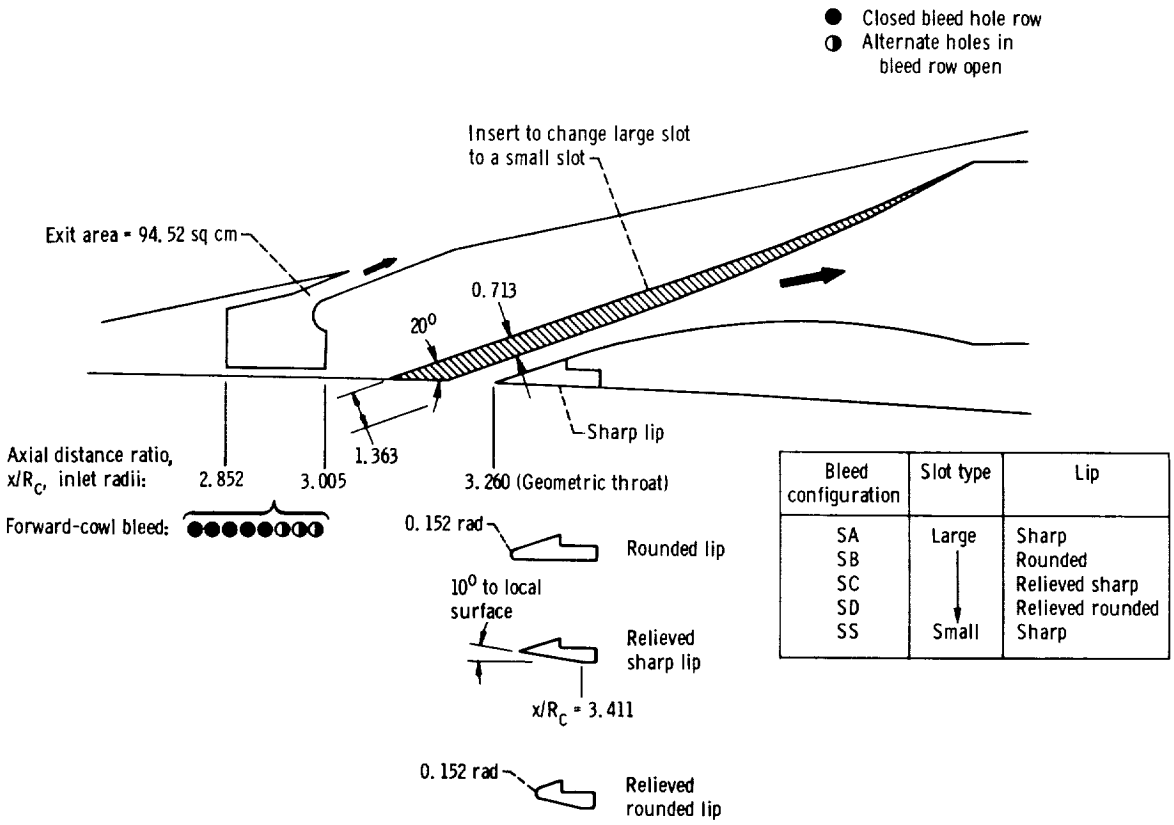

Figure 8. - Forward-slanted-slot throat bypass. Dimensions are in centimeters.

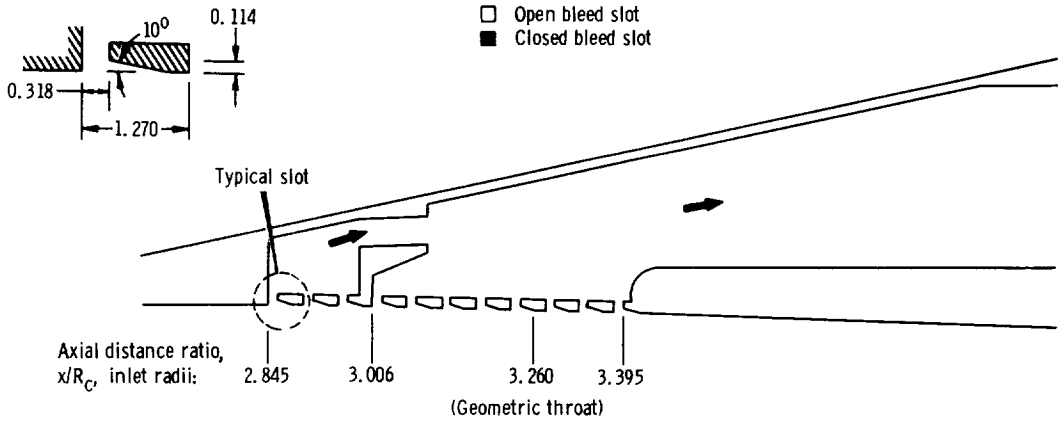

Bleed config-uration	Forward-cowl bleed	Throat-bypass bleed
EA	■ ■ ■	□ □ □ □ □ □ □ □
EB	□ □ □	□ □ □ □ □ □ □ □

Figure 9. - Distributed educated-throat bypass. Dimensions are in centimeters.

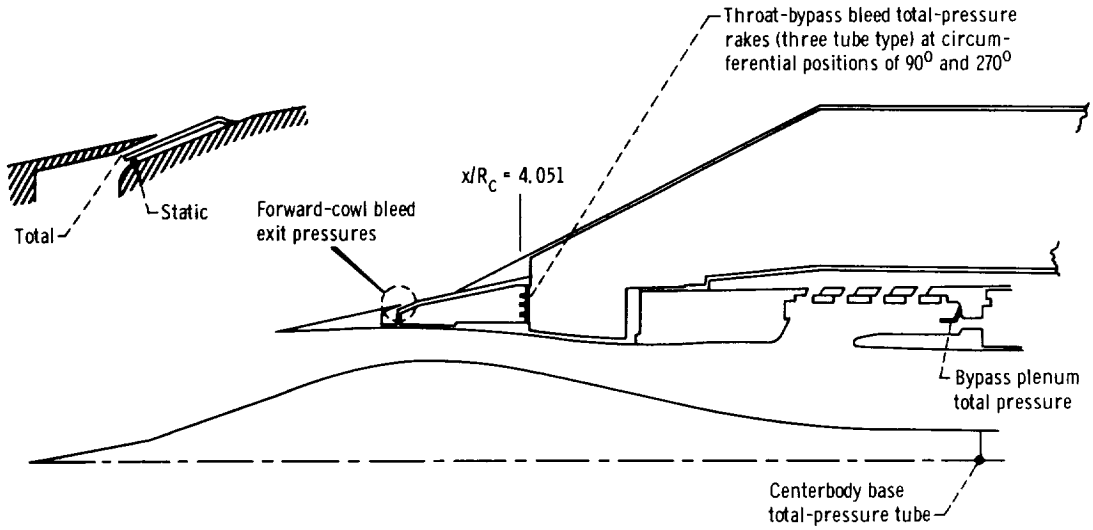

(a) Bleed pressures.

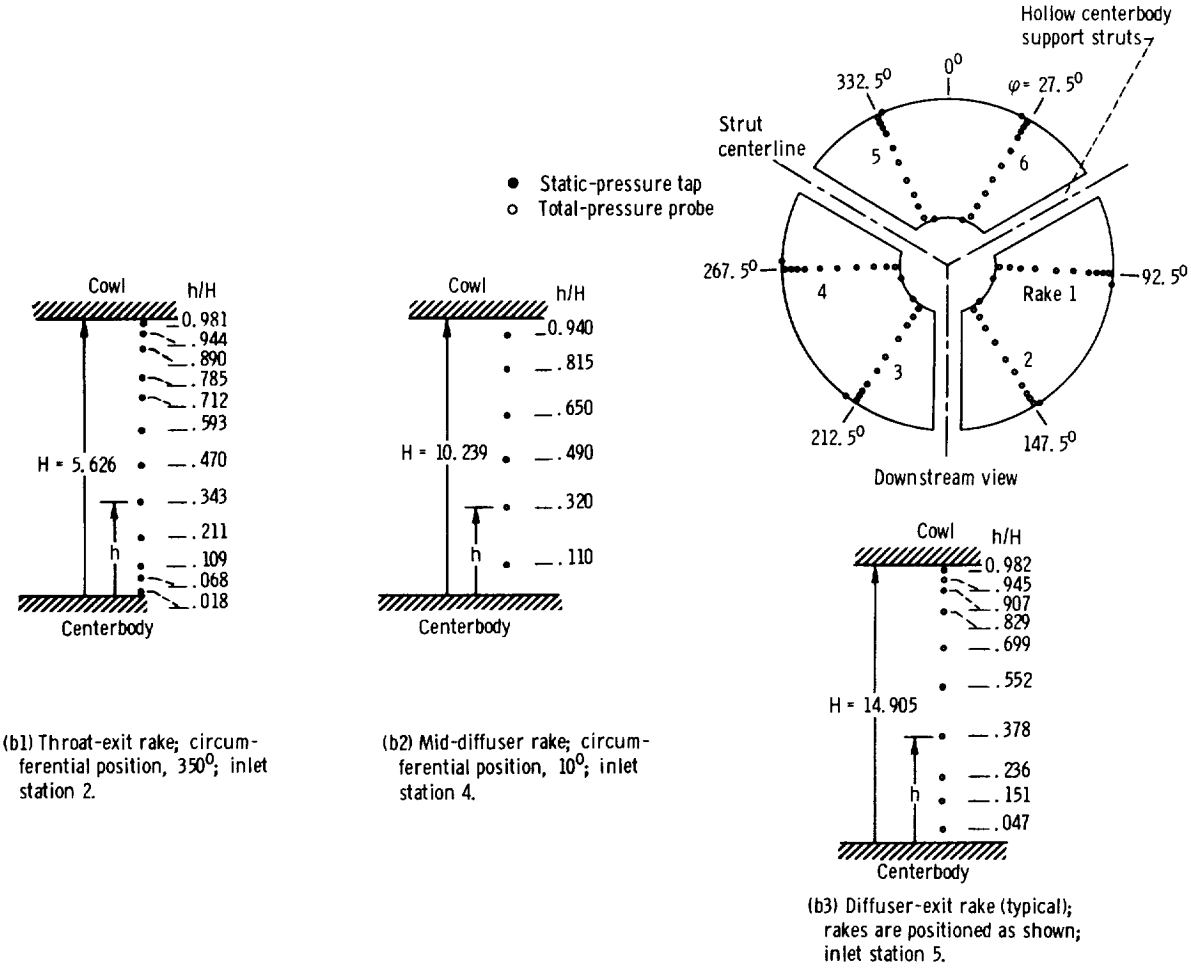

(b1) Throat-exit rake; circumferential position, 350°; inlet station 2.

(b2) Mid-diffuser rake; circumferential position, 10°; inlet station 4.

(b3) Diffuser-exit rake (typical); rakes are positioned as shown; inlet station 5.

(b) Subsonic diffuser total-pressure rakes.

Figure 10. - Bleed and inlet diffuser total-pressure instrumentation.

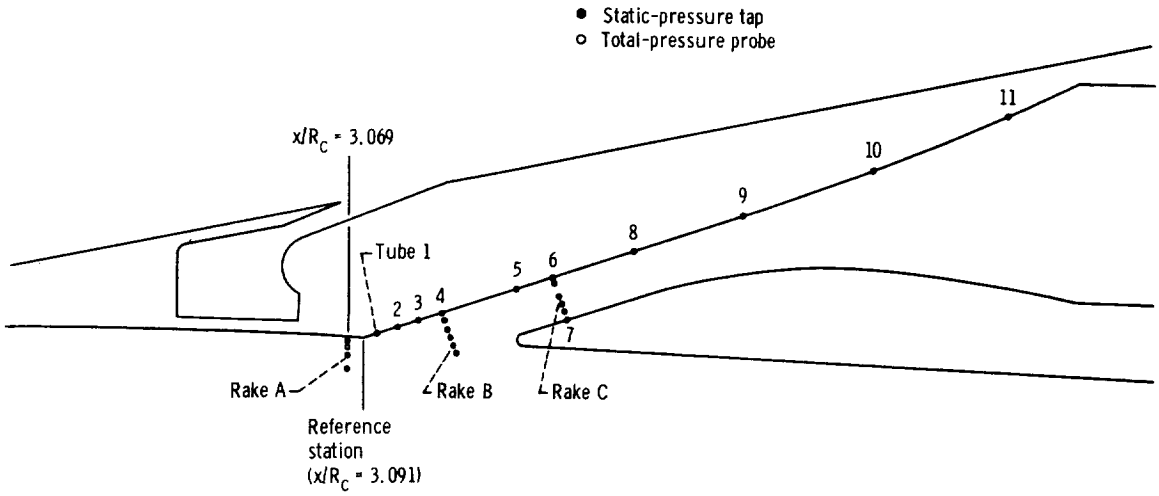

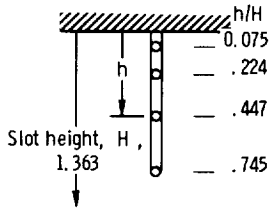

(a) Rake A; axial distance ratio, $x/R_C = 3.069$; circumferential position, 5^0.

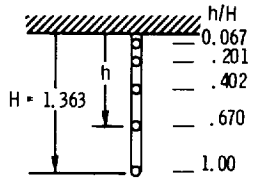

(b) Rake B; axial distance ratio, $x/R_C = 3.215$; circumferential position, 20^0.

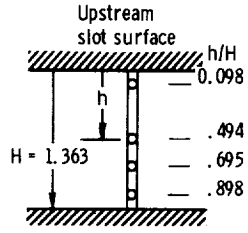

(c) Rake C; axial distance ratio, $x/R_C = 3.335$; circumferential position, 350^0.

Slot static-pressure taps, top centerline	
Tube	Axial distance from reference station, L/R_C
1	0.015
2	.052
3	.088
4	.124
5	.200
6	.244
7	.264
8	.347
9	.470
10	.613
11	.760

Figure 11. - Forward-slanted-slot pressure instrumentation.

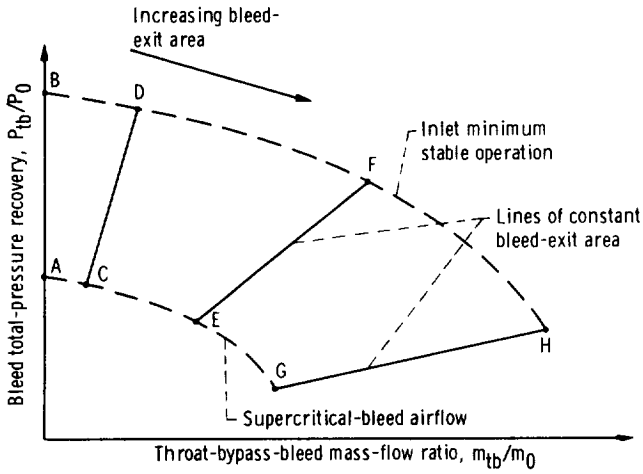

(a) Throat-bypass performance.

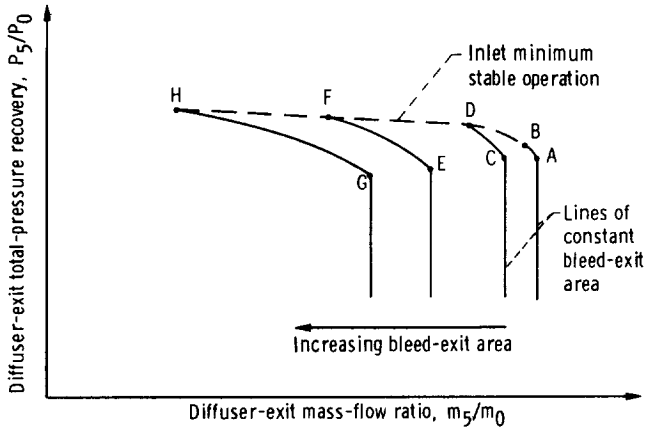

(b) Inlet performance.

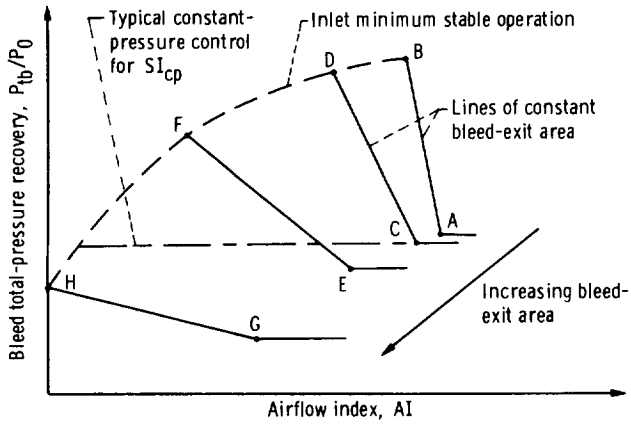

(c) Airflow index.

Figure 12. - Inlet stability data.

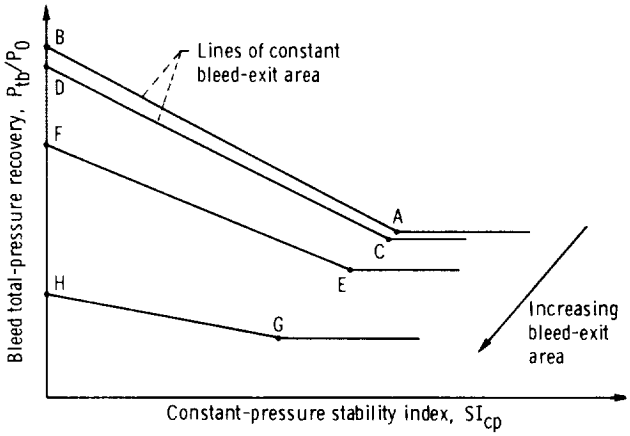

(d) Stability index for constant throat-bypass bleed recovery.

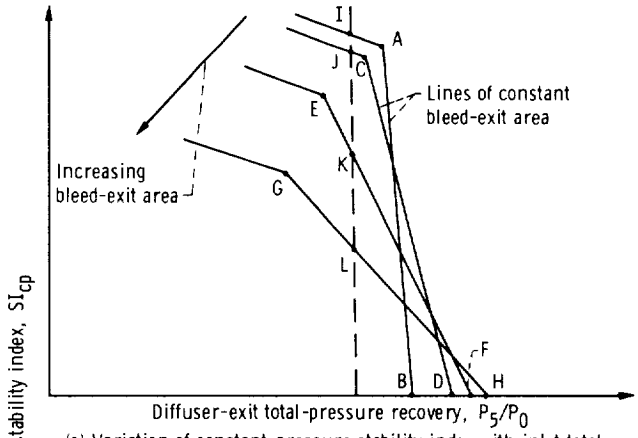

(e) Variation of constant-pressure stability index with inlet total-pressure recovery.

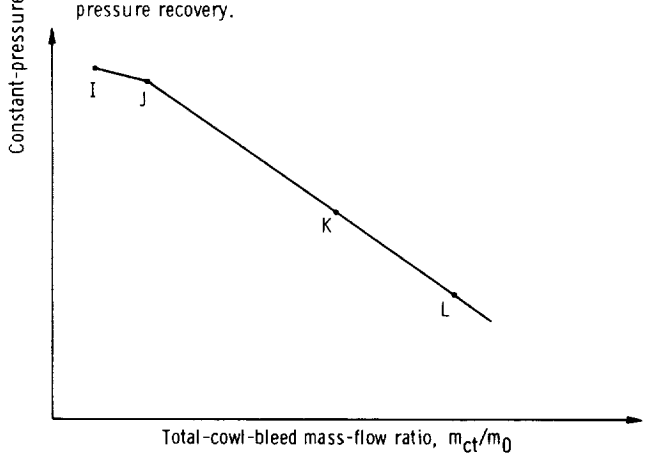

(f) Constant-pressure stability index for an initial inlet total-pressure recovery of 0.89.

Figure 12. - Continued.

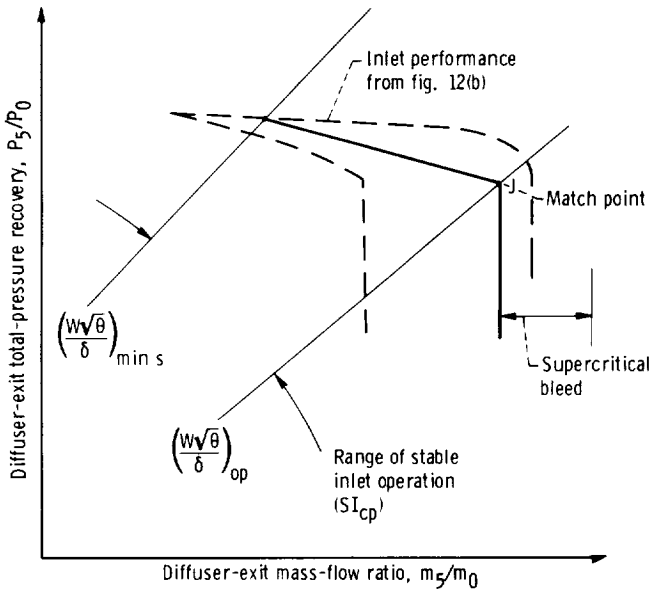

(g) Inlet performance for point J as match condition and with constant-pressure control on throat-bypass bleed.

Figure 12. - Concluded.

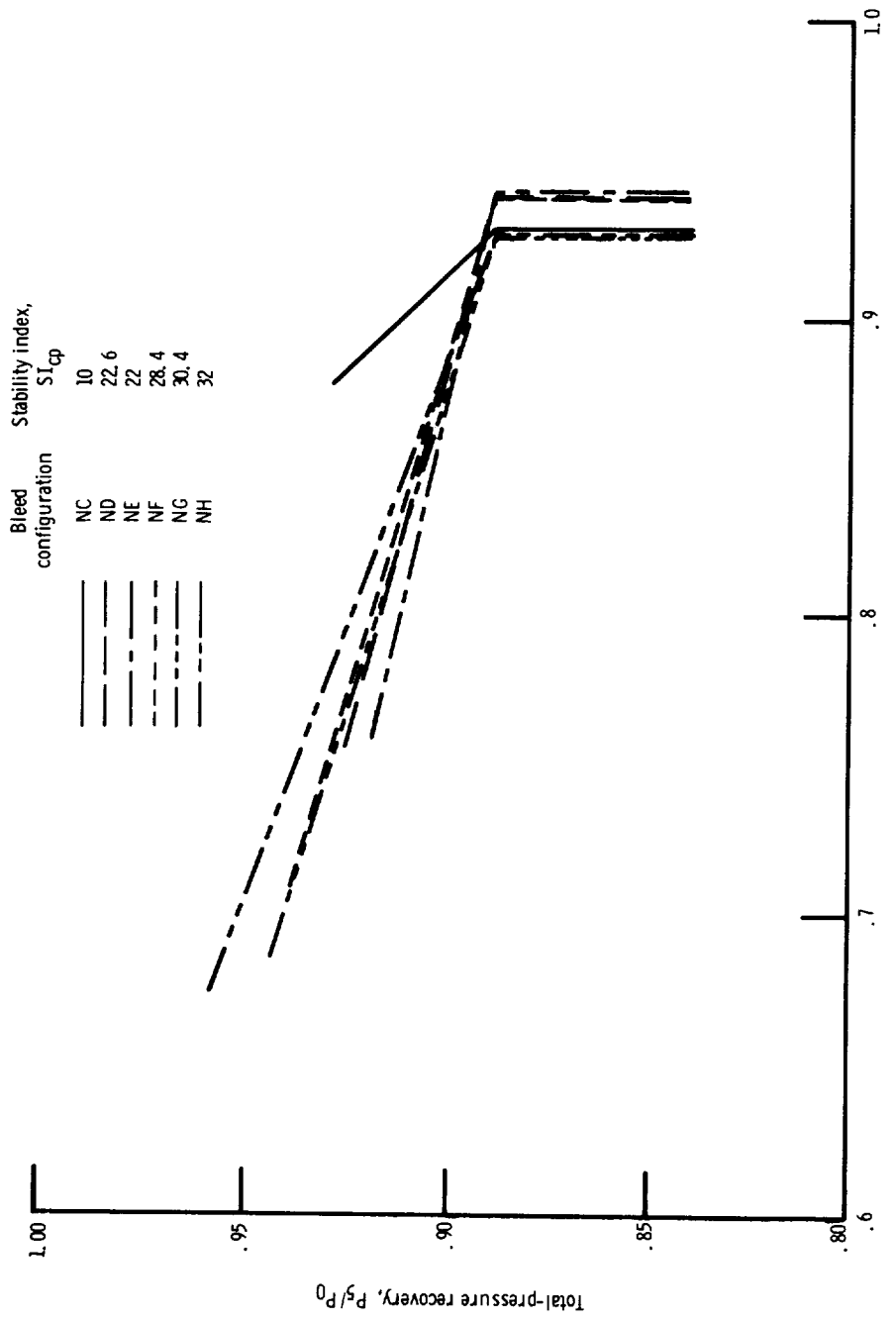

Figure 13. - Comparison of inlet performance for distributed porous throat-bypass configurations based on a constant throat-bypass recovery to unstart limit from initial inlet conditions of 89-percent total-pressure recovery and a total-cowl-bleed mass-flow ratio of 0.02 to 0.03. Free-stream Mach number, $M_0 = 2.50$; angle of attack, $\alpha = 0^0$; overboard-bypass mass-flow ratio, $m_{by}/m_0 = 0.0175$.

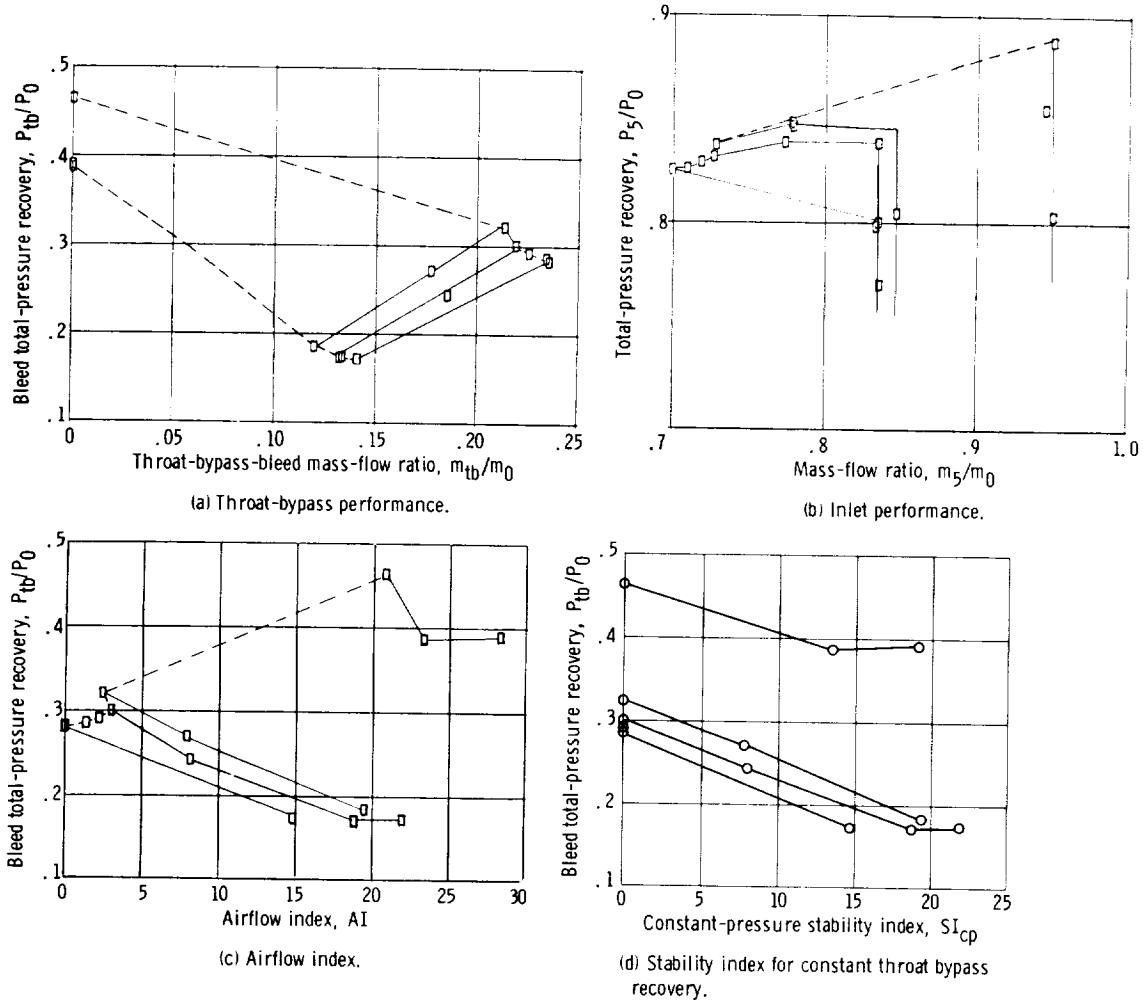

(a) Throat-bypass performance.

(b) Inlet performance.

(c) Airflow index.

(d) Stability index for constant throat bypass recovery.

Figure 14. - Performance of distributed porous configuration NA. Free-stream Mach number, $M_0 = 2.50$; angle of attack, $\alpha = 0^0$; overboard-bypass mass-flow ratio, $m_{by}/m_0 = 0.0175$.

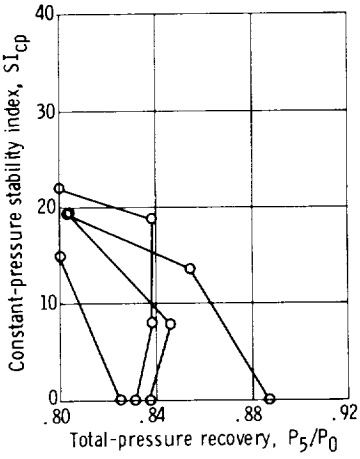

(e) Variation of constant-pressure stability index with inlet total-pressure recovery.

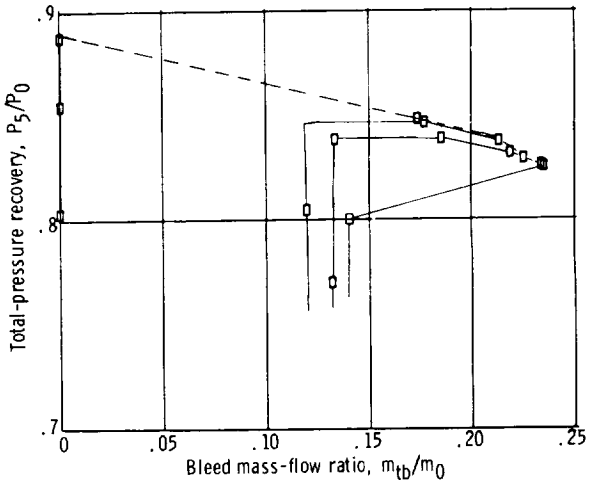

(f) Variation of inlet recovery with throat-bypass bleed.

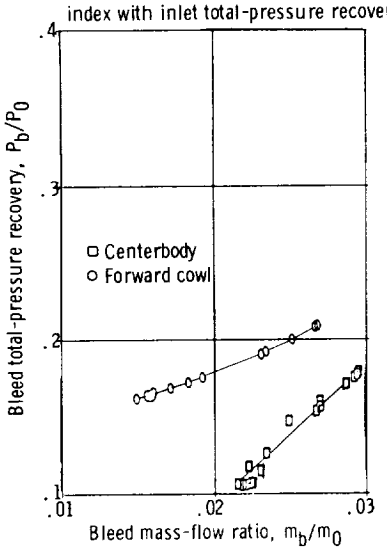

(g) Forward-cowl and centerbody bleed performance.

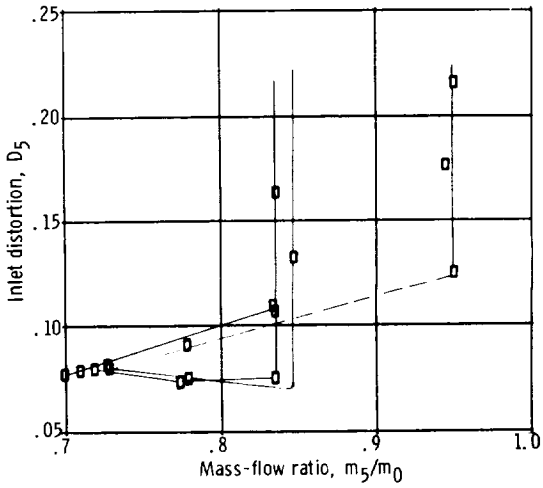

(h) Distortion.

Figure 14. - Concluded.

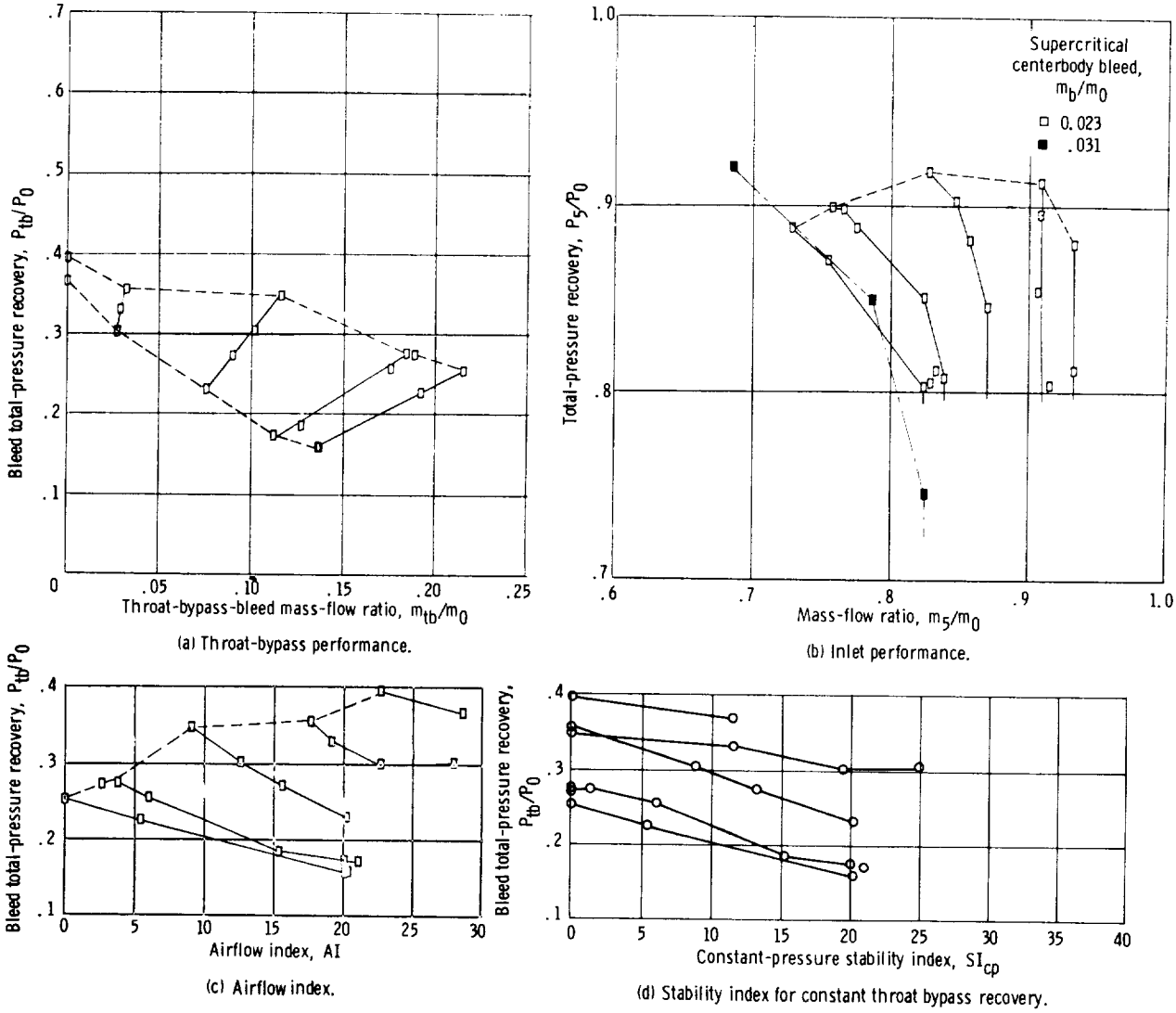

(a) Throat-bypass performance.

(b) Inlet performance.

(c) Airflow index.

(d) Stability index for constant throat bypass recovery.

Figure 15. - Performance of distributed porous configuration NB. Free-stream Mach number, $M_0 = 2.50$; angle of attack, $\alpha = 0^0$; overboard-bypass mass-flow ratio, $m_{by}/m_0 = 0.0175$.

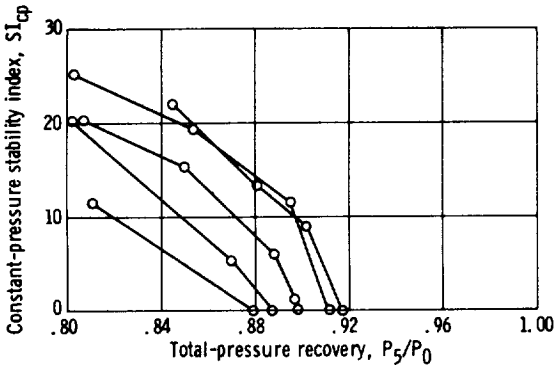

(e) Variation of constant-pressure stability index with inlet total-pressure recovery.

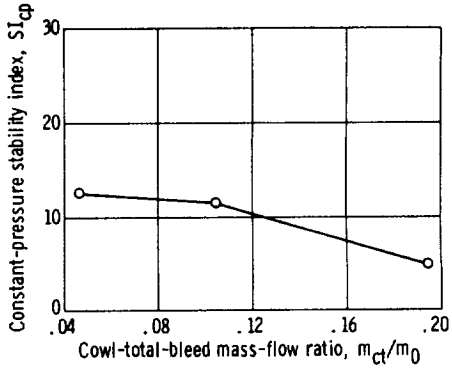

(f) Constant-pressure stability index for an initial inlet total-pressure recovery of 0.89.

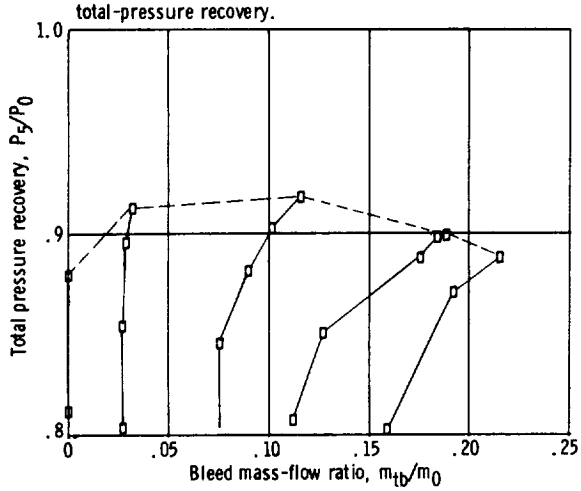

(g) Variation of inlet recovery with throat-bypass bleed.

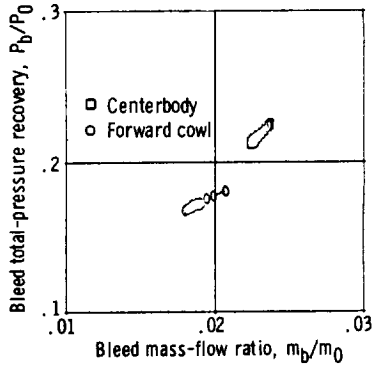

(h) Forward-cowl and centerbody bleed performance.

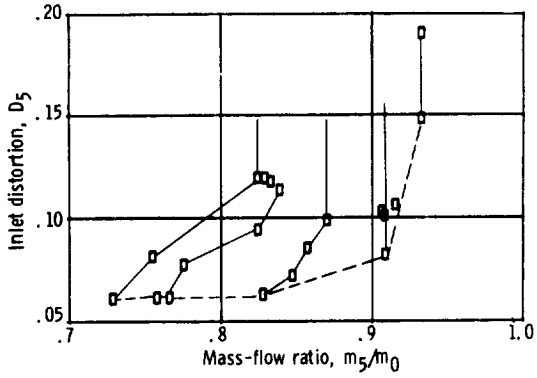

(i) Distortion.

Figure 15. - Concluded.

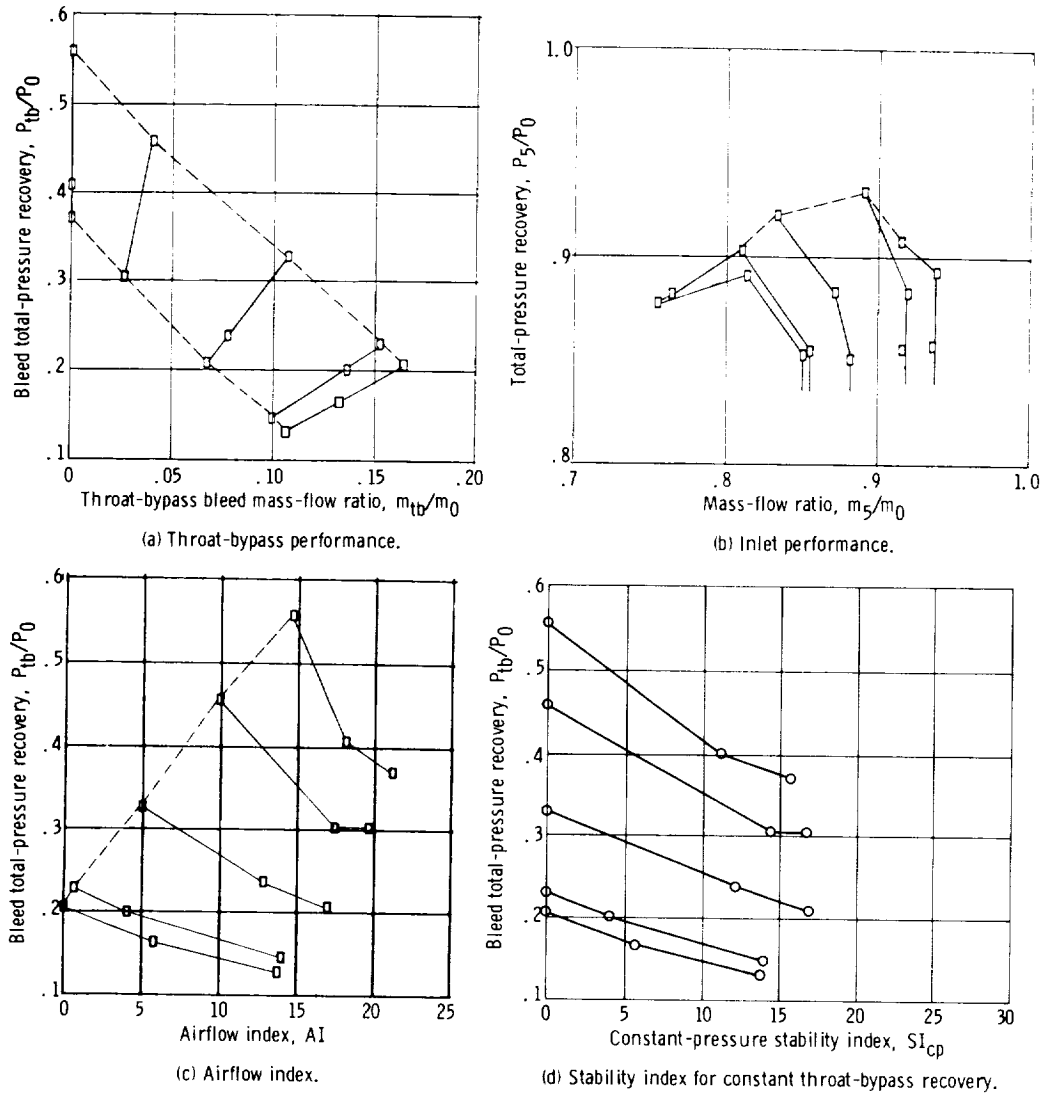

(a) Throat-bypass performance.

(b) Inlet performance.

(c) Airflow index.

(d) Stability index for constant throat-bypass recovery.

Figure 16. - Performance of distributed porous configuration NC. Free-stream Mach number, $M_0 = 2.50$; angle of attack, $\alpha = 0^0$; overboard-bypass mass-flow ratio, $m_{by}/m_0 = 0.0175$.

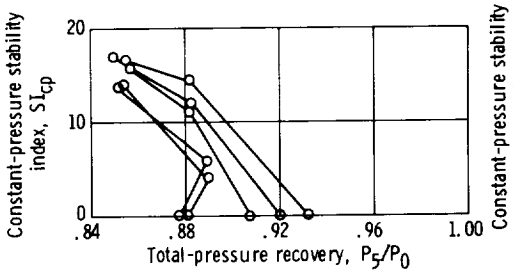

(e) Variation of constant-pressure stability index with inlet total-pressure recovery.

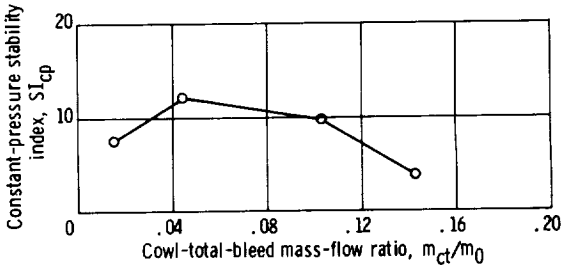

(f) Constant-pressure stability index for an initial inlet total-pressure recovery of 0.89.

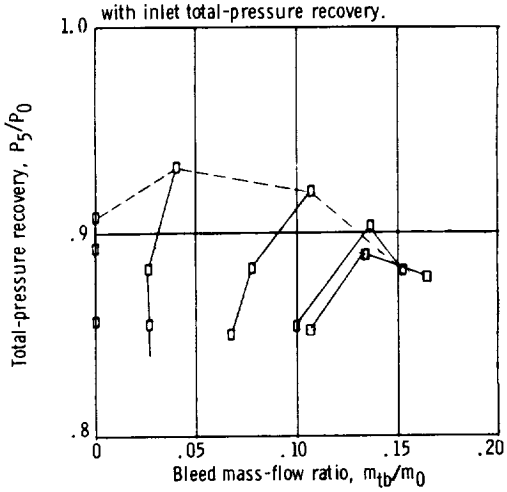

(g) Variation of inlet recovery with throat-bypass bleed.

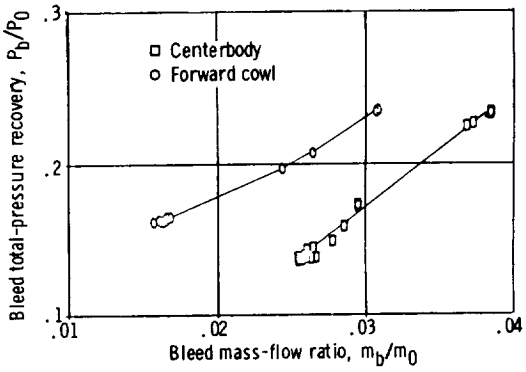

(h) Forward-cowl and centerbody bleed performance.

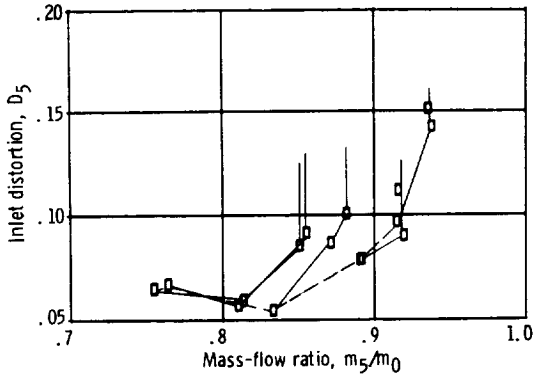

(i) Distortion.

Figure 16. - Concluded.

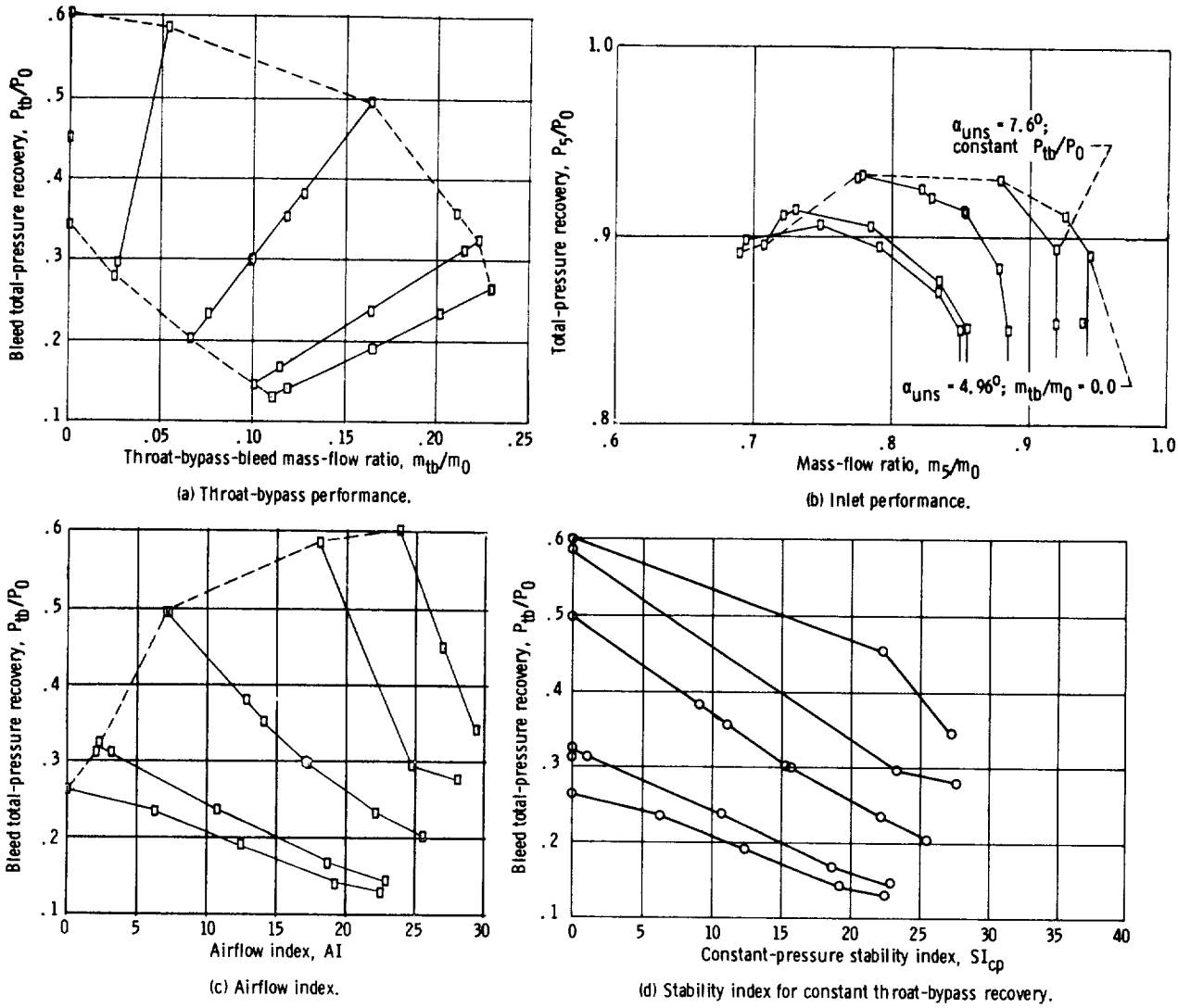

(a) Throat-bypass performance.

(b) Inlet performance.

(c) Airflow index.

(d) Stability index for constant throat-bypass recovery.

Figure 17. - Performance for distributed porous configuration ND. Free-stream Mach number, M_0 = 2.50; angle of attack, α = 0°; overboard-bypass mass-flow ratio, m_{by}/m_0 = 0.0175.

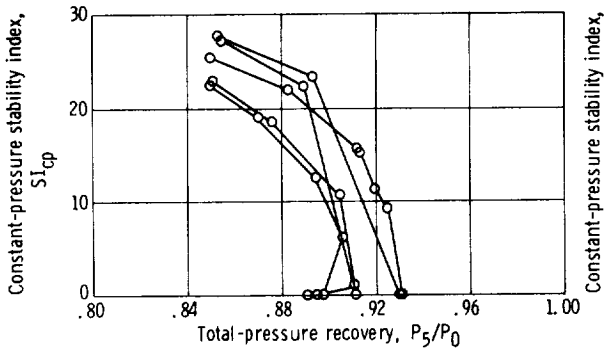

(e) Variation of constant-pressure stability index with inlet total-pressure recovery.

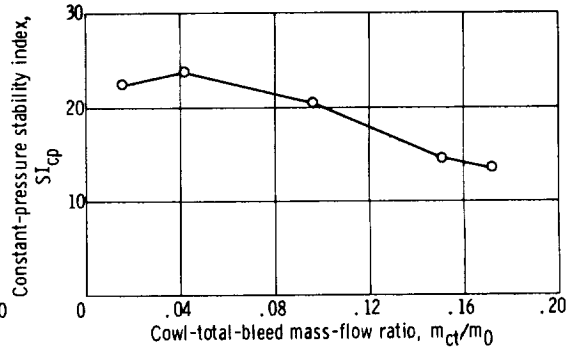

(f) Constant-pressure stability index for an initial inlet total-pressure recovery of 0.89.

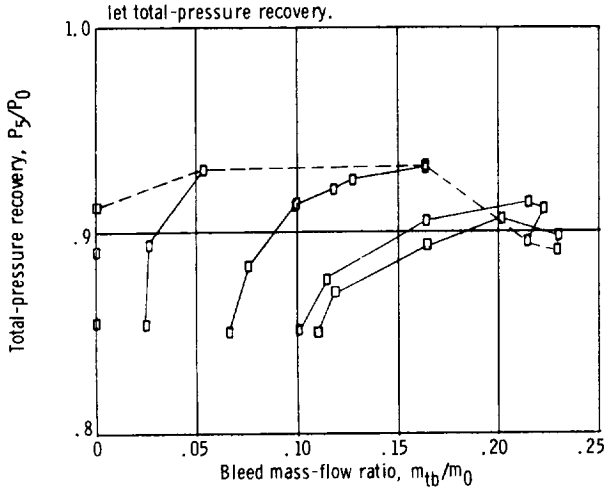

(g) Variation of inlet recovery with throat-bypass bleed.

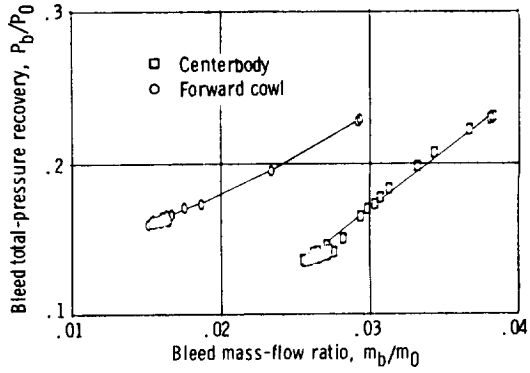

(h) Forward-cowl and centerbody bleed performance.

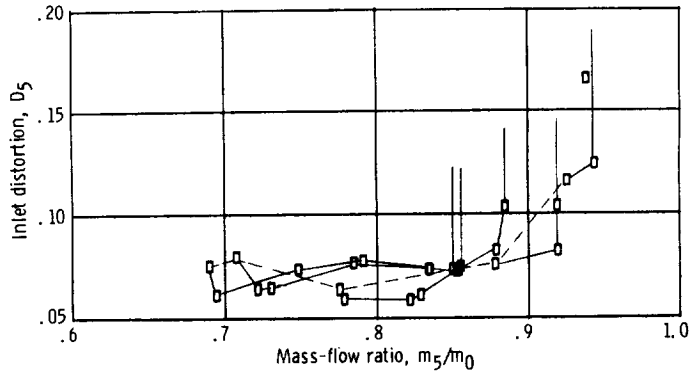

(i) Distortion.

Figure 17. - Concluded.

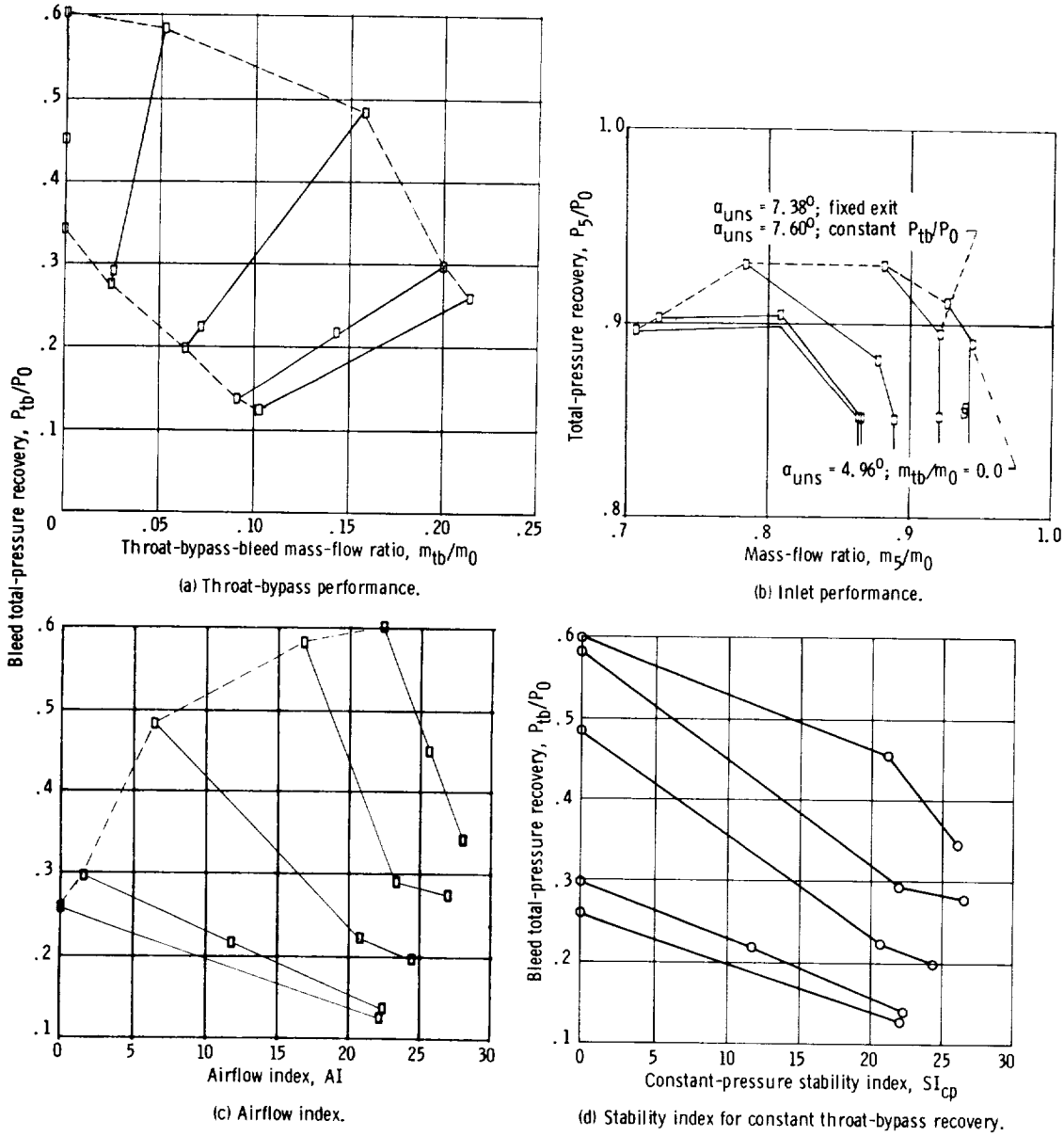

Figure 18. - Performance for distributed porous configuration NE. Free-stream Mach number, M_0 = 2.50; angle of attack, α = 0°; overboard-bypass mass-flow ratio, m_{by}/m_0 = 0.0175.

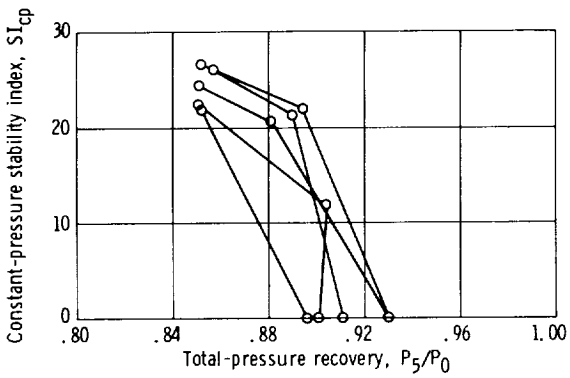

(e) Variation of constant-pressure stability index with inlet total-pressure recovery.

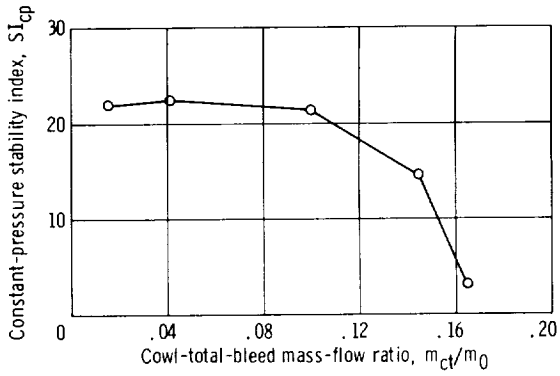

(f) Constant-pressure stability index for an initial inlet total-pressure recovery of 0.89.

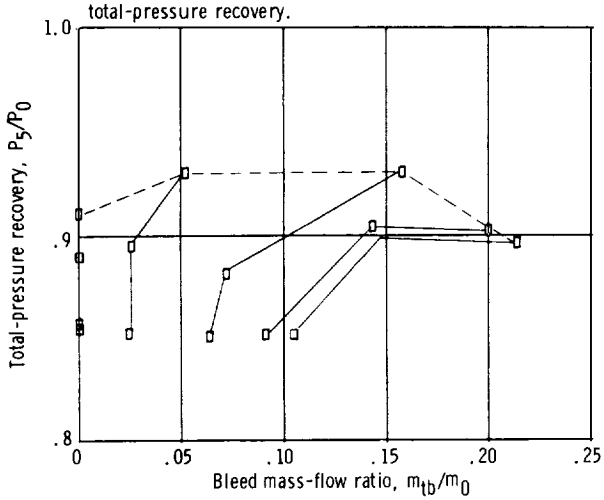

(g) Variation of inlet recovery with throat-bypass bleed.

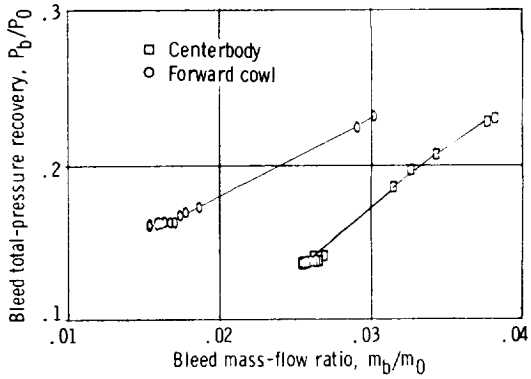

(h) Forward-cowl and centerbody bleed performance.

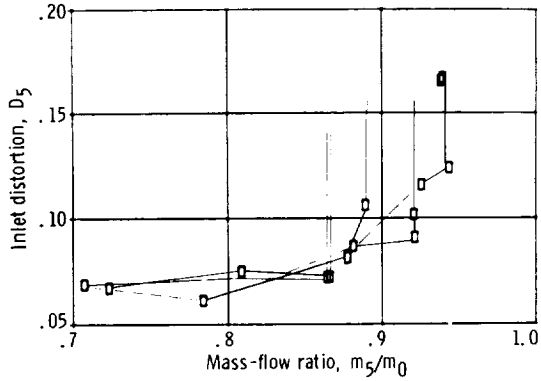

(i) Distortion.

Figure 18. - Concluded.

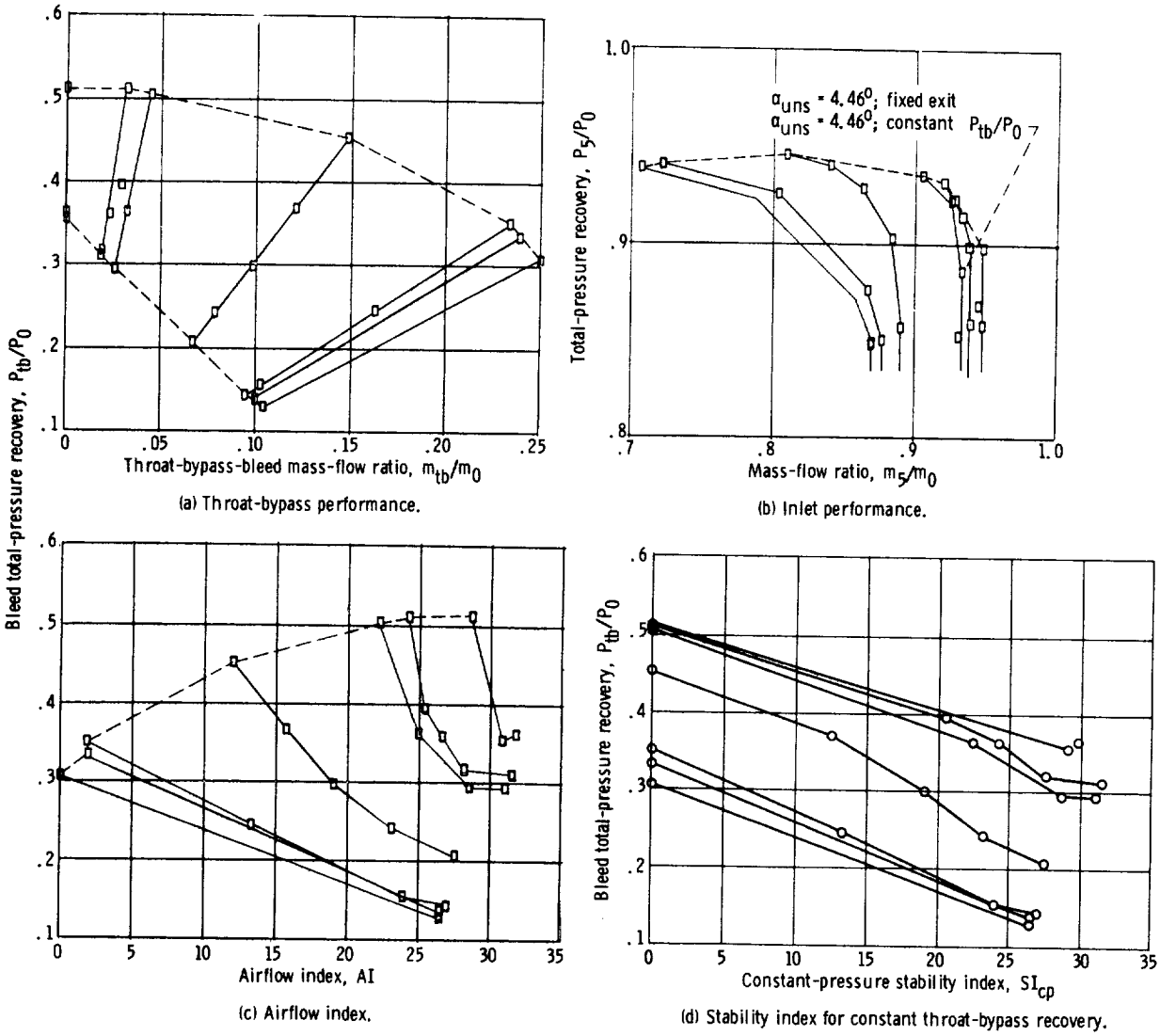

Figure 19. - Performance of distributed porous configuration NF. Free-stream Mach number, M_0 = 2.50; angle of attack, α = 0°; overboard-bypass mass-flow ratio, m_{by}/m_0 = 0.0175.

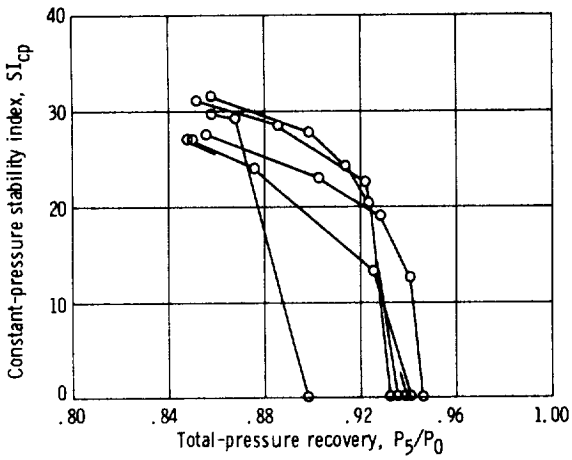

(e) Variation of constant-pressure stability index with inlet total-pressure recovery.

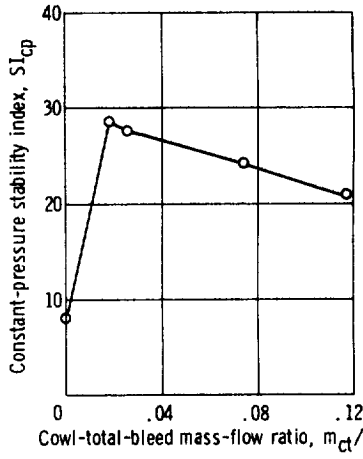

(f) Constant-pressure stability index for an initial inlet total-pressure recovery of 0.89.

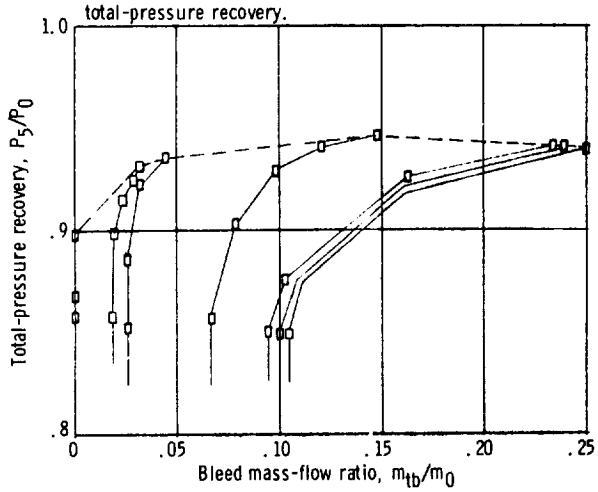

(g) Variation of inlet recovery with throat-bypass bleed.

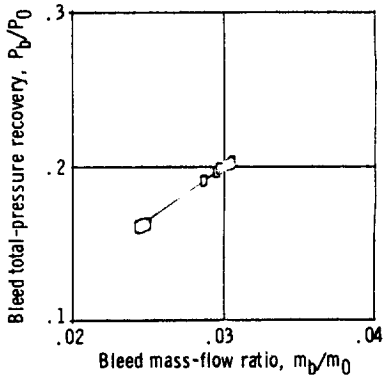

(h) Centerbody bleed performance.

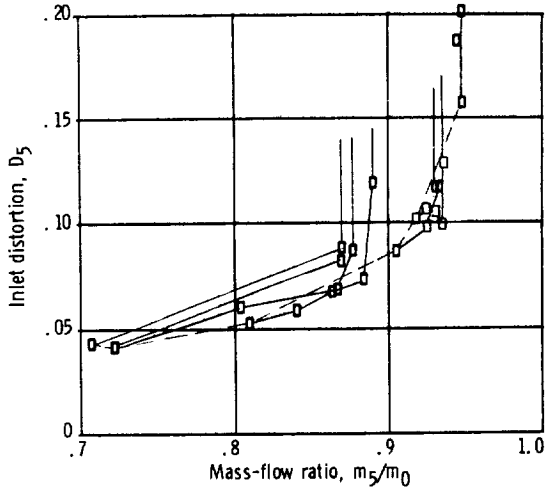

(i) Distortion.

Figure 19. - Concluded.

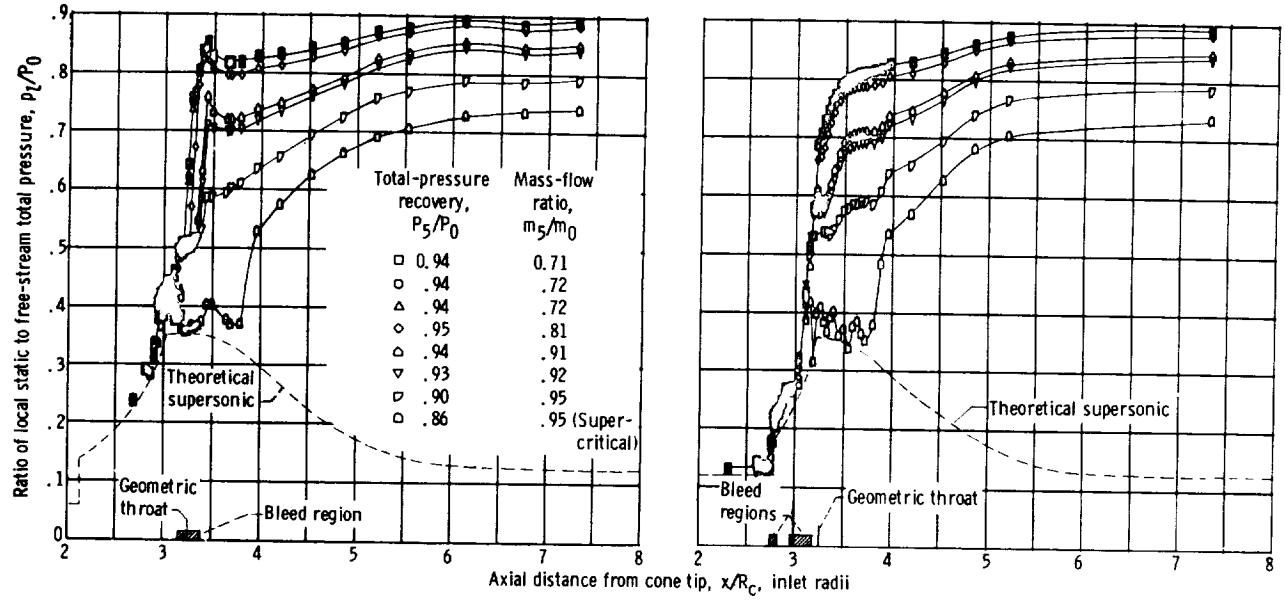

(a) Internal cowl surface pressure distributions.

(b) Centerbody surface pressure distributions.

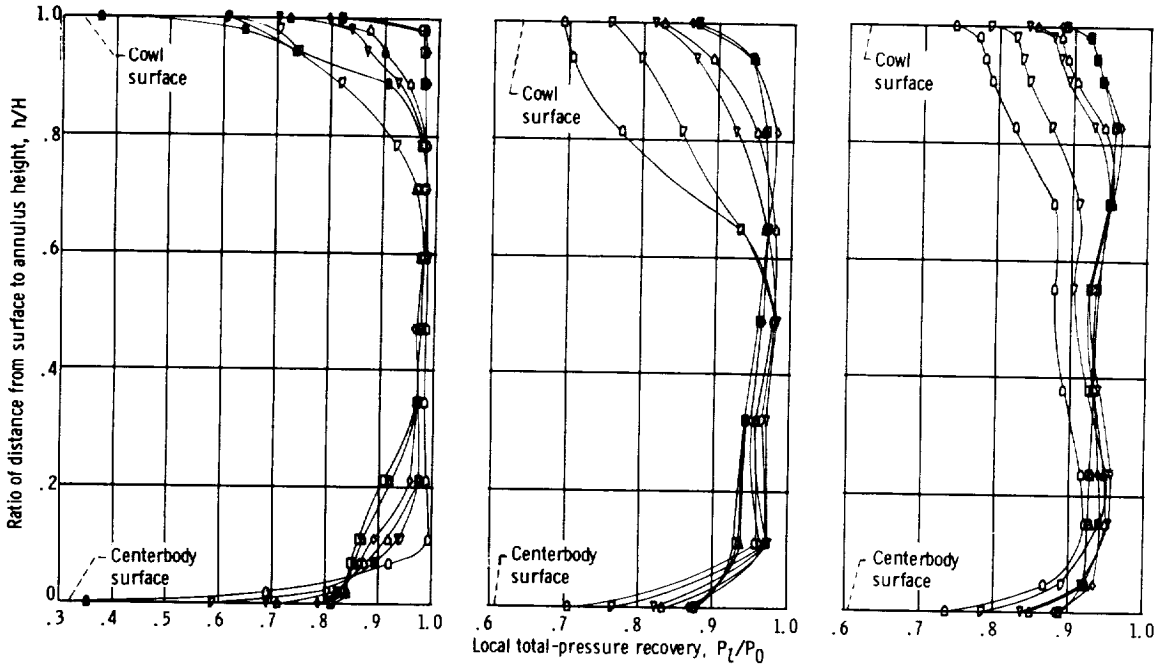

(c) Throat exit, station 2. Symbols at h/H of 0 and 1.0 represent inlet surface static pressures.

(d) Mid-diffuser, station 4. Symbols at h/H of 0 and 1.0 represent inlet surface static pressures.

(e) Diffuser exit rake 6, station 5. Symbols at h/H of 0 and 1.0 represent inlet surface static pressures.

Figure 20. - Diffuser static- and total-pressure distributions for configuration NF. Distributions are presented for one supercritical condition (throat-bypass mass-flow ratio, $m_{tb}/m_0 = 0$) and for all unstart limit data.

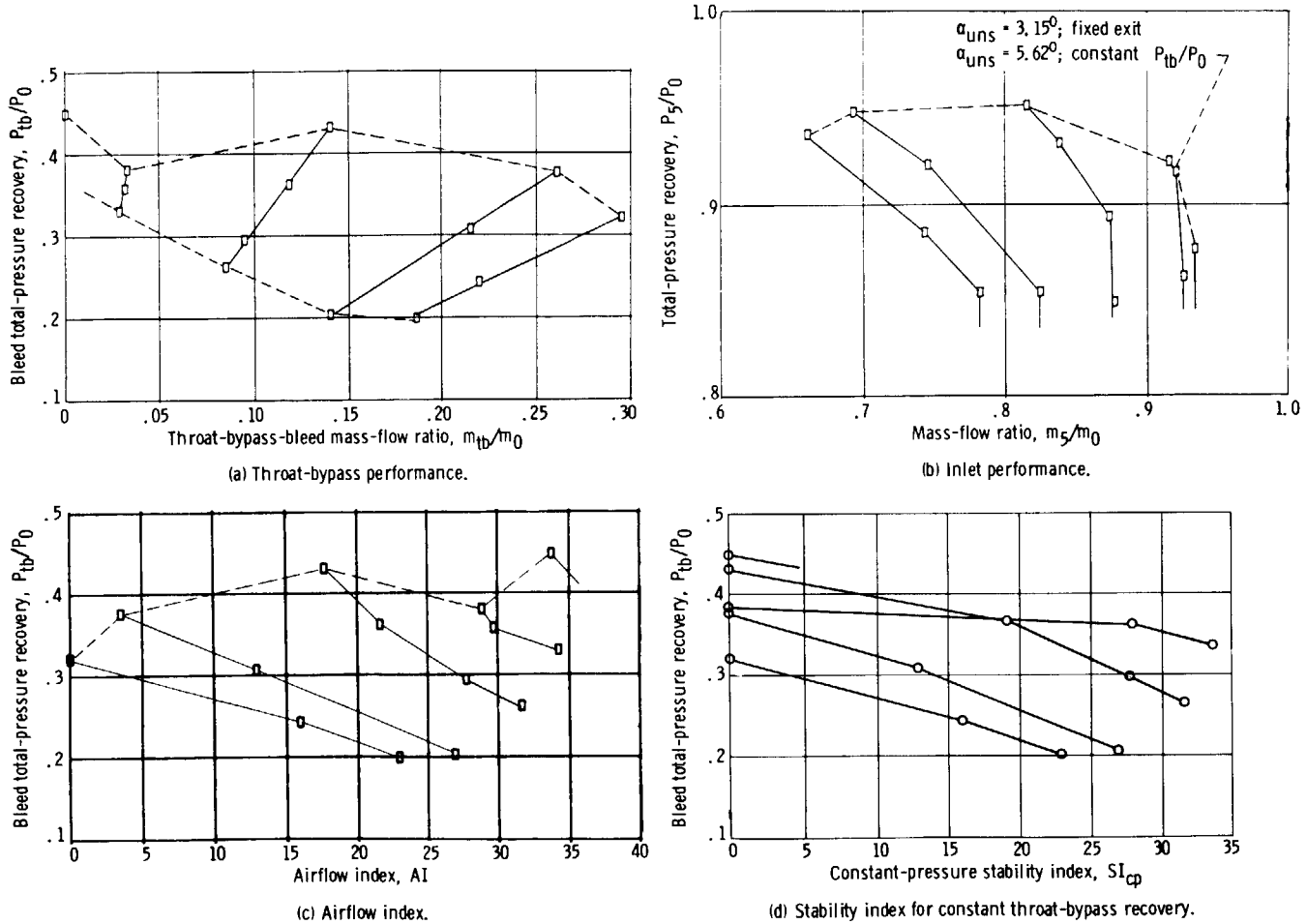

Figure 21. - Performance of distributed porous configuration NG. Free-stream Mach number, M_0 = 2.50; angle of attack, α = 0°; overboard-bypass mass-flow ratio, m_{by}/m_0 = 0.0175.

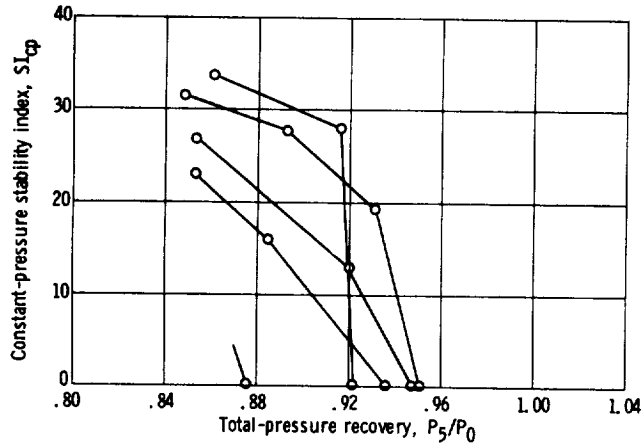

(e) Variation of constant-pressure stability index with inlet total-pressure recovery.

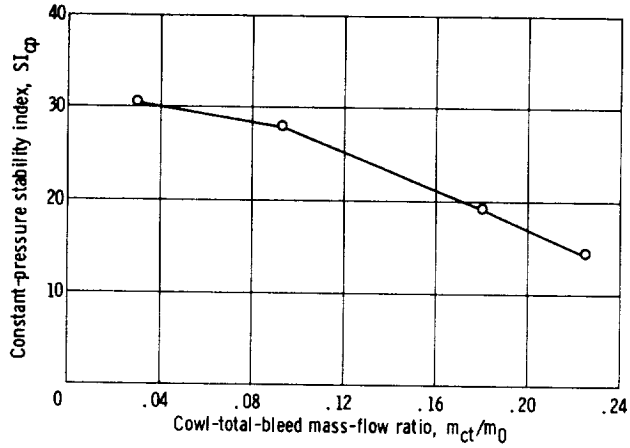

(f) Constant-pressure stability index for an initial inlet total-pressure recovery of 0.89.

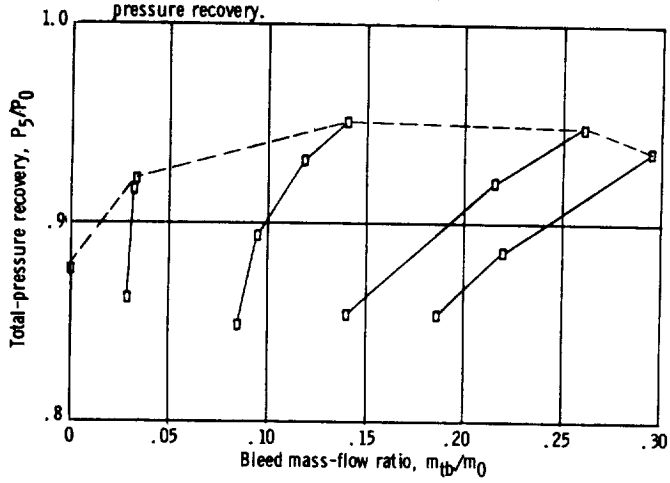

(g) Variation of inlet recovery with throat-bypass bleed.

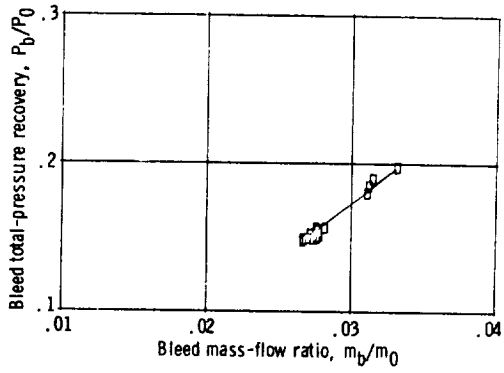

(h) Centerbody bleed performance.

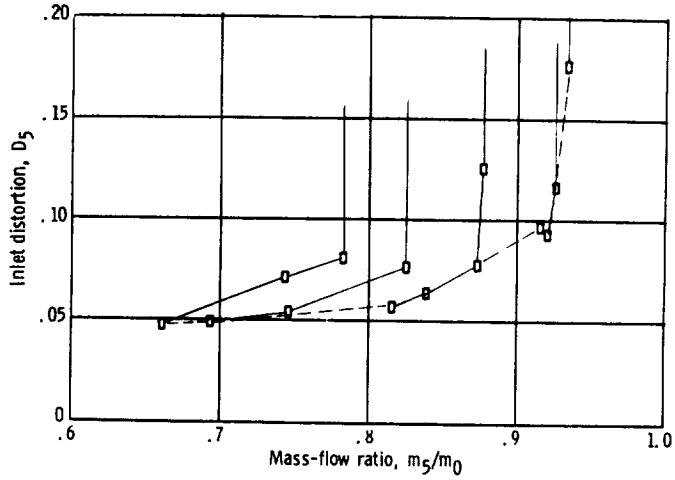

(i) Distortion.

Figure 21. - Concluded.

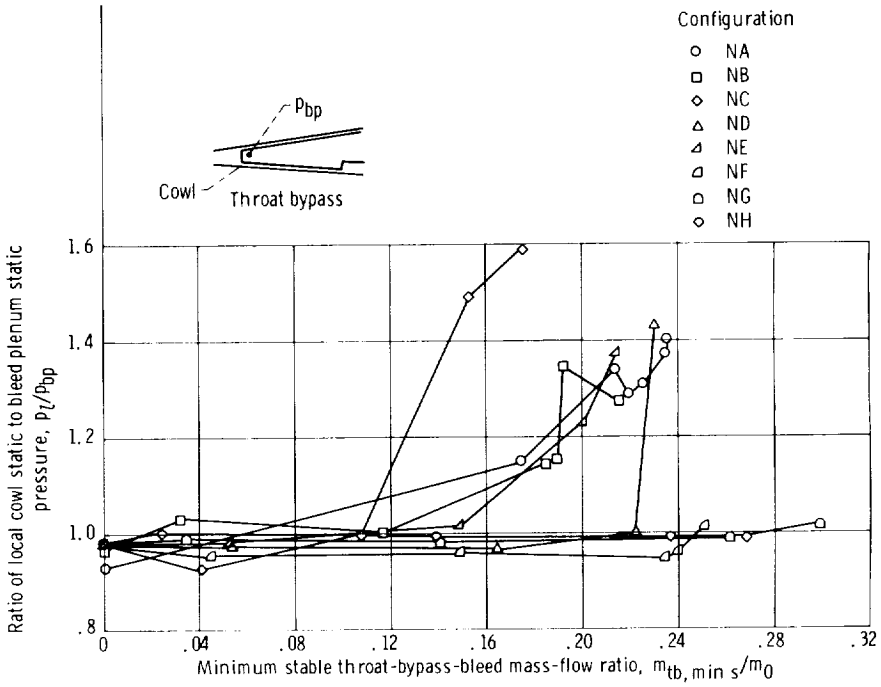

Figure 22. - Distributed-porous-cowl bleed recirculation pressure ratios for minimum stable conditions.

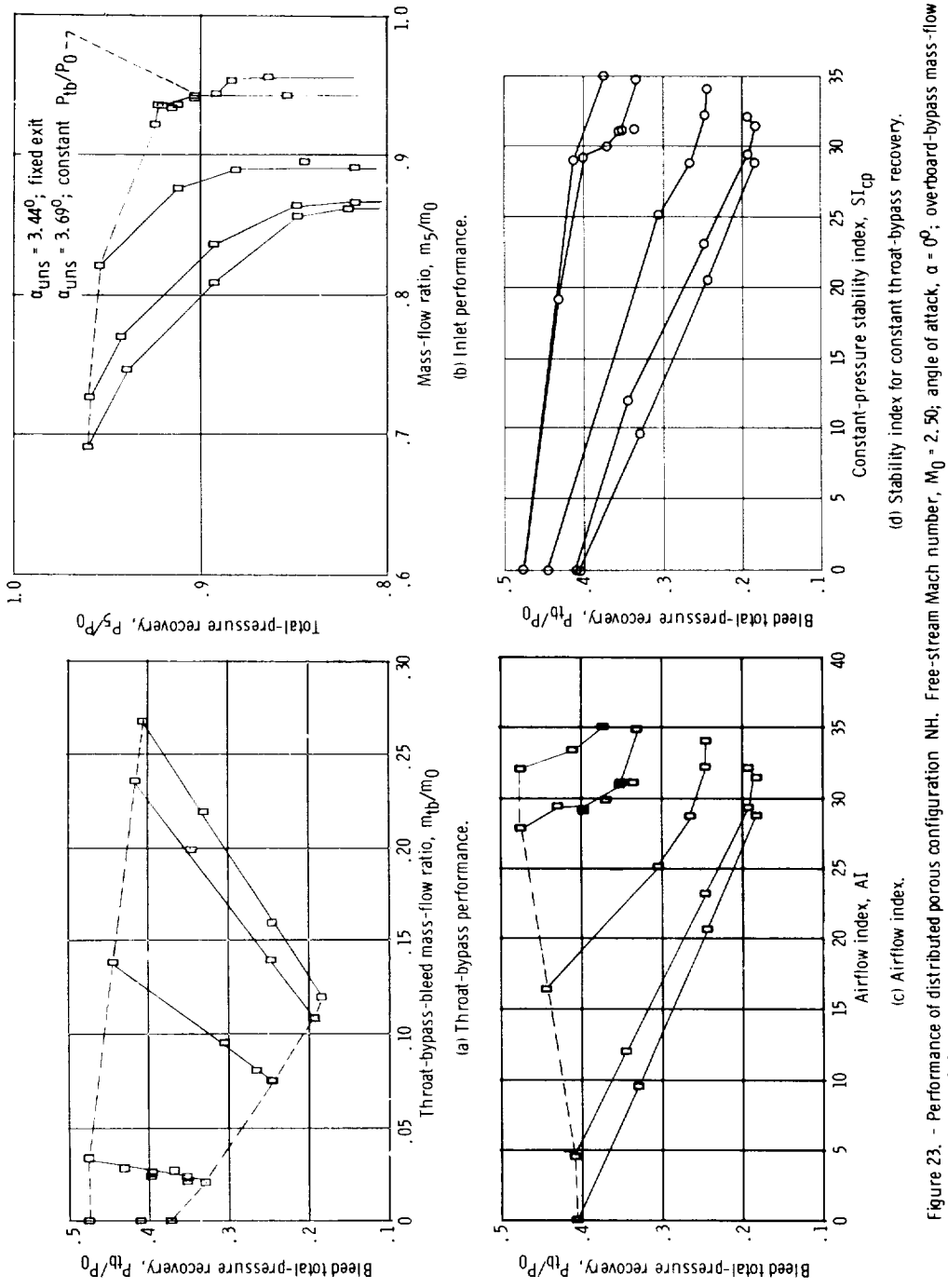

Figure 23. - Performance of distributed porous configuration NH. Free-stream Mach number, $M_0 = 2.50$; angle of attack, $\alpha = 0^0$; overboard-bypass mass-flow ratio, $m_{by}/m_0 = 0.01$.

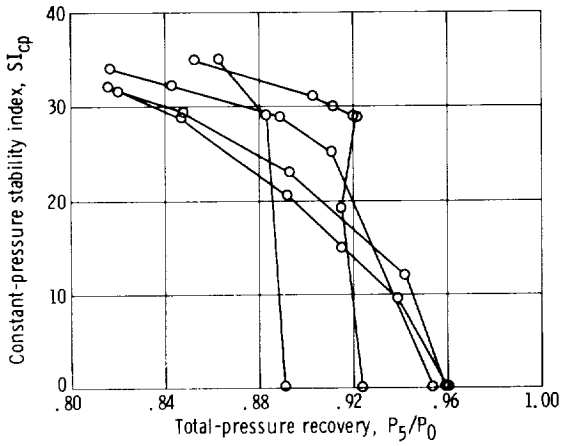

(e) Variation of constant-pressure stability index with inlet total-pressure recovery.

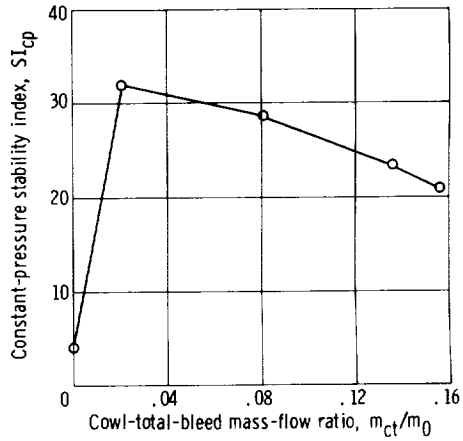

(f) Constant-pressure stability index for an initial inlet total-pressure recovery of 0.89.

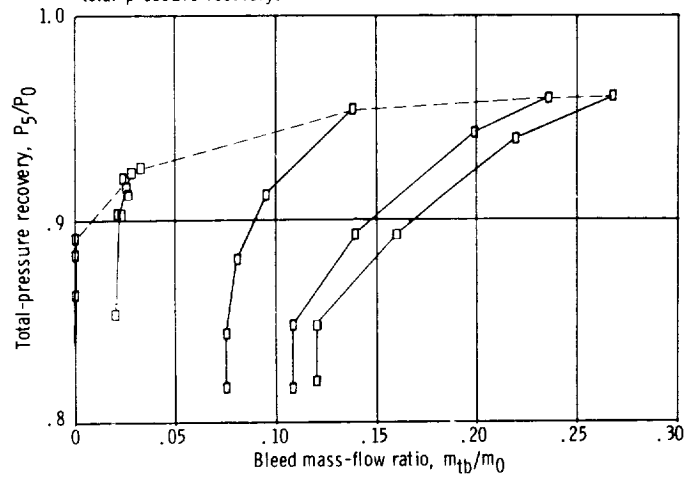

(g) Variation of inlet recovery with throat-bypass bleed.

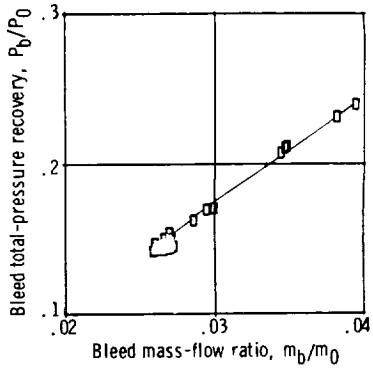

(h) Centerbody-bleed performance.

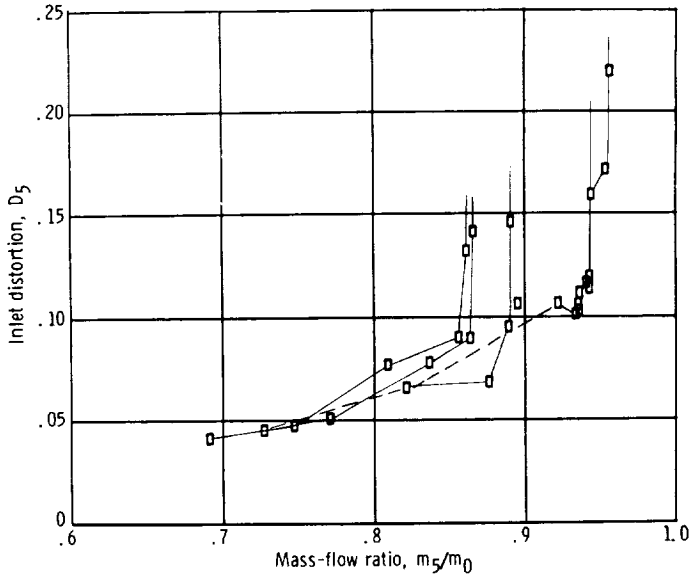

(i) Distortion.

Figure 23. - Concluded.

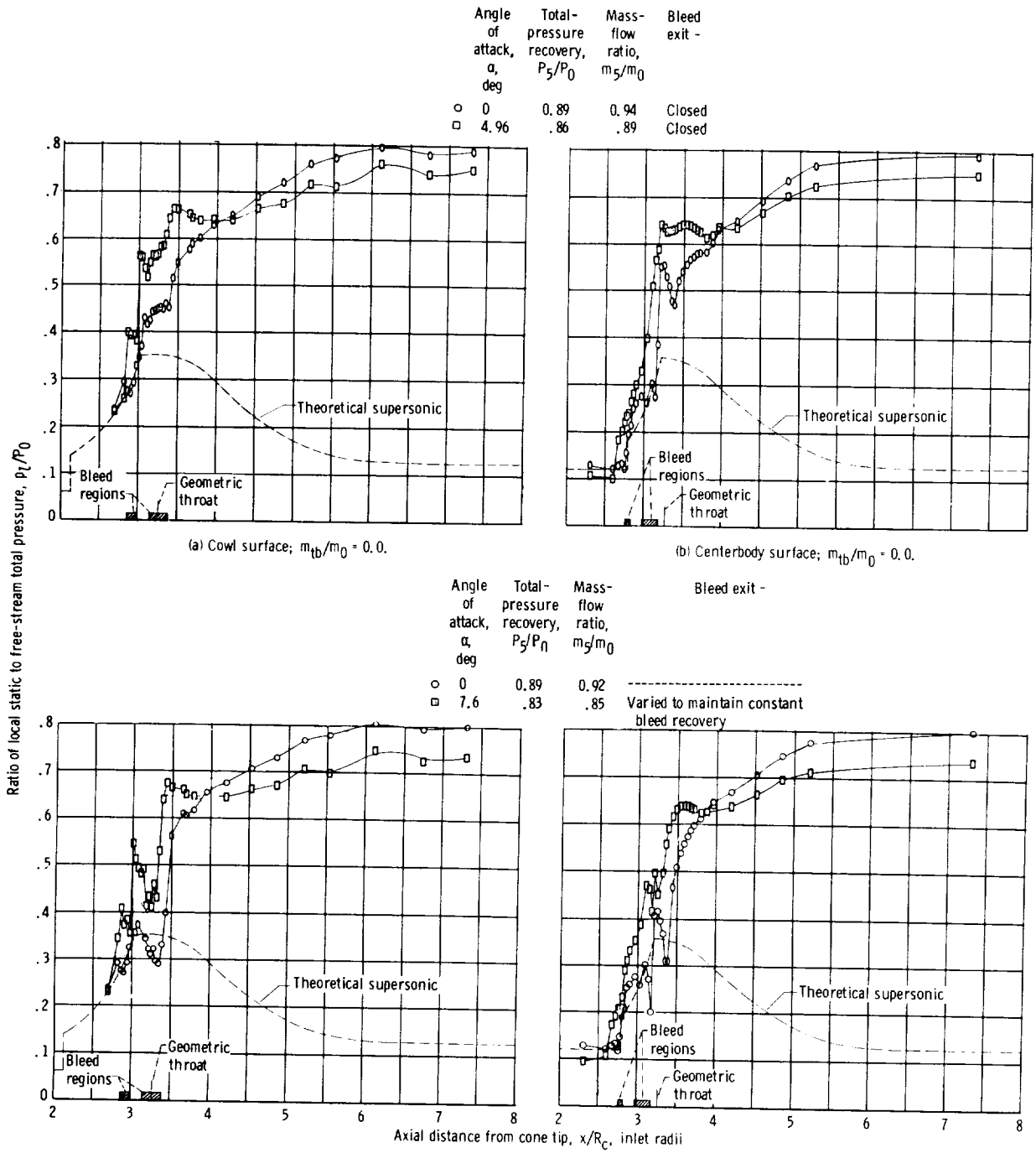

Figure 24. - Diffuser static-pressure distributions for configuration ND for an initial operating condition and for the unstart angle-of-attack limit, for throat-bypass mass-flow ratios m_{tb}/m_0 of 0 and 0.026.

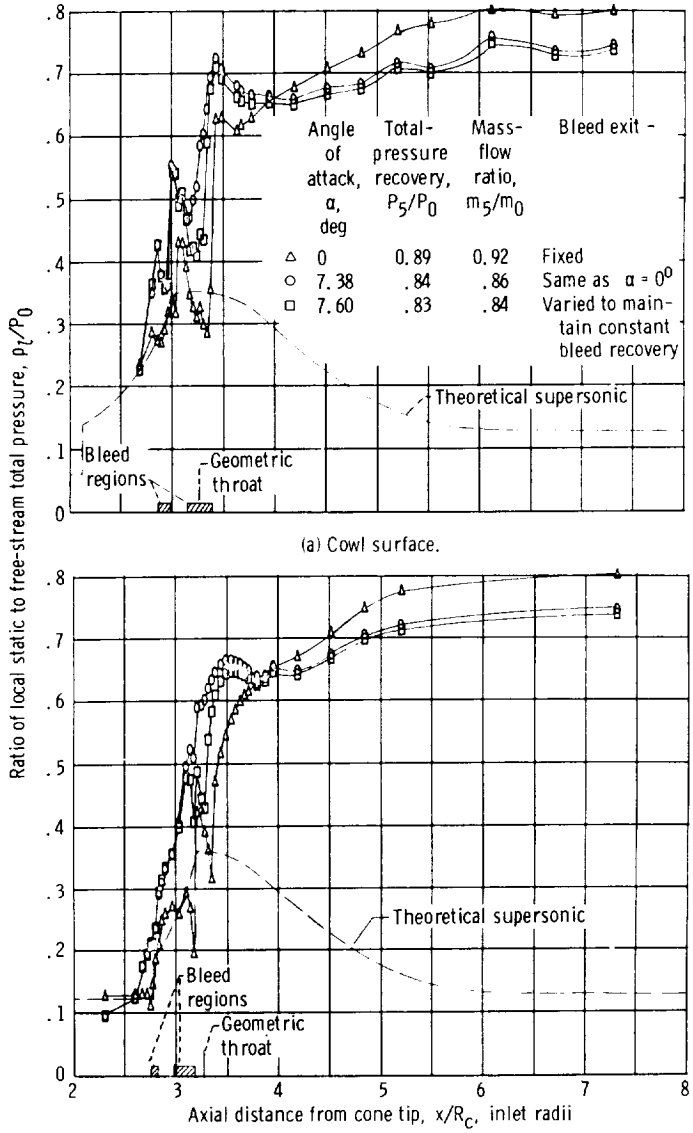

Figure 25. - Diffuser static-pressure distributions for configuration NE for an initial operating condition for angle of attack of zero degrees and for the unstart angle-of-attack limits with fixed bleed exits and variable bleed exits to maintain a constant bleed recovery.

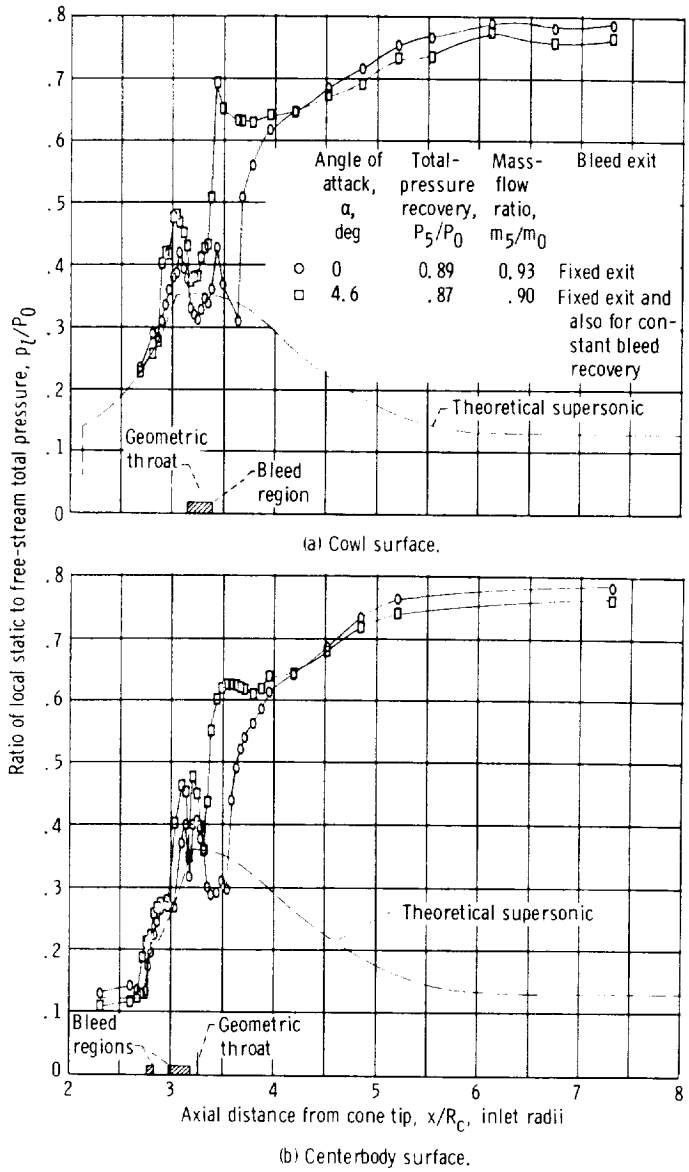

(a) Cowl surface.

(b) Centerbody surface.

Figure 26. - Diffuser static-pressure distributions for configuration NF for an initial operating condition for angle of attack of zero degrees and for the unstart angle-of-attack limit with fixed bleed exits and variable bleed exits to maintain a constant bleed recovery.

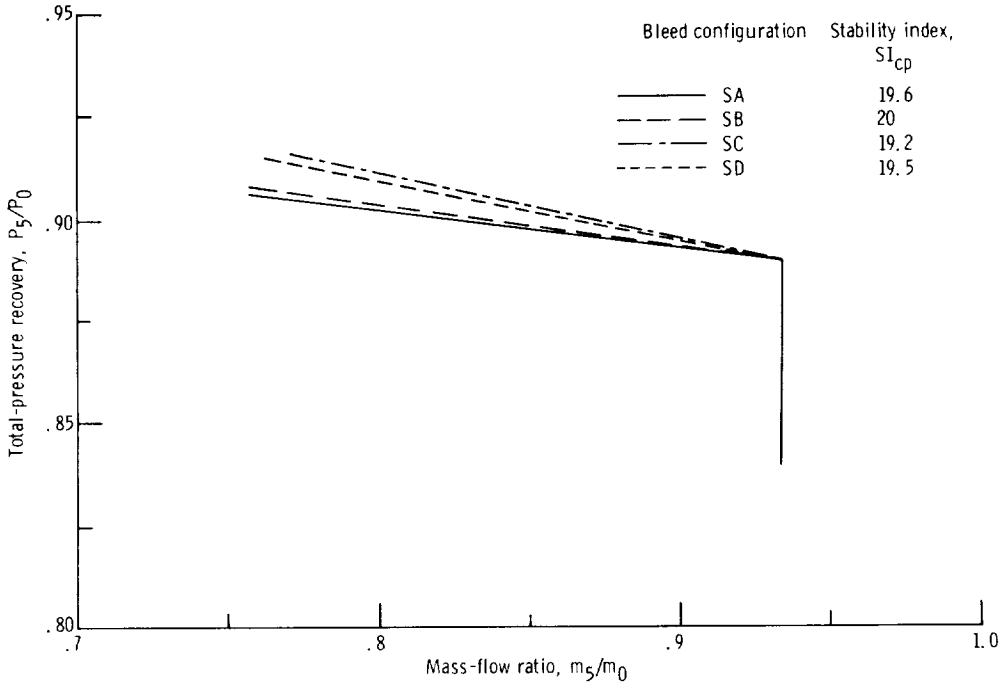

Figure 27. - Comparison of inlet performance for large-forward-slanted-slot throat-bypass configurations based on a constant throat-bypass recovery to unstart limit from initial inlet conditions of 89-percent total-pressure recovery and total-cowl-bleed mass-flow ratio of 0.02. Free-stream Mach number, $M_0 = 2.50$; angle of attack, $\alpha = 0^0$; overboard-bypass mass-flow ratio, $m_{by}/m_0 = 0.0175$.

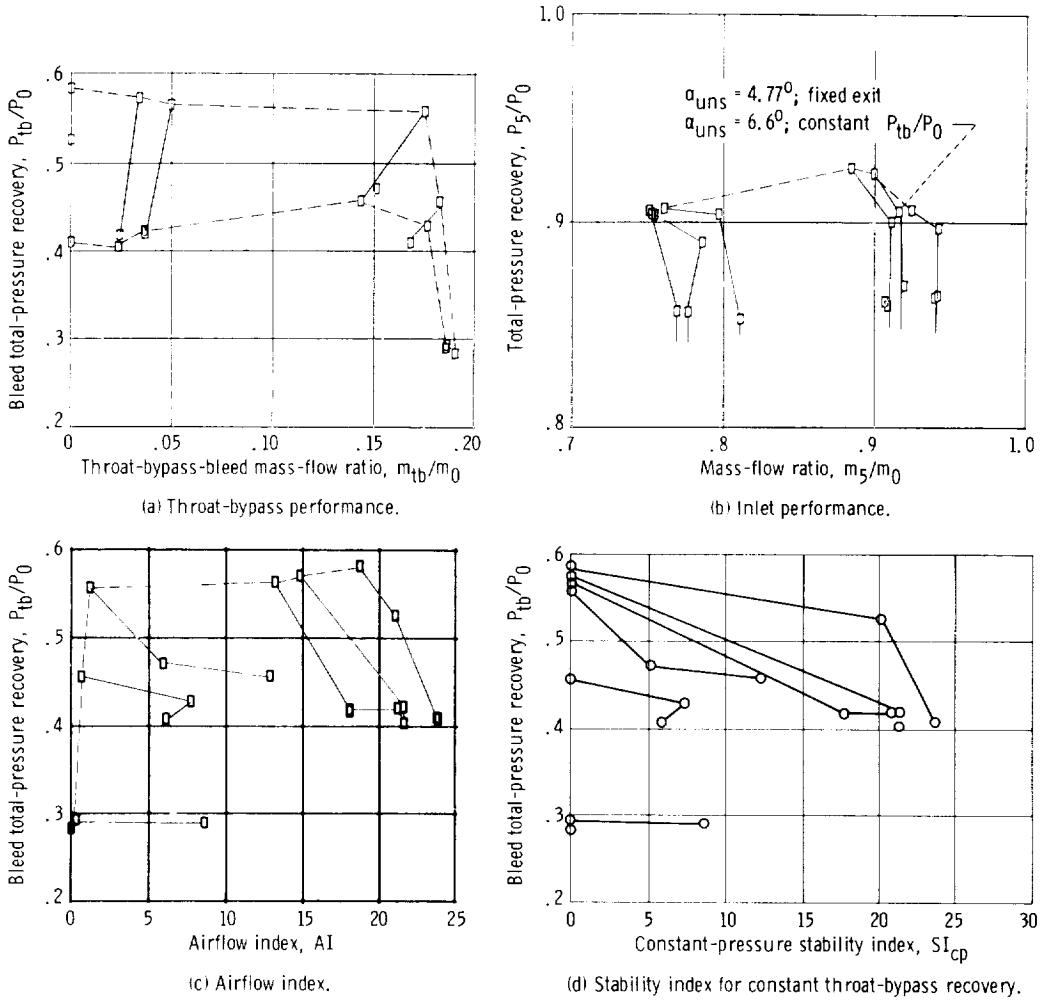

Figure 28. - Performance of forward-slanted-slot configuration SA. Free-stream Mach number, M_0 = 2.50; angle of attack, α = 0°; overboard-bypass mass-flow ratio, m_{by}/m_0 = 0.0175.

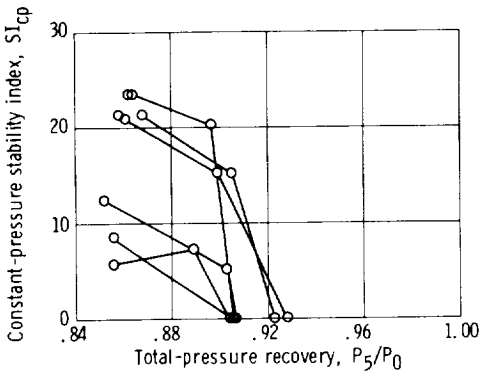

(e) Variation of constant-pressure stability index with inlet total-pressure recovery.

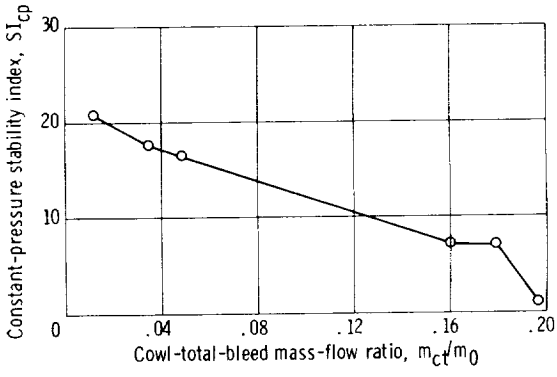

(f) Constant-pressure stability index for an initial inlet total-pressure recovery of 0.89.

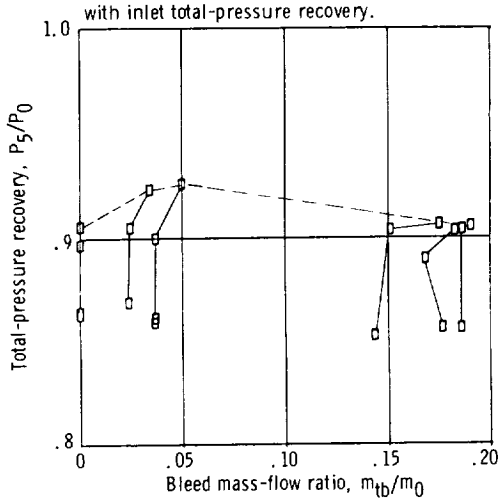

(g) Variation of inlet recovery with throat-bypass bleed.

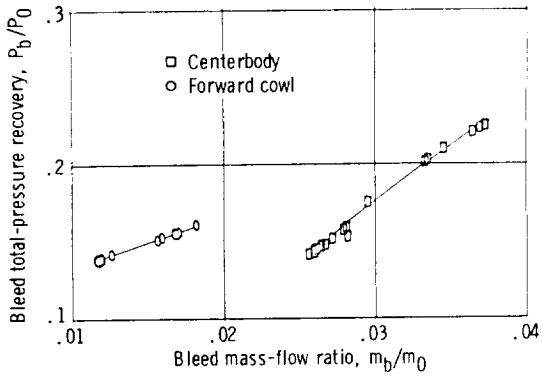

(h) Forward-cowl and centerbody bleed performance.

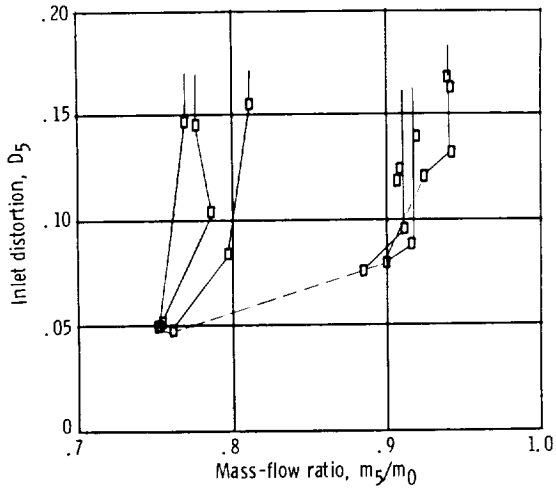

(i) Distortion.

Figure 28. - Concluded.

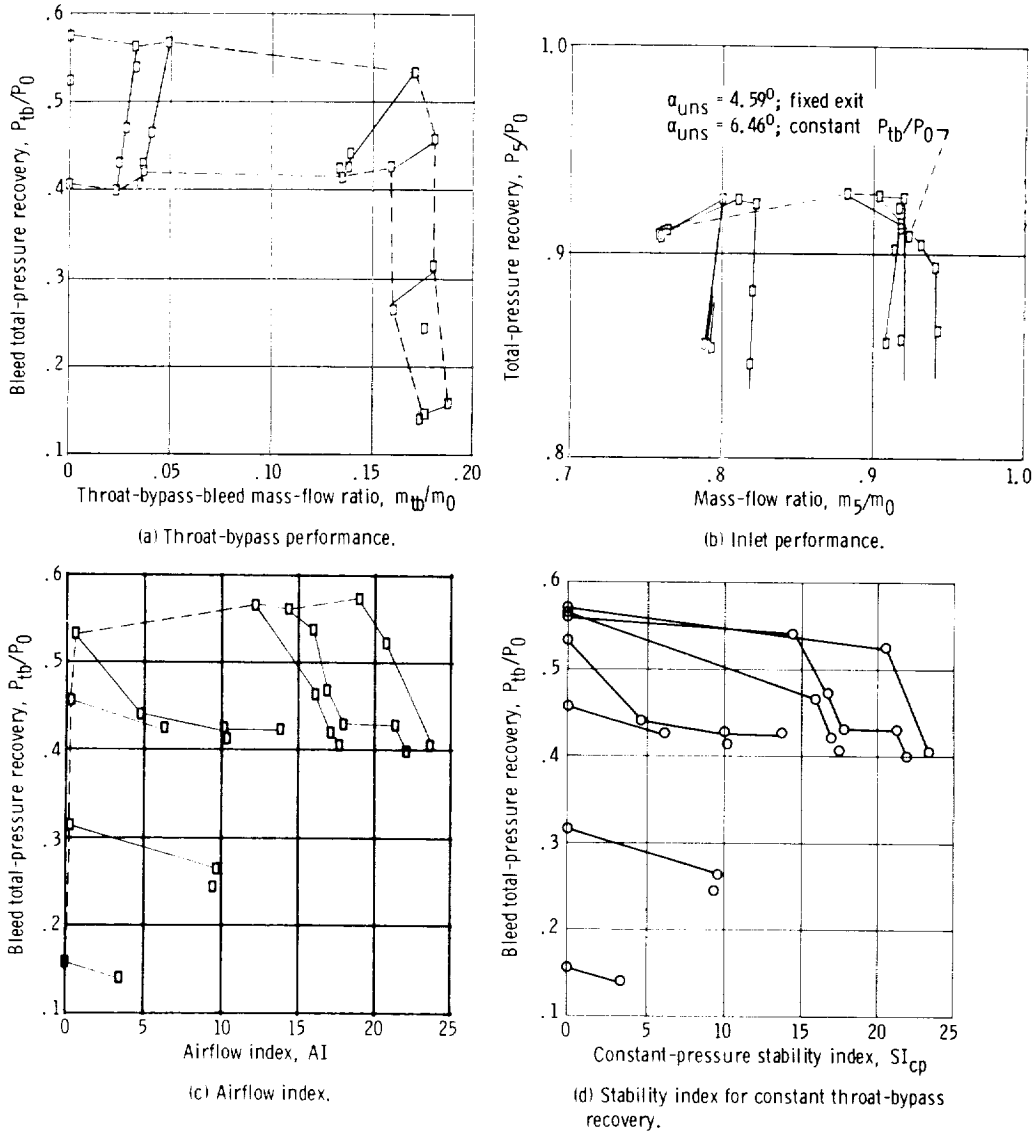

Figure 29. - Performance of forward-slanted-slot configuration SB. Free-stream Mach number, M_0 = 2.50; angle of attack, α = 0°; overboard-bypass mass-flow ratio, m_{by}/m_0 = 0.0175.

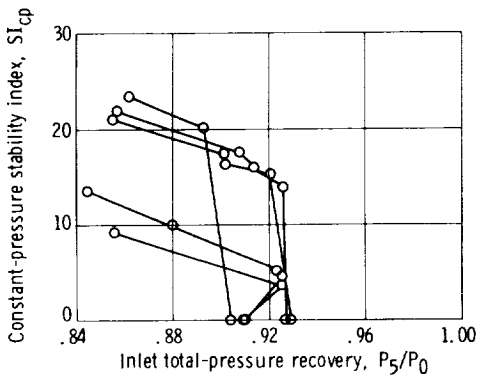

(e) Variation of constant-pressure stability index with inlet total-pressure recovery.

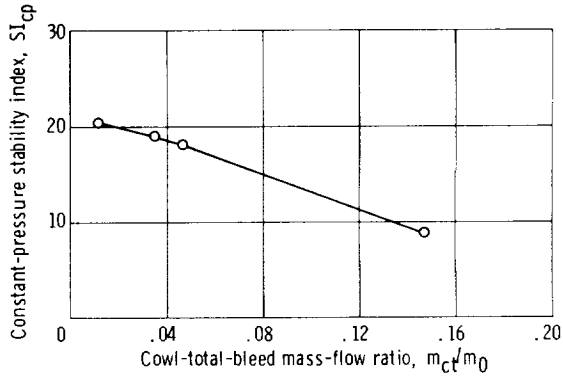

(f) Constant-pressure stability index for an initial inlet total-pressure recovery of 0.89.

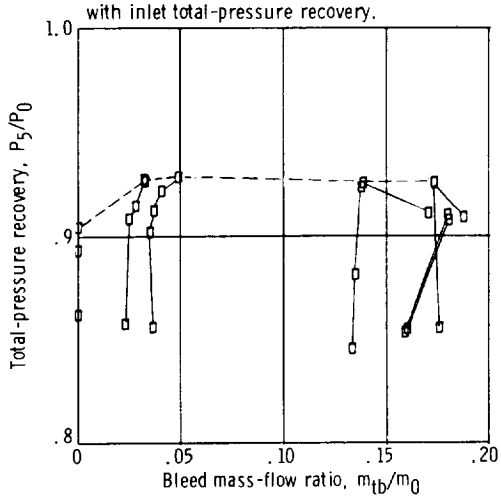

(g) Variation of inlet recovery with throat-bypass bleed.

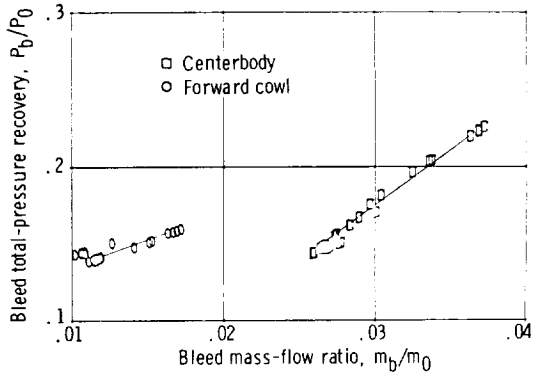

(h) Forward-cowl and centerbody bleed performance.

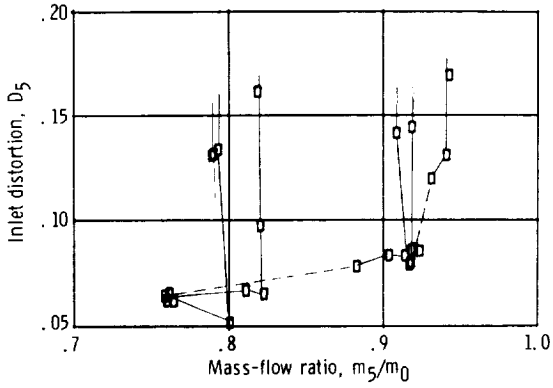

(i) Distortion.

Figure 29. - Concluded.

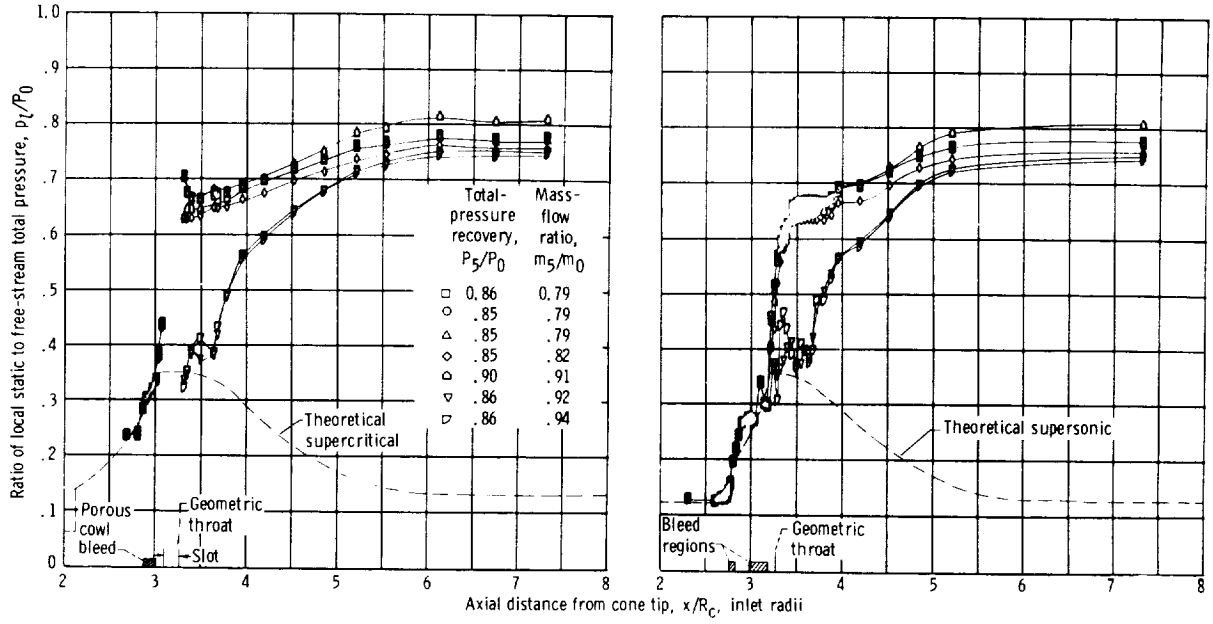

(a) Internal cowl surface pressure distributions.

(b) Centerbody surface pressure distributions.

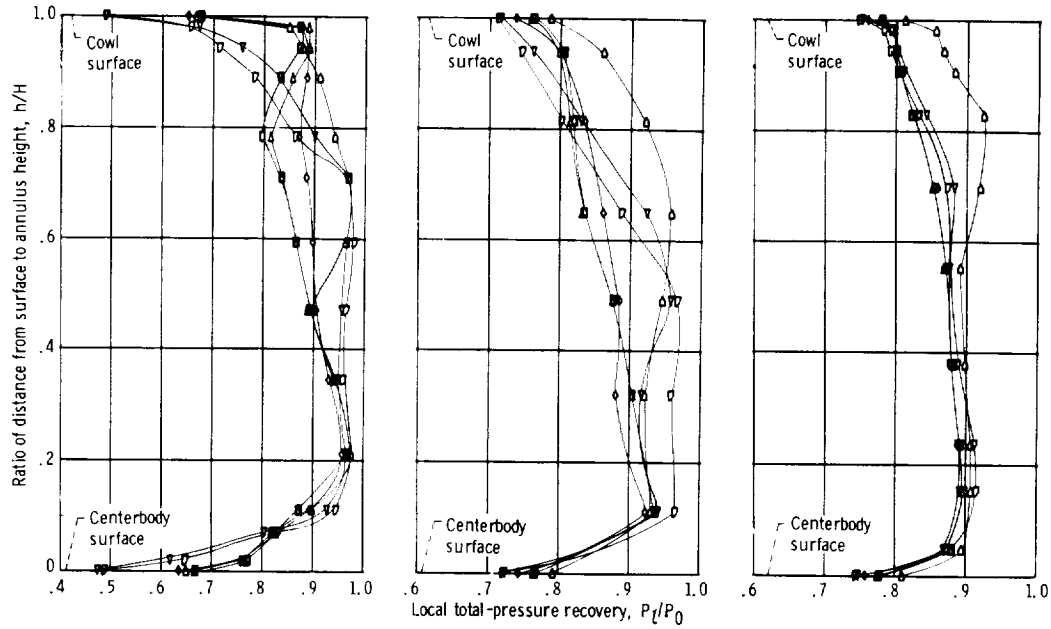

(c) Throat-exit local total-pressure recovery, station 2. Symbols at h/H of 0 and 1.0 represent inlet surface static pressures.

(d) Mid-diffuser local total-pressure recovery, station 4. Symbols at h/H of 0 and 1.0 represent inlet surface static pressures.

(e) Diffuser-exit rake 6 local total-pressure recovery, station 5. Symbols at h/H of 0 and 1.0 represent inlet surface static pressures.

Figure 30. - Inlet diffuser and throat-bypass slot static- and total-pressure distributions for configuration SB. These pressure distributions are for supercritical conditions that were obtained for several fixed exits.

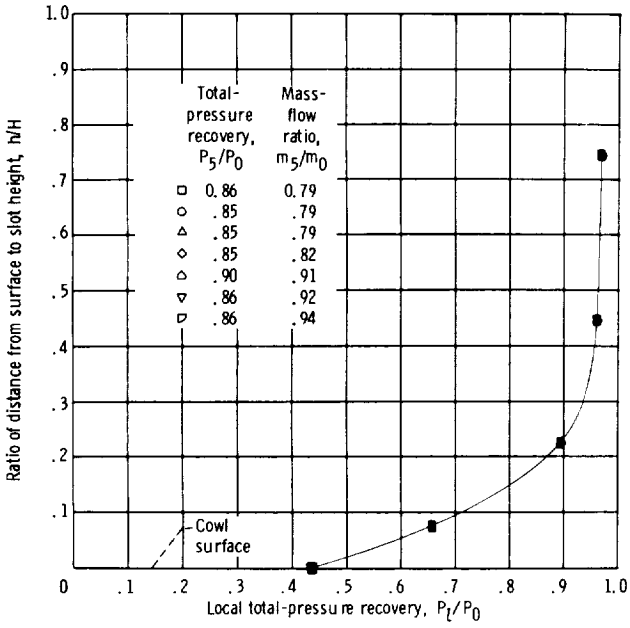

(f) Local total-pressure recovery for slot rake A. Symbols at h/H of 0 represent inlet surface static pressures.

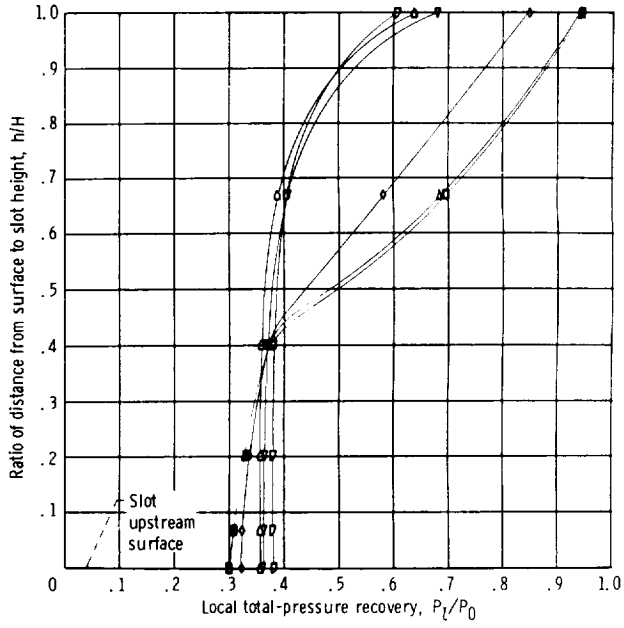

(g) Local total-pressure recovery for slot rake B. Symbols at h/H of 0 represent inlet surface static pressures.

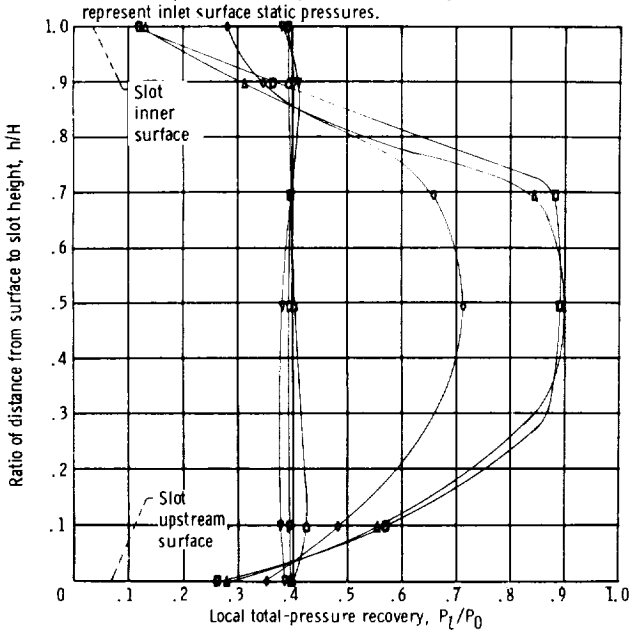

(h) Local total-pressure recovery for slot rake C. Symbols at h/H of 0 and 1.0 represent inlet surface static pressures.

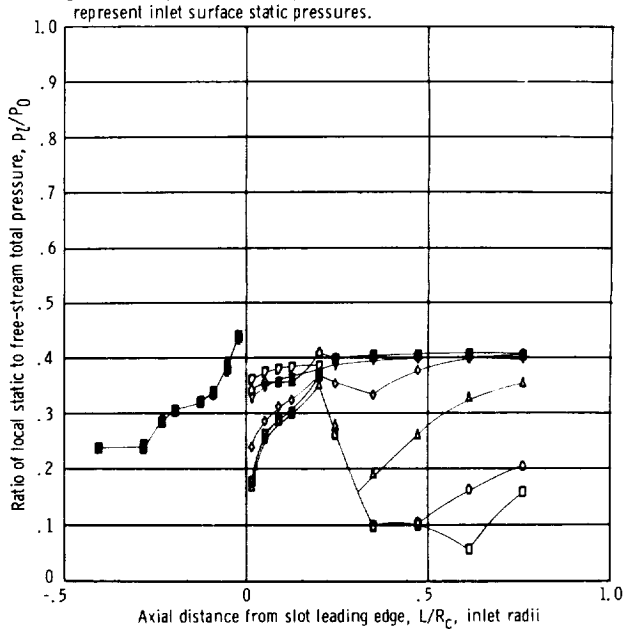

(i) Local pressure distributions on upstream surface of bleed slot.

Figure 30. - Concluded.

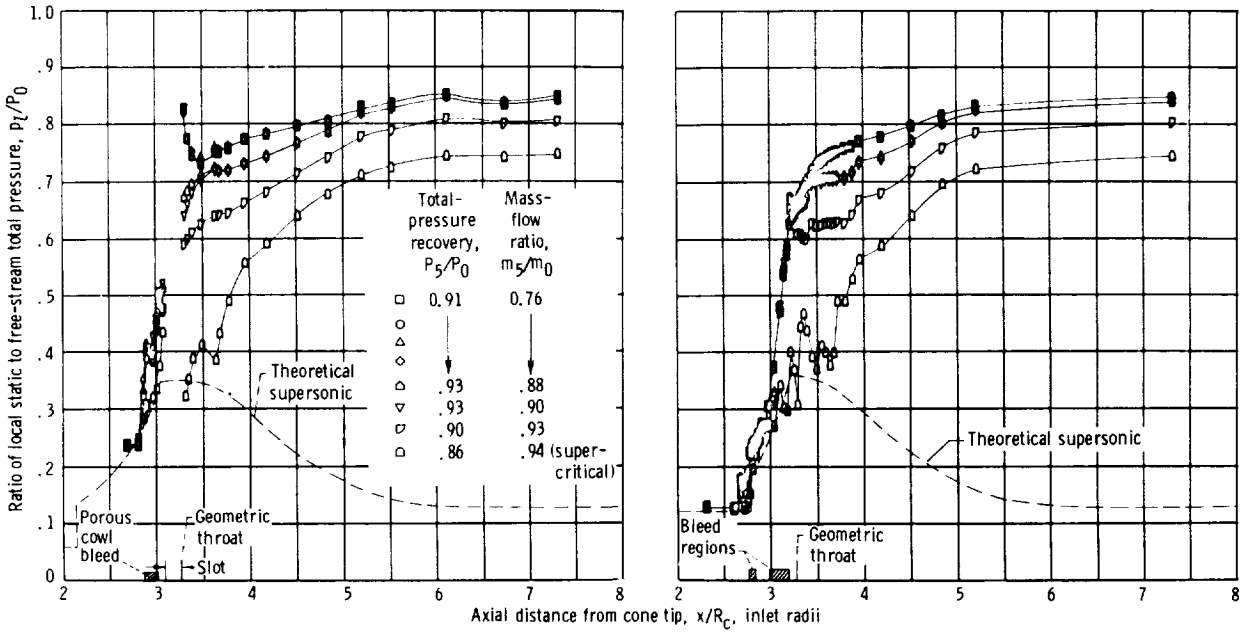

(a) Internal cowl surface pressure distributions.

(b) Centerbody surface pressure distributions.

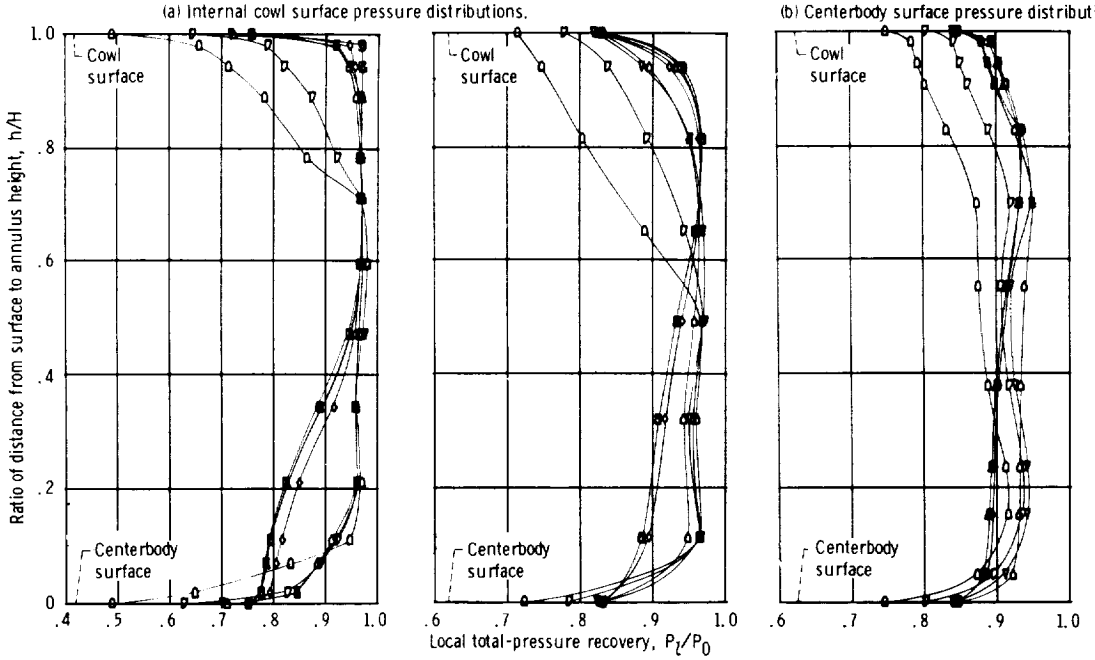

(c) Throat-exit local total-pressure recovery, station 2. Symbols at h/H of 0 and 1.0 represent inlet surface static pressures.

(d) Mid-diffuser local total-pressure recovery, station 4. Symbols at h/H of 0 and 1.0 represent inlet surface static pressures.

(e) Diffuser-exit rake 6 local total-pressure recovery, station 5. Symbols at h/H of 0 and 1.0 represent inlet surface static pressures.

Figure 31. - Inlet diffuser and throat-bypass slot static- and total-pressure distributions for configuration SB. Pressure distributions are for one supercritical condition (throat-bypass mass-flow ratio, $m_{tb}/m_0 = 0$) and all unstart limit data.

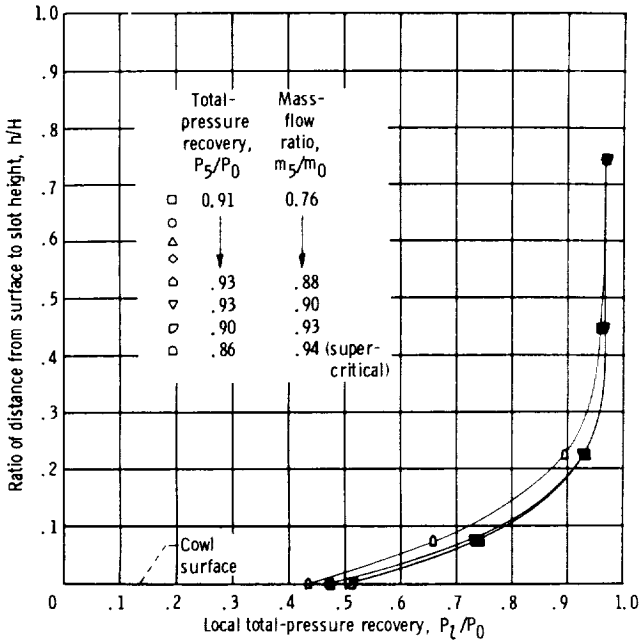

(f) Local total-pressure recovery for slot rake A. Symbols at h/H of 0 represent inlet surface static pressures.

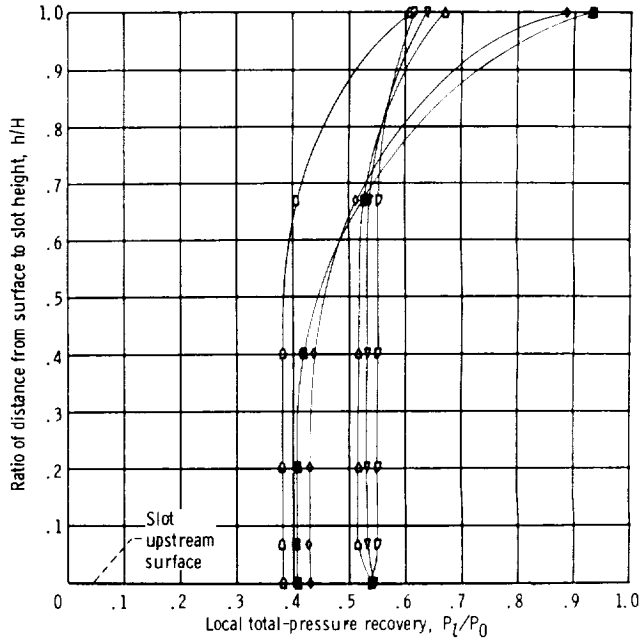

(g) Local total-pressure recovery for slot rake B. Symbols at h/H of 0 represent inlet surface static pressures.

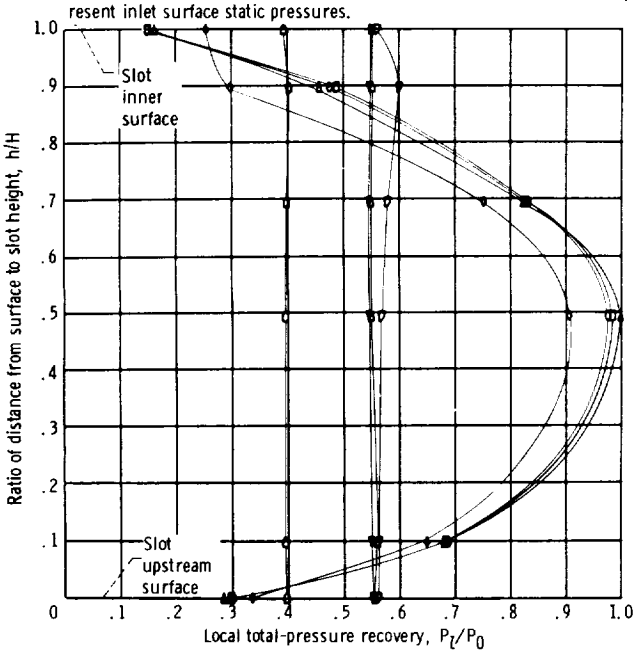

(h) Local total-pressure recovery for slot rake C. Symbols at h/H of 0 and 1.0 represent inlet surface static pressures.

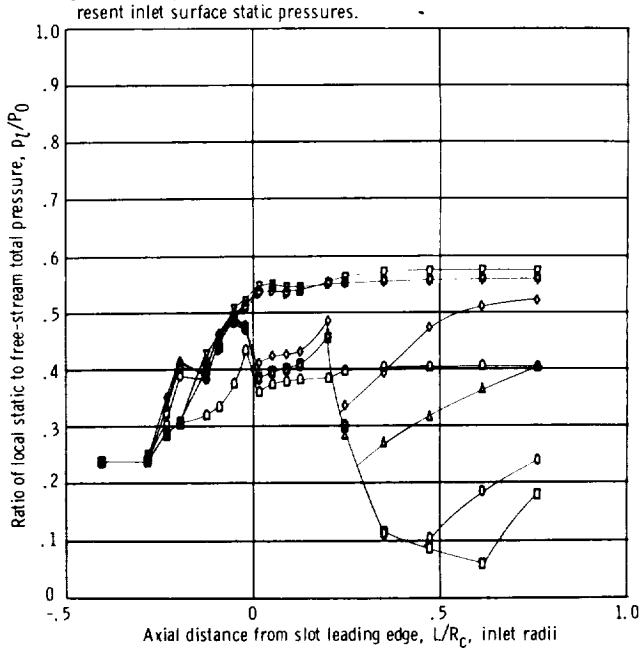

(i) Local pressure distributions on upstream surface of bleed slot.

Figure 31. - Concluded.

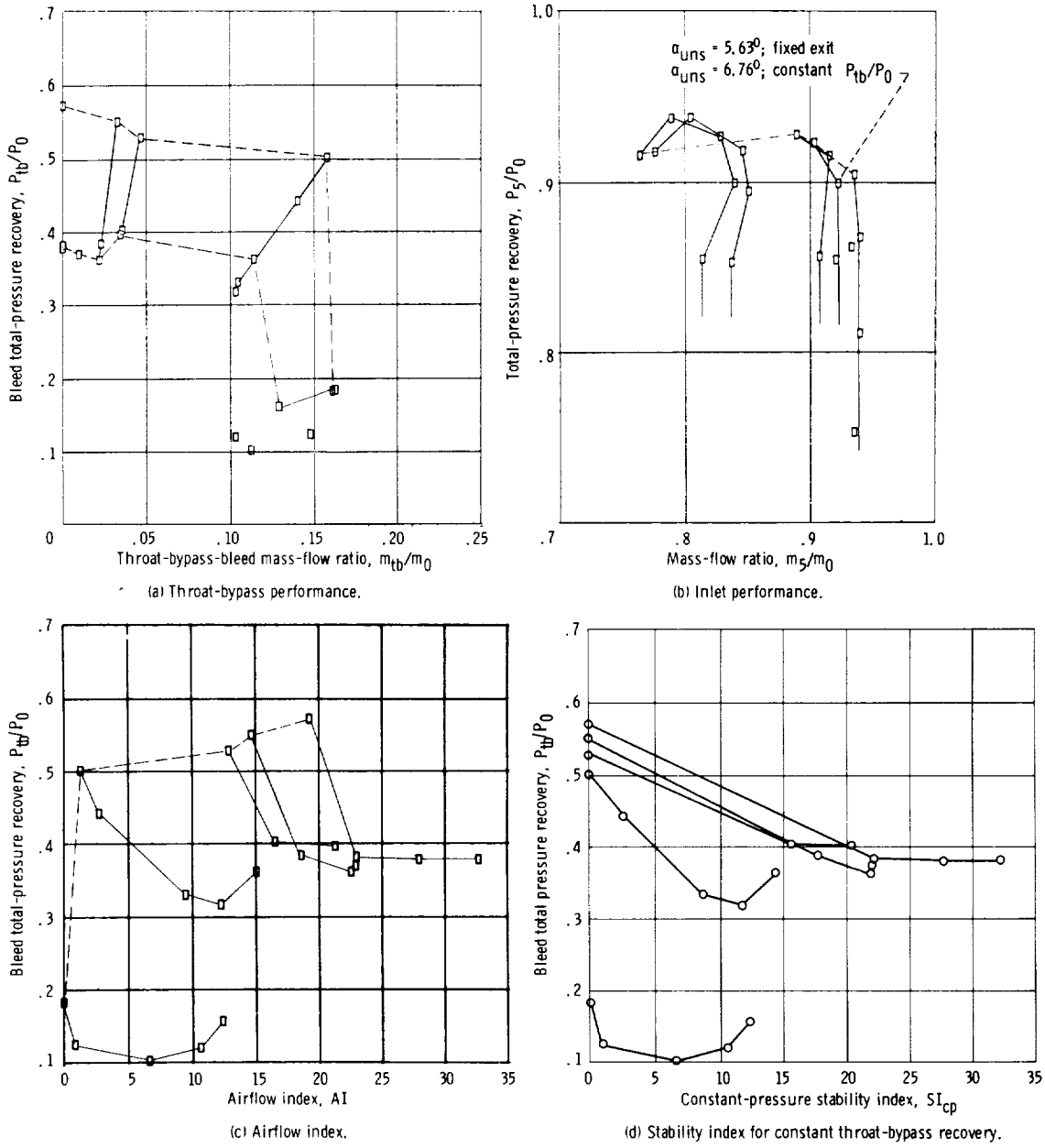

Figure 32. - Performance of forward-slanted-slot configuration SC. Free-stream Mach number, M_0 = 2.50; angle of attack, α = 0°; overboard-bypass mass-flow ratio, m_{by}/m_0 = 0.0175.

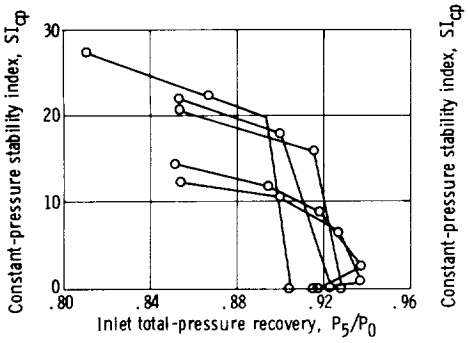

(e) Variation of constant-pressure stability index with inlet total-pressure recovery.

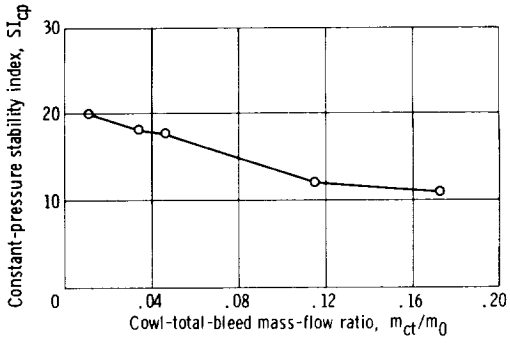

(f) Constant-pressure stability index for an initial inlet total-pressure recovery of 0.89.

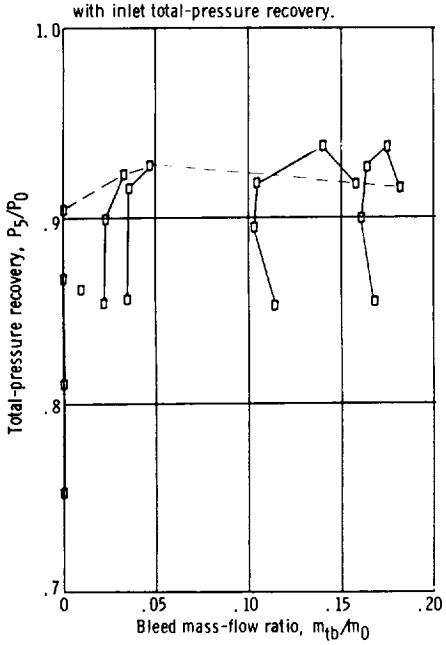

(g) Variation of inlet recovery with throat-bypass bleed.

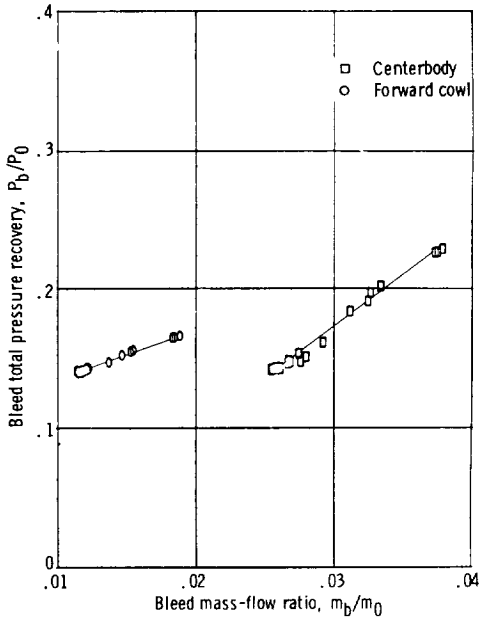

(h) Forward-cowl and centerbody bleed performance.

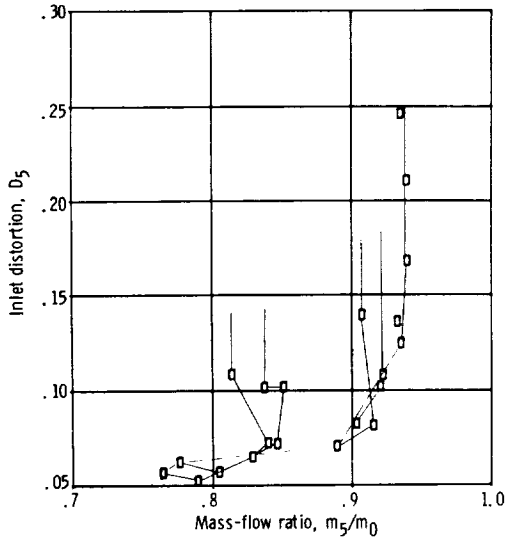

(i) Distortion.

Figure 32. - Concluded.

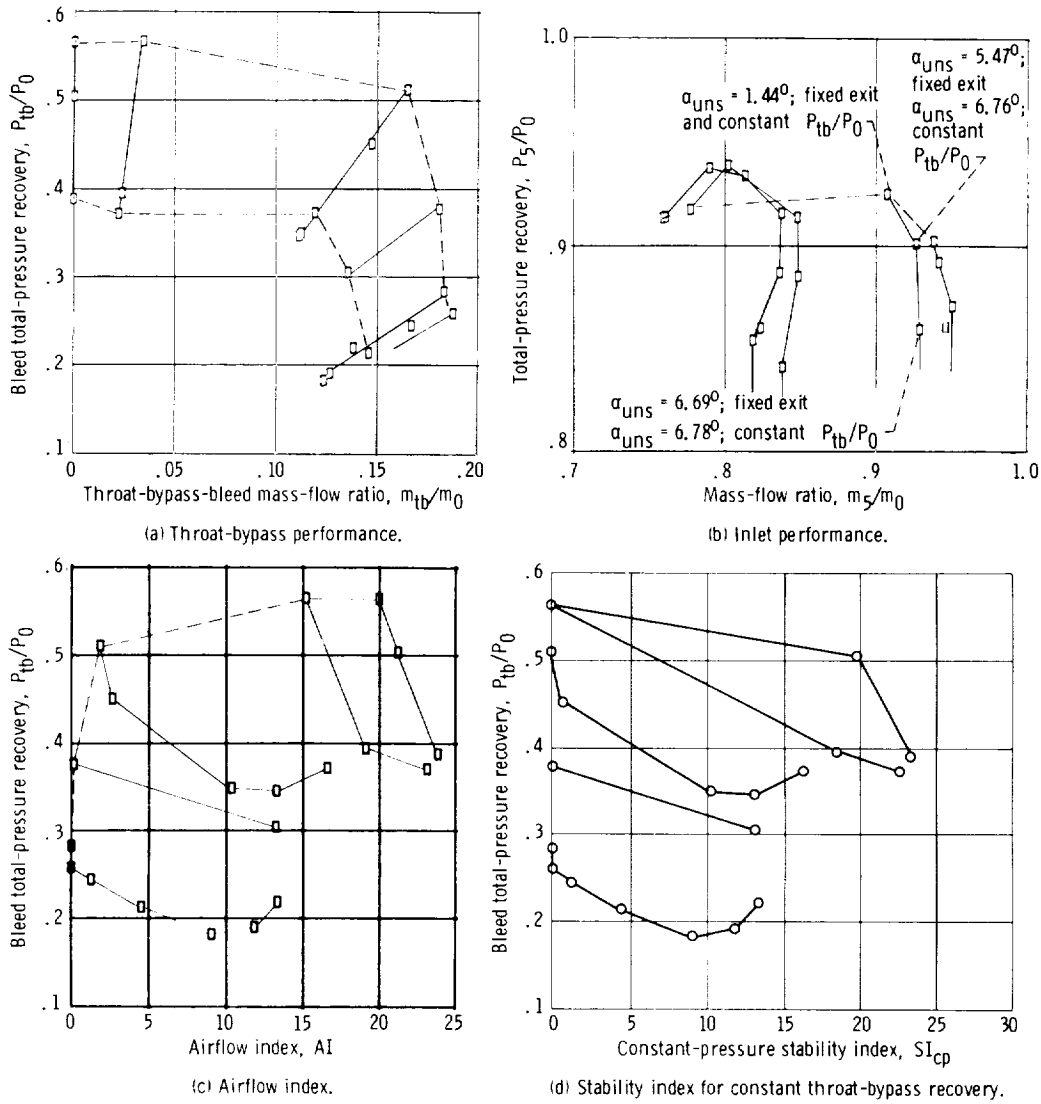

Figure 33. - Performance of forward-slanted-slot configuration SD. Free-stream Mach number, M_0 = 2.50; angle of attack, α = 0°; overboard-bypass mass-flow ratio, m_{by}/m_0 = 0.01.

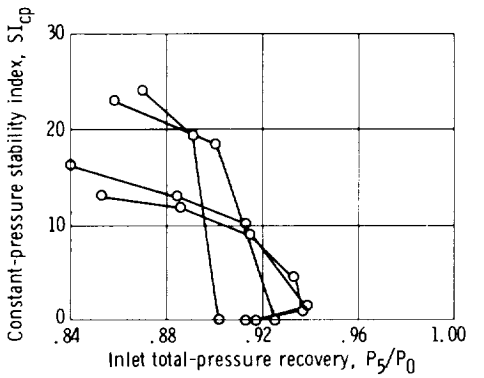

(e) Variation of constant-pressure stability index with inlet total-pressure recovery.

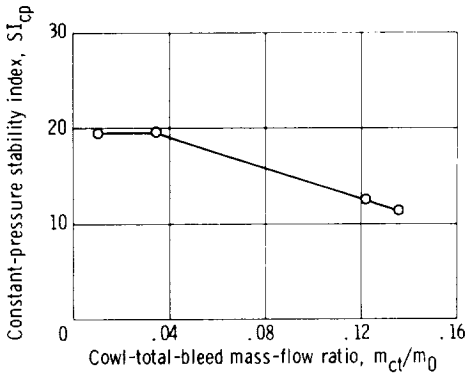

(f) Constant-pressure stability index for an initial inlet total-pressure recovery of 0.89.

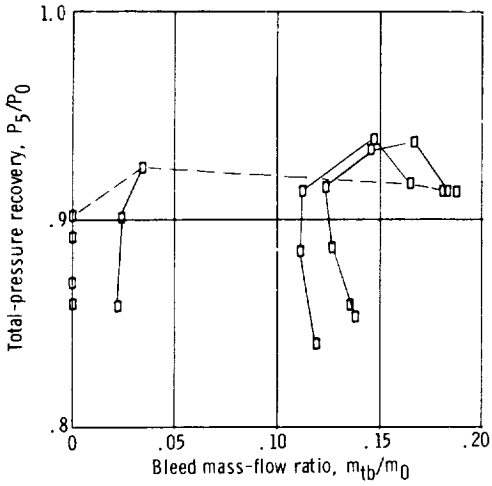

(g) Variation of inlet recovery with throat-bypass bleed.

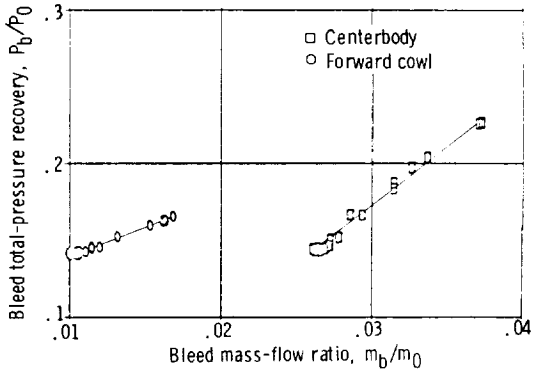

(h) Forward-cowl and centerbody bleed performance.

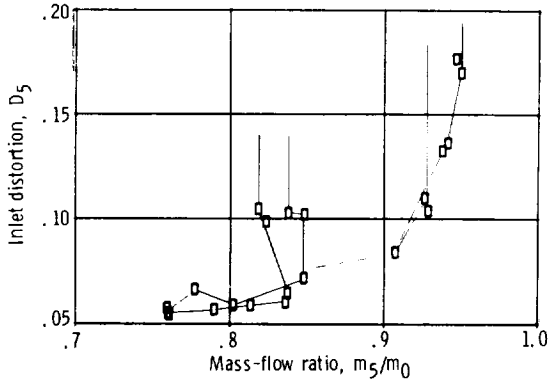

(i) Distortion.

Figure 33. - Concluded.

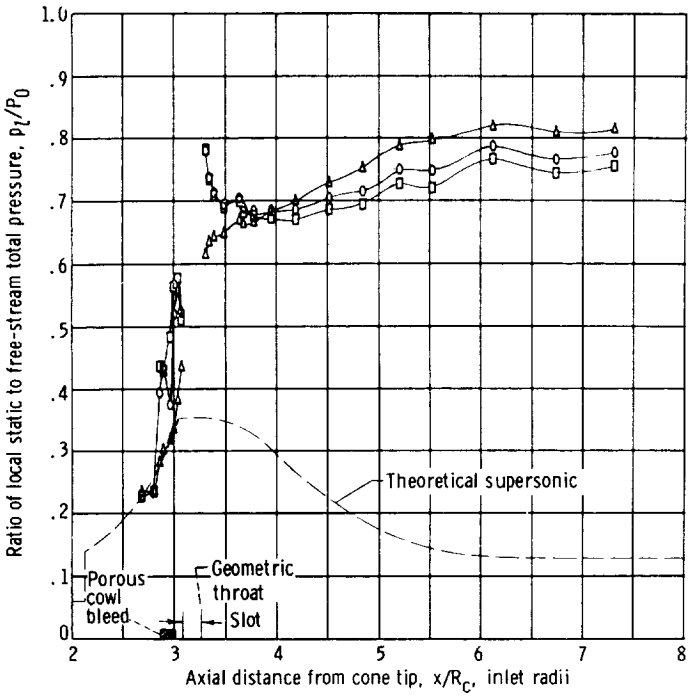

(a) Cowl surface.

Angle of attack, α, deg	Total-pressure recovery, P_5/P_0	Mass-flow ratio, m_5/m_0	Bleed exit -
△ 0	0.91	0.92	Fixed exit
○ 4.59	.87	.88	Same as $\alpha = 0^0$
□ 6.46	.85	.85	Constant bleed recovery

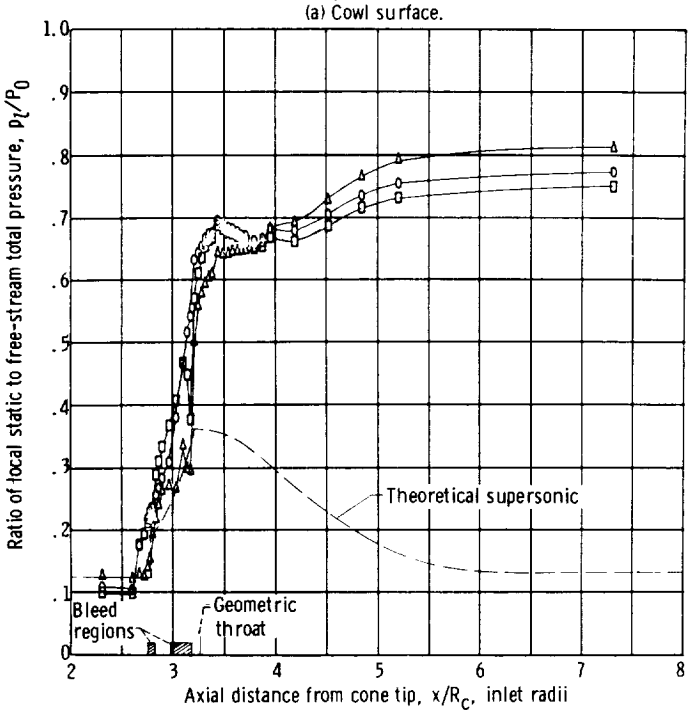

(b) Centerbody surface.

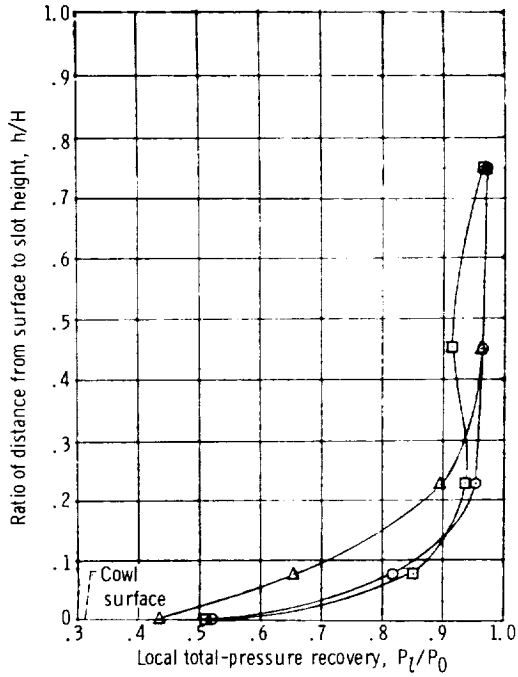

(c) Slot rake A. Symbols at a h/H of 0 represent inlet surface static pressures.

Figure 34. - Diffuser static-pressure distributions for configuration SB for an initial operating condition and for unstart angles of attack. Slot rake A data are also presented.

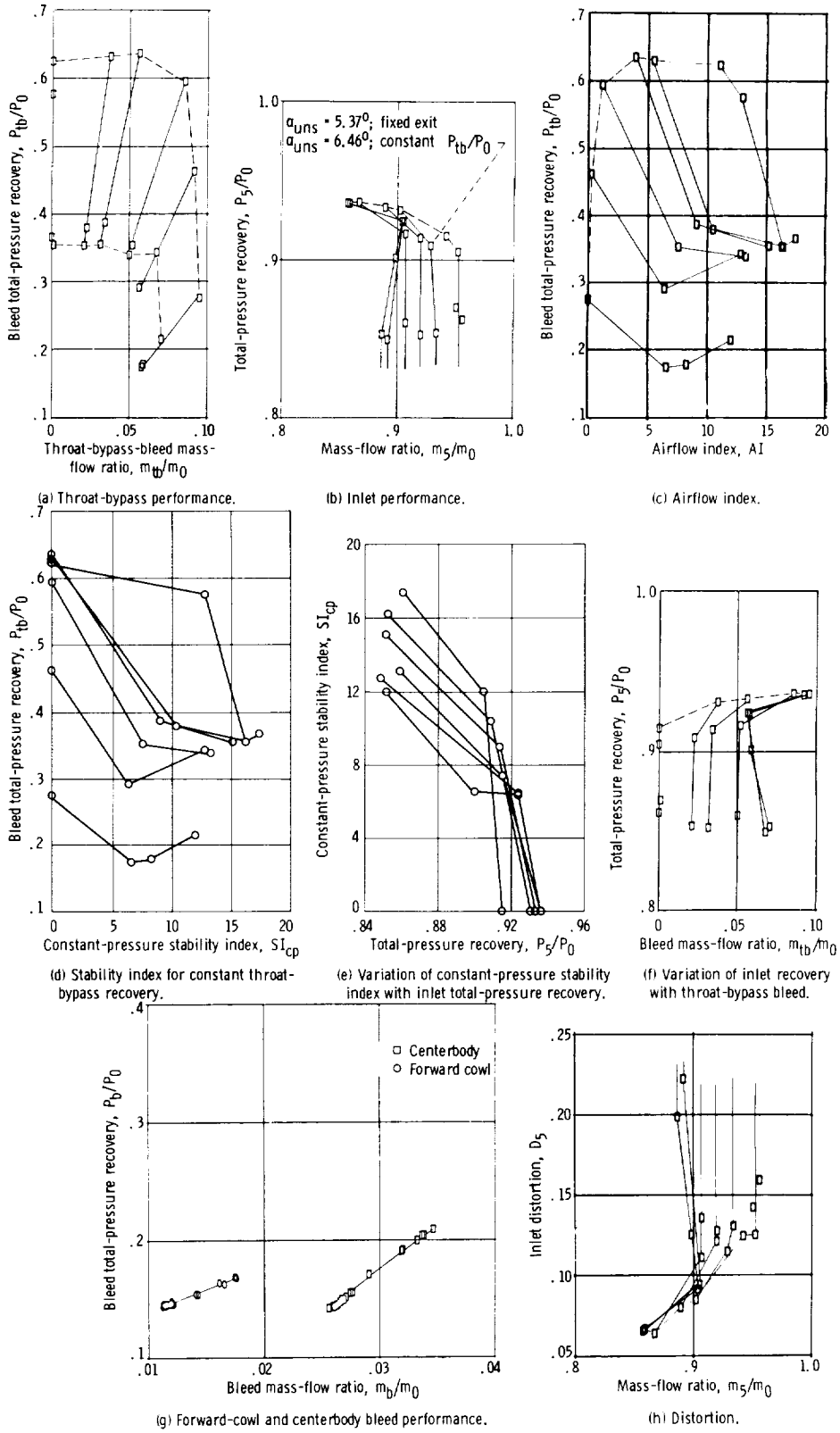

Figure 35. - Performance of forward-slanted slot configuration SS. Free-stream Mach number, M_0 = 2.50; angle of attack, α = 0°; overboard-bypass mass-flow ratio, m_{by}/m_0 = 0.01.

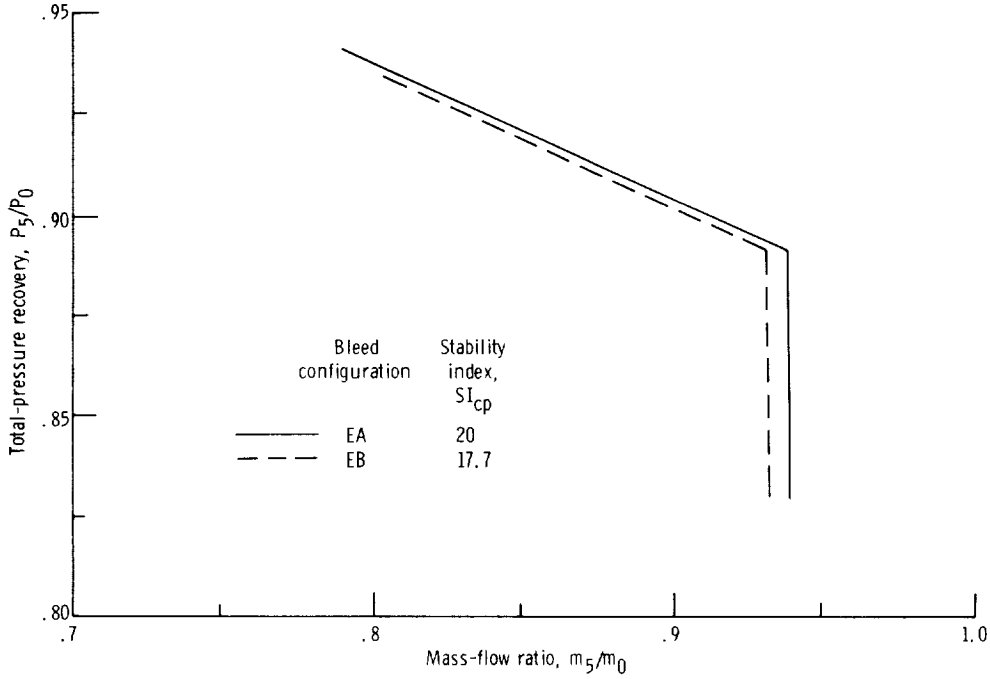

Figure 36. - Comparison of inlet performance for distributed educated-throat-bypass configurations based on constant throat-bypass recovery to unstart limit from initial inlet conditions of 89-percent total-pressure recovery and total-cowl-bleed mass-flow ratio of 0.02 to 0.03. Free-stream Mach number, $M_0 = 2.50$; angle of attack, $\alpha = 0^0$; overboard-bypass mass-flow ratio, $m_{by}/m_0 = 0.01$.

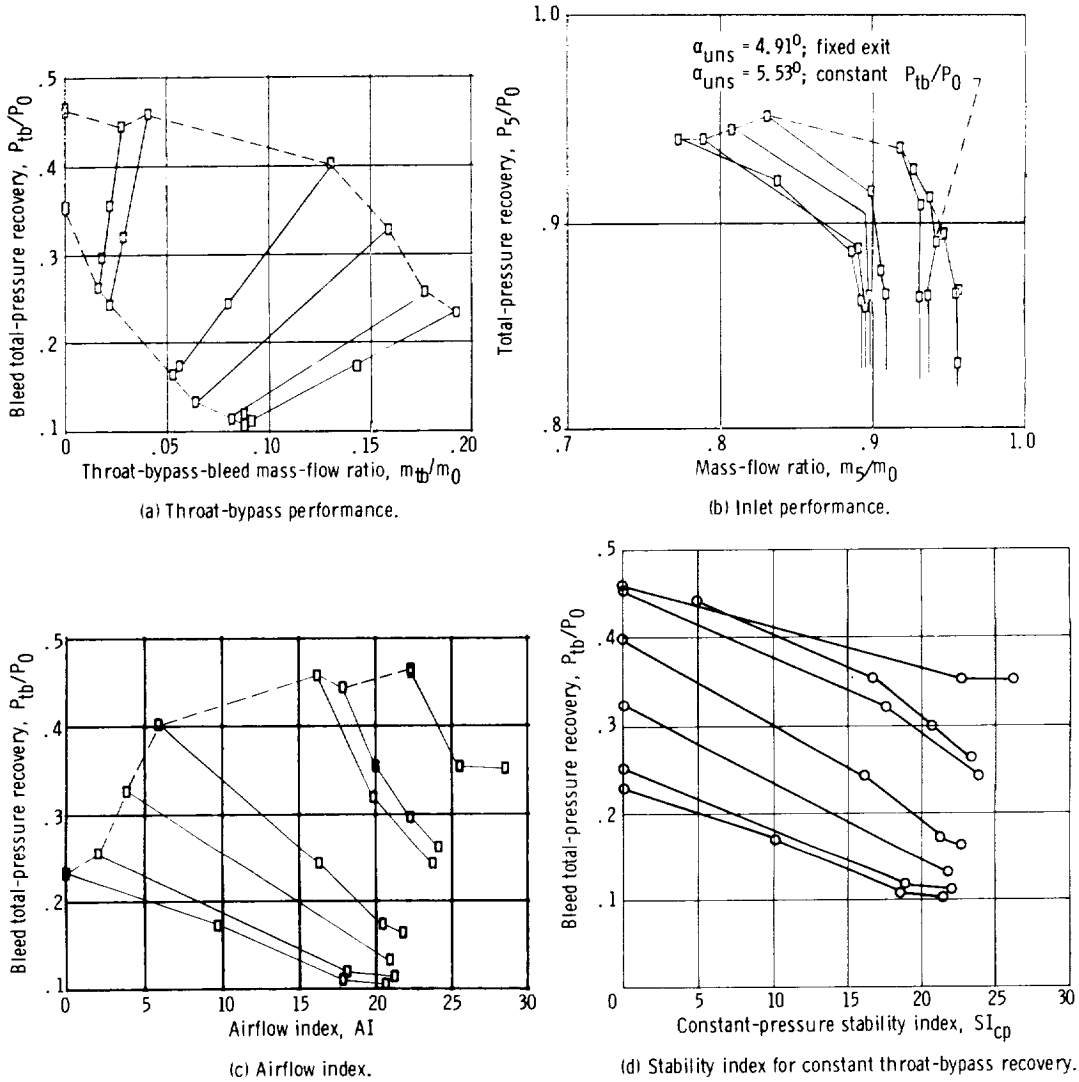

Figure 37. - Performance of distributed educated configuration EA. Free-stream Mach number, $M_0 = 2.50$; angle of attack, $\alpha = 0^0$; overboard-bypass mass-flow ratio, $m_{by}/m_0 = 0.01$.

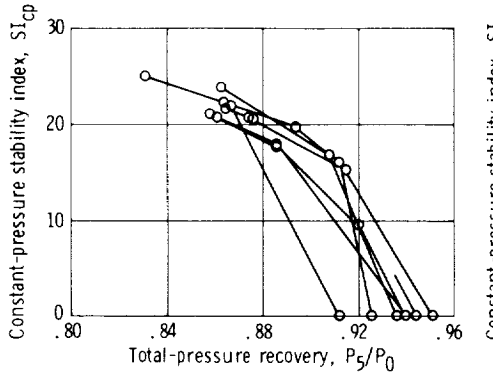

(e) Variation of constant-pressure stability index with inlet total-pressure recovery.

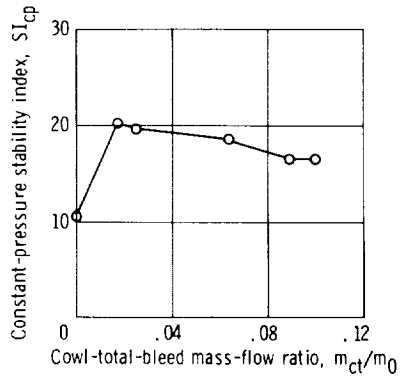

(f) Constant-pressure stability index for an initial inlet total-pressure recovery of 0.89.

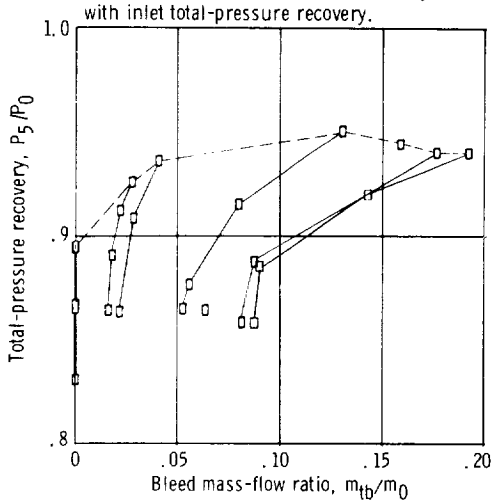

(g) Variation of inlet recovery with throat-bypass bleed.

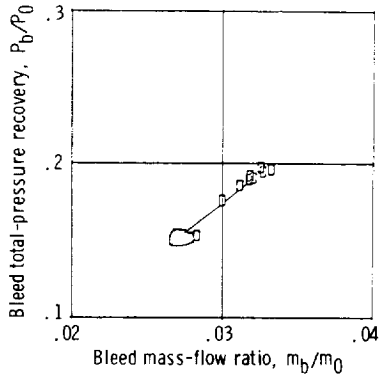

(h) Centerbody bleed performance.

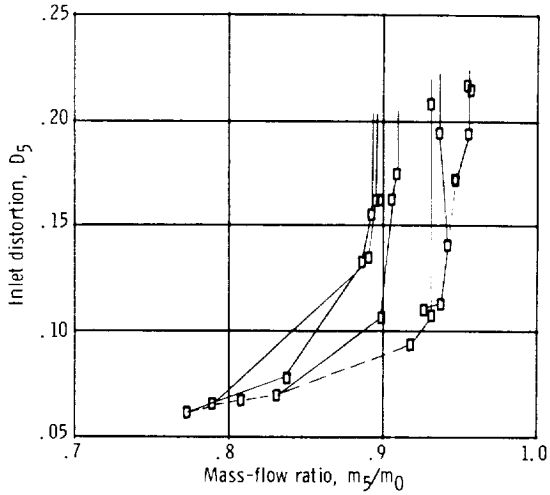

(i) Distortion.

Figure 37. - Concluded.

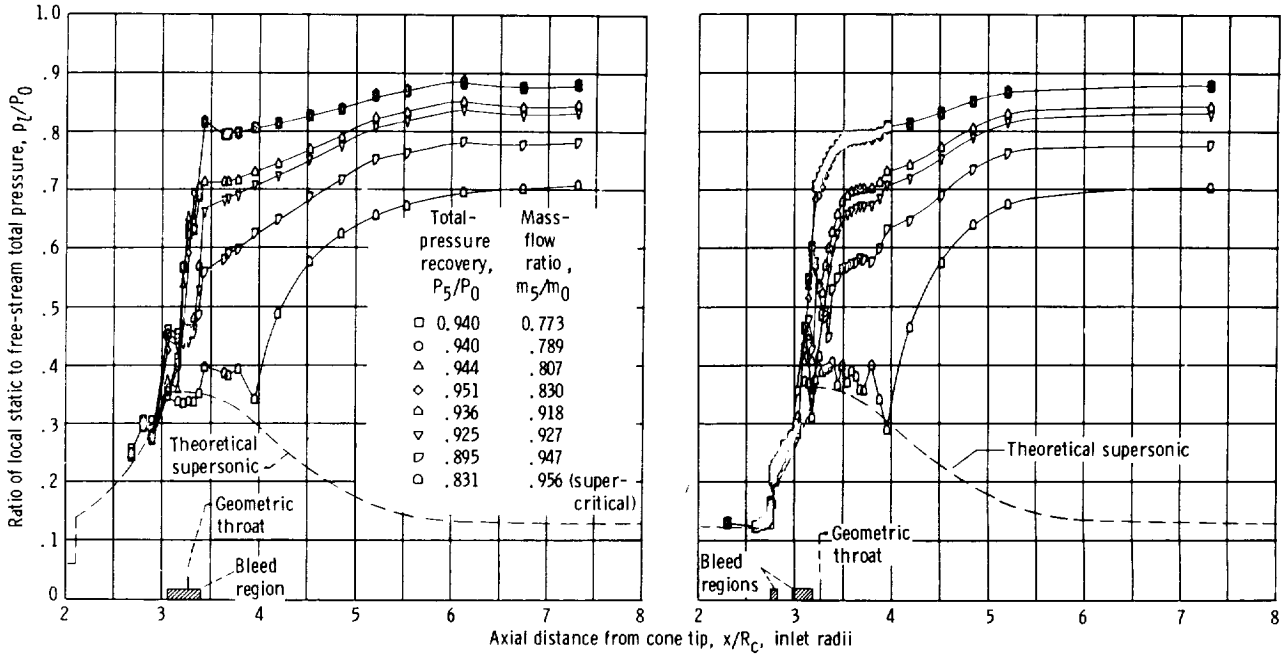

(a) Internal cowl surface pressure distributions.

(b) Centerbody surface pressure distributions.

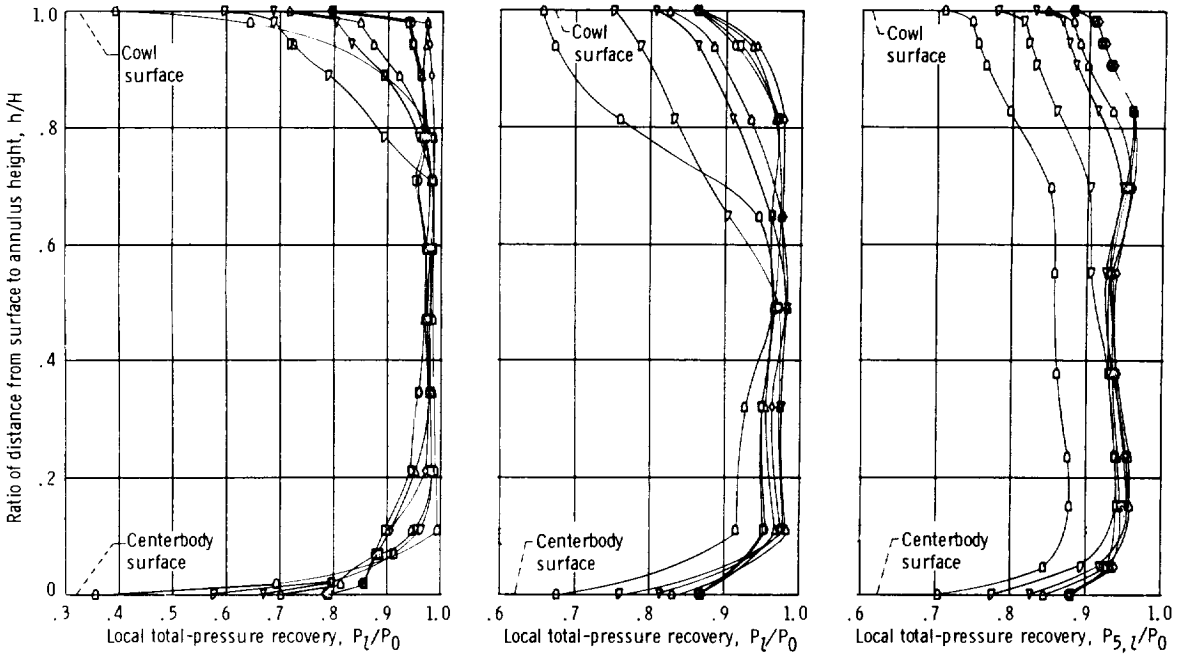

(c) Throat exit, station 2. Symbols at h/H of 0 and 1.0 represent inlet surface static pressures.

(d) Mid-diffuser, station 4. Symbols at h/H of 0 and 1.0 represent inlet surface static pressures.

(e) Diffuser rake 6, station 5. Symbols at h/H of 0 and 1.0 represent inlet surface static pressures.

Figure 38. - Inlet diffuser static- and total-pressure distributions for configuration EA. Distributions are presented for one supercritical condition and all unstart limit data.

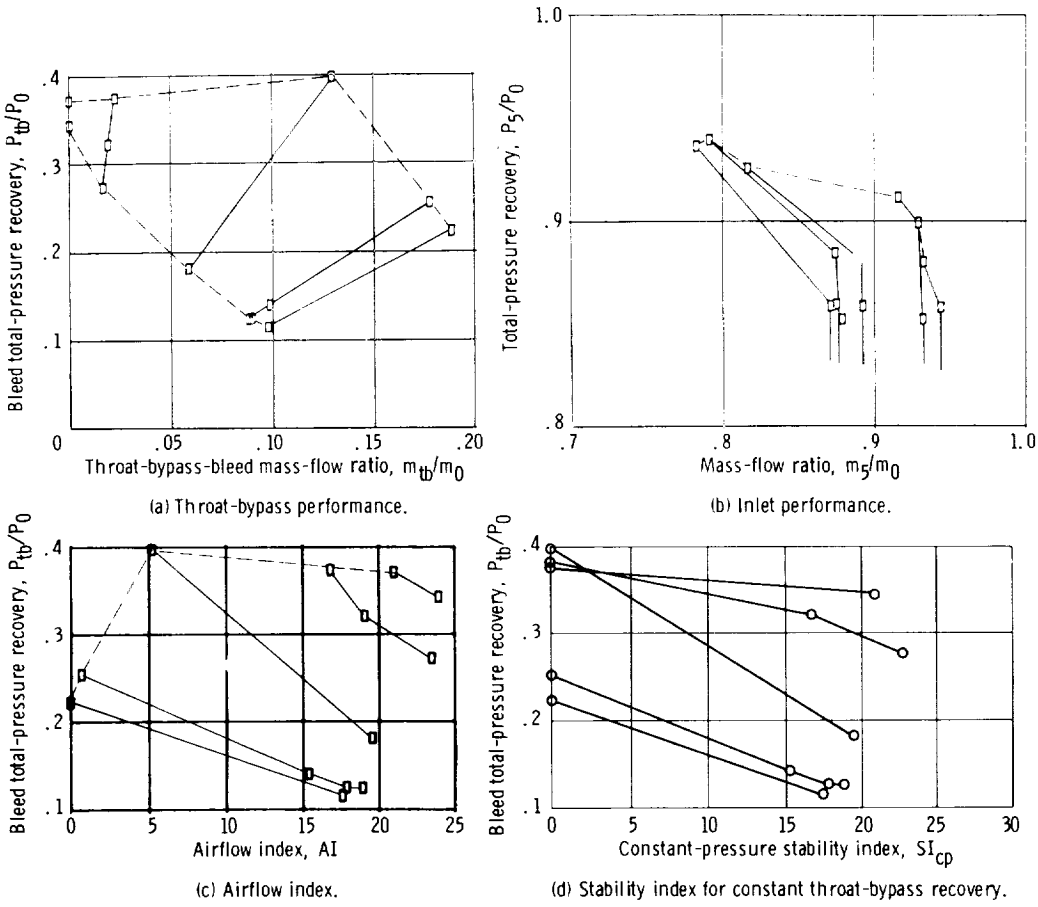

(a) Throat-bypass performance.

(b) Inlet performance.

(c) Airflow index.

(d) Stability index for constant throat-bypass recovery.

Figure 39. - Performance of distributed educated bleed configuration EB. Free-stream Mach number, $M_0 = 2.50$; angle of attack, $\alpha = 0^o$; overboard-bypass mass-flow ratio, $m_{by}/m_0 = 0.01$.

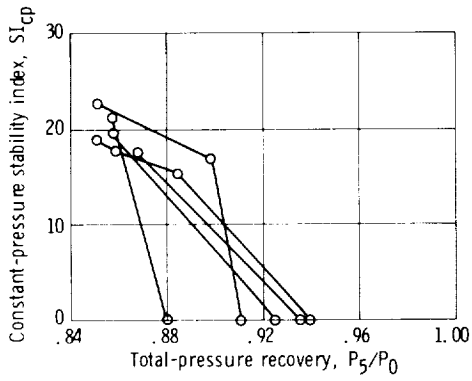

(e) Variation of constant-pressure stability index with inlet total-pressure recovery.

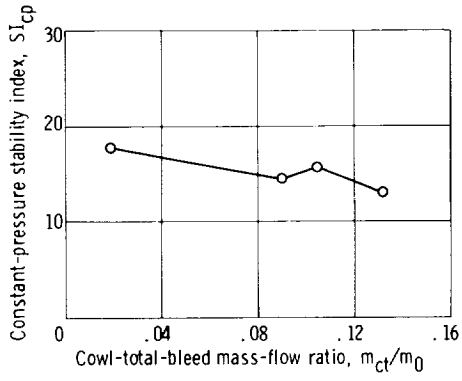

(f) Constant-pressure stability index for an initial inlet total-pressure recovery of 0.89.

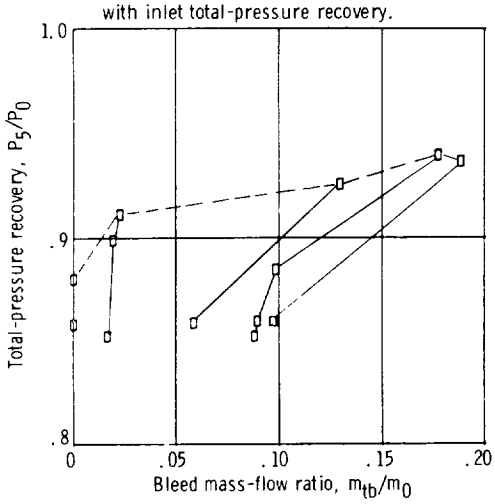

(g) Variation of inlet recovery with throat-bypass bleed.

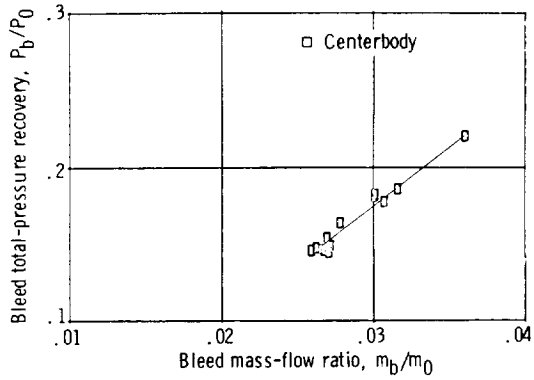

(h) Centerbody bleed performance.

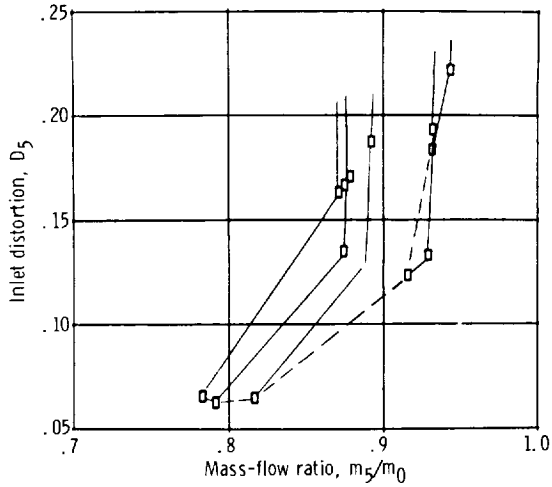

(i) Distortion.

Figure 39. - Concluded.

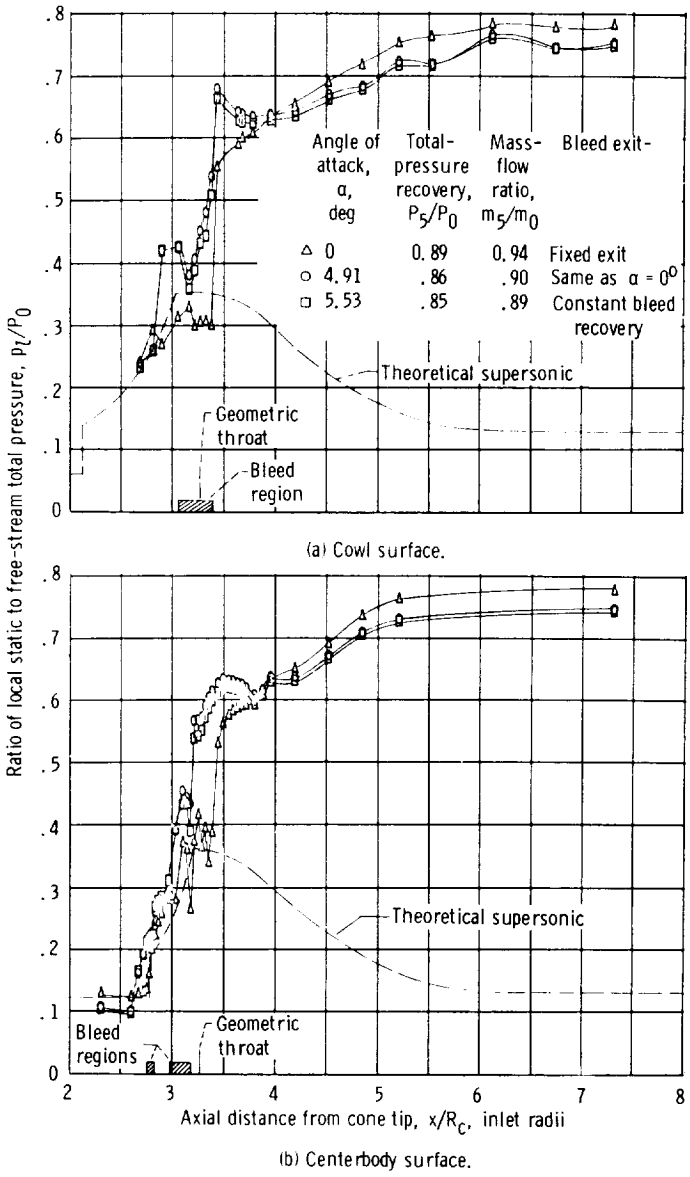

Figure 40. - Diffuser static-pressure distribution for configuration EA for an initial operating condition and for unstart angles of attack.

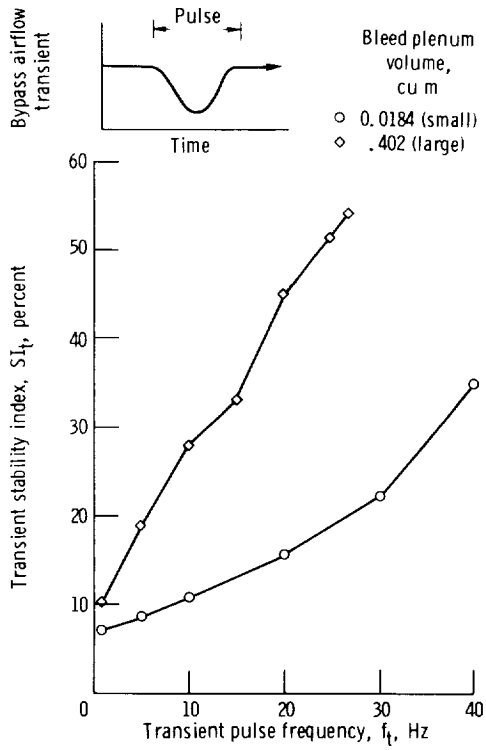

Figure 41. - Unstart limits of inlet system utilizing throat-bypass configuration NF when subjected to transient internal disturbances. Free-stream Mach number, M_0 = 2.50; angle of attack, α = 0°.